8-2014

Structural Dynamics and Charge Transport in Room Temperature Ionic Liquids

Philip James Griffin
University of Tennessee - Knoxville, pgriffi5@vols.utk.edu

To the Graduate Council:

I am submitting herewith a dissertation written by Philip James Griffin entitled "Structural Dynamics and Charge Transport in Room Temperature Ionic Liquids." I have examined the final electronic copy of this dissertation for form and content and recommend that it be accepted in partial fulfillment of the requirements for the degree of Doctor of Philosophy, with a major in Physics.

Alexei P. Sokolov, Major Professor

We have read this dissertation and recommend its acceptance:

Takeshi Egami, Mark Dadmun, Robert Compton

Accepted for the Council:

Carolyn R. Hodges

Vice Provost and Dean of the Graduate School

(Original signatures are on file with official student records.)

Structural Dynamics and Charge Transport in Room Temperature Ionic Liquids

A Dissertation Presented for the

Doctor of Philosophy

Degree

The University of Tennessee, Knoxville

Philip James Griffin

August 2014

Acknowledgements

This dissertation would not have come to fruition if it were not for the important contributions and collaborative efforts of my colleagues and friends in Prof. Alexei Sokolov's research group at the University of Tennessee. I would like to thank Dr. Alexander Kisliuk for teaching me in the early days about light scattering and the glass transition. He may not agree, but much of what I know now started as his answer to one of my many questions in the optics lab several years ago. I am especially thankful that during my doctoral studies I had the opportunity to work with Dr. Joshua Sangoro, who was so helpful to me and taught me many things about how to be a good scientist. I would also like to acknowledge the collaborative efforts and many discussions with Adam Holt, Dr. Alexander Agapov, Dr. Yangyang Wang, and Dr. Vladimir Novikov. Thanks as well to the members of my committee, Prof. Takeshi Egami, Prof. Mark Dadmun, and Prof. Robert Compton, for taking the time and effort to serve on my committee and review this dissertation. Last, but not least, I would like to extend my sincere gratitude to Prof. Alexei Sokolov for giving me the opportunity to work on these interesting research problems, and also for providing me the support and freedom to learn how to become an independent scientist.

Finally, I want to send my love to my family and friends who were there for me before, during, and who will be there after this saga in my life is complete. Thanks to all of you. To my fiancée, Haylie, I give my deepest love and appreciation…I can't wait to spend my life with you and to see what comes next!

Abstract

Room temperature ionic liquids are an important class of materials due to their chemical tunability and numerous advantageous physicochemical properties. As a result, ionic liquids are currently being investigated for use in a wide array of chemical and electrochemical applications. Despite their great potential, however, the relationship between the chemical structure and physicochemical properties of ionic liquids is not well understood.

To this end, this dissertation presents experimental studies of the reorientational structural dynamics and charge transport properties of a variety of room temperature ionic liquids using quasielastic light scattering spectroscopy and broadband dielectric spectroscopy.

Studies of a series of 1-butyl-3-methylimidazolium based ionic liquids, in which the anion was systematically varied, have revealed that the anion chemical structure has a significant impact on the structural dynamics and charge transport properties of ionic liquids. As the anion becomes larger and more asymmetrical, ionic mobility increases strongly as a result of an increased fluidity. Surprisingly, the mole fraction of free ions remains unaffected by the anion chemical structure.

The influence of cation chemical structure on the transport properties of ionic liquids was explored in a homologous series of tetra-alkylammonium based ionic liquids. It was found that pronounced chemical heterogeneity causes ionic liquids to exhibit complex and strongly heterogeneous molecular dynamics. Furthermore, when aliphatic side-groups of cations occupy a large liquid volume fraction, both the ion mobility as well as the mole fraction of free ions were found to decrease strongly as a consequence of pronounced nanophase segregation.

The transport properties of a novel carboxylic acid-tertiary amine based protic ionic liquid were also studied in this dissertation. The structural dynamics and charge transport

mechanism in this protic ionic liquid are surprisingly very similar to the aprotic ionic liquids, despite the fundamental differences in the intrinsic charge carrier.

Through these comparative studies, this dissertation not only provides a fundamental understanding of the unique dynamical properties of room temperature ionic liquids, but it also elucidates the complex interrelationship between key chemical structure variations and molecular transport properties of these important materials.

Table of Contents

List of Figures

1. Introduction

Room temperature ionic liquids are salts with normal melting temperatures at or below 100°C.[1] These materials have many unique physical properties such as low vapor pressure, high electrochemical and thermal stability, as well as high ionic conductivity which make them potentially ideal materials for use in a manifold of technological applications.[2] In addition, ionic liquids may be synthesized using a wide array of various counterion combinations and ion side-group functionalities, leading many to consider ionic liquids as truly "designer solvents".[3] Despite the great potential of ionic liquids to be used to solve numerous chemical and electrochemical challenges, there remains much to be understood about these important materials.

One of the major goals in the field of ionic liquid research is to develop a predictive understanding of the relationship between molecular structure and the physicochemical properties of these materials. As a result of the seemingly limitless numbers of potential ionic liquids which may be synthesized, there are many opportunities to contribute to the resolution of this great challenge in both theoretical and experimental capacities. To this end, this dissertation presents experimental studies of the reorientational structural dynamics and charge transport properties of a variety of room temperature ionic liquids and addresses three major questions related to molecular transport in ionic liquids: (i) How does the anion chemical structure influence structural dynamics and charge transport, as well as the interrelationship between these dynamical processes? (ii) What effect does the presence of nanophase segregated structures and large alkyl moieties have on the structural dynamics and charge transport of ionic liquids? (iii) To what extent is charge transport in protic ionic liquids similar to, or different from, transport in aprotic ionic liquids?

Chapter two presents an overview of the dynamical properties of supercooled liquids and the glass transition, and also discusses the physicochemical properties of ionic liquids. Chapter three describes the experimental techniques used in this dissertation to measure the reorientational structural dynamics and charge transport properties of the studied ionic liquids. In chapter four, a homologous series of three 1-butyl-3-methylimidazolium based ionic liquids are investigated with the goal of understanding the role that the anion chemical structure plays in controlling the molecular transport mechanism. In chapter five, the influence of nanophase segregation and the presence of long alkyl side chain on the molecular transport mechanism is explored in a homologous series of three tetra-alkylammonium based ionic liquids. Whereas chapters four and five are concerned with aprotic room temperature ionic liquids, chapter six presents studies of the structural dynamics and charge transport properties of a carboxylic acid-tertiary amine based protic ionic liquid. Concluding remarks and a brief outlook are presented in chapter seven.

2. Properties of Molecular and Ionic Liquids

2.1. Dynamics in Supercooled Liquids and the Glass Transition

The general feature that defines all glass forming materials is the capability to be supercooled below the thermodynamic melting point T_m.[4-6] Nearly all liquids can be supercooled to some extent and avoid crystallization.[7] Not all liquids, however, may be supercooled deeply enough to reach the temperature where the rate of cooling becomes faster than the rate of molecular motion. At this temperature T_g, the liquid falls out of equilibrium because the constituent molecules are no longer able to rearrange fast enough to reach the newly imposed ground state. This kinetic trapping process is called the glass transition.[4-8]

The ease with which a liquid may reach and remain in the metastable supercooled state depends on several factors such as chemical structure, local symmetry, and the type of intermolecular interactions present in the liquid.[8, 9] The most common types of liquids that can be easily supercooled are organic molecules with dominant hydrogen bonds such as glycerol, inorganic molecular liquids with strong covalent bonds such as silica, and asymmetric molecular liquids exhibiting Van der Waals interactions such as ortho-terphenyl.[7] The room temperature ionic liquids that will be studied in this dissertation are also stable in the supercooled liquid state and can be considered "good glass-formers". The reasons as to why some liquids are good glass-formers are still not well understood. A simple, qualitative hypothesis is that the locally preferred ordering of neighbor molecules is not compatible with the order that is favored by the long range crystalline state. This concept of competition between local and long range order is an essential part of the theories of glass transition proposed by Tanaka (Two-order parameter model)[10, 11] and Kivelson (Frustration limited domain theory).[12, 13] Using this picture we can qualitatively understand that molten salts (e.g. NaCl), due to the high degree of ionic symmetry, possess a

correspondingly large compatibility between local and long range order and are very unstable in the supercooled liquid state. Room temperature ionic liquids, on the other hand, generally consist of large, asymmetric, and charge delocalized cations, while the anion is usually smaller with different structural and electrostatic symmetry.[14] The intrinsic molecular incompatibility of ionic liquids frustrates the crystal lattice and results in a highly stable supercooled liquid. It is thus critical to understand how the chemical structure influences the physicochemical properties of glass forming liquids, as it is perhaps the most crucial variable in determining the unique qualities of these materials.

2.1.1. Non-Arrhenius structural dynamics and "fragility"

Upon cooling toward the glass transition temperature, dramatic changes in the molecular dynamics (e.g. viscosity, translational diffusion rate, molecular rotation rate, and ionic conductivity) of a glass forming liquid occur. For a prototypical glass forming liquid, the viscosity increases by an extraordinary fourteen orders of magnitude when the liquid is cooled from the high temperature regime down to the glass transition.[8] Most liquids near the glass transition would take years to measurably flow, and the liquid at or below the glass transition is a solid for all practical purposes. A key distinction to make is that unlike liquids that undergo crystallization or some other type of thermodynamic phase transition, supercooled liquids do not exhibit any discontinuous changes in the dynamical properties as the melting point or glass transition temperature is traversed. Instead, they exhibit a continuous increase of their viscosity, etc. with decreasing temperature.[4, 8]

The most common way of presenting dynamic relaxation data of glass forming liquids are on the so called "Angell plot", in which the viscosity, relaxation time, etc. of a specific liquid is plotted as a function of relative temperature T_g/T.[15] As can be seen in Fig. 2.1, supercooled

liquids approach their respective glass transition temperatures on their own unique kinetic pathway. This pathway is non-Arrhenius for practically all glass forming liquids, with the notable exceptions of the covalent network oxides. On the plot in Fig. 2.1, the Arrhenius law[16]

$$\tau_\alpha = \tau_0 \exp(\frac{E_A}{k_B T}) \tag{2.1}$$

where τ_α is the characteristic structural relaxation time (or viscosity, diffusion rate, etc.), τ_0 is the relaxation attempt time, E_A is the characteristic activation energy, and k_B is Boltzmann's constant, would appear as a straight line with a slope proportional to the characteristic activation energy E_A required to overcome the potential energy barrier against molecular motion.

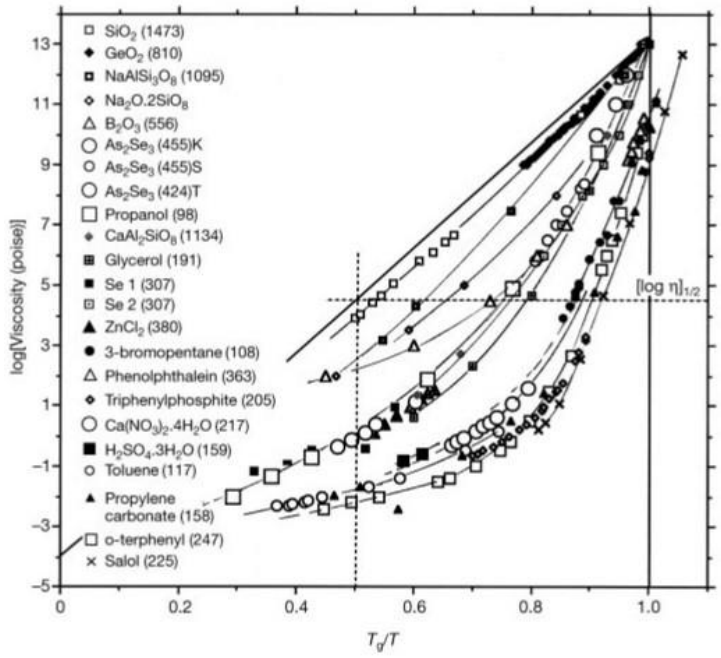

Figure 2.1. "Angell plot" of shear viscosity as a function of T_g-scaled inverse temperature for several molecular glass forming liquids.[17]

The Arrhenius law describes a kinetic process where the free energy barrier does not depend on temperature, and it was first used to characterize the temperature dependent rate of chemical

reactions.[16] Molecular motion in glass forming liquids clearly does not follow the Arrhenius law (except at temperatures far from T_g), and it can be seen in Fig. 2.1 that the apparent free energy barrier increases as T_g is approached (the derivative of each curve monotonically increases as the temperature decreases toward T_g).

The Vogel-Fulcher-Tammann (VFT) equation[18, 19] is commonly employed to fit measurements of the temperature dependent structural relaxation data of many supercooled liquids, and it will be employed throughout this dissertation. It introduces an additional fit parameter to the Arrhenius equation such that

$$\tau_\alpha = \tau_0 \exp\left(\frac{B}{T-T_0}\right) \tag{2.2}$$

where B and T_0 are empirical fit parameters. The VFT equation fits relaxation data of most glass forming liquids fairly well over a very broad temperature range. One potentially unphysical aspect of it, however, is the equation implies that there exists a finite temperature T_0 where the structural relaxation time in the liquid becomes infinite. It is near this temperature that the so called Kauzmann paradox[20] is postulated to occur in which the extrapolated entropy of the supercooled liquid apparently becomes lower than the entropy of the corresponding crystal. There are some authors who suggest that the Kauzmann paradox is resolved by a thermodynamic phase transition to an ideal glass state near T_0, and that this transition is the underlying cause of viscous slowdown in supercooled liquids.[21, 22] However, the VFT temperature dependence of relaxation times and the Kauzmann paradox remain great puzzles because a phase transition of this kind has never been observed experimentally in prototypical glass forming liquids.[23, 24]

It is seen in Fig. 2.1 that the relaxation times for some of the liquids are much more curved and deviate much more strongly from the Arrhenius law than other glass forming liquids. Angell et al. introduced the concept of fragility in order to quantify this difference.[4, 25] Liquids

that closely follow the Arrhenius temperature dependence and have less curvature in the temperature dependence of structural relaxation are called "strong", while liquids that deviate significantly from Arrhenius temperature dependence are called "fragile". Fragility *m* is determined by calculating the derivative of the relaxation time data in Fig. 2.1 at T_g, where

$$m = \left. \frac{d \log \tau_\alpha}{d\frac{T_g}{T}} \right|_{T=Tg} \tag{2.3}$$

The fragility of the covalent network oxides (eg. SiO_2) is usually in the range $m \approx 20–30$, most small molecule liquids have $m \approx 50–100$ (e.g. glycerol and ortho-terphenyl), while polymeric liquids exhibit a wide range of fragilities with $m \approx 20–200$.[26] The microscopic mechanism responsible for the non-Arrhenius temperature dependence of structural relaxation in supercooled liquids is still not understood, although there are several phenomenological theories which have been developed in an attempt to understand this important property of supercooled liquid dynamics.

One of the most important phenomenological theories describing the temperature dependence of relaxation times in supercooled liquids is the Adam-Gibbs theory.[27] In this theory, a single molecular rearrangement may only occur with the simultaneous, cooperative rearrangement of neighboring molecules. This group of molecules is called the cooperatively rearranging region (CRR). The smallest possible CRR consists of z^* molecules and possesses one additional configurational state to which it may transition. The average time between collective rearrangements within the CRR is then given by

$$\tau = Aexp(\frac{z^* \Delta\mu}{k_B T}) \tag{2.4}$$

where *A* is the rearrangement attempt time, z^* is the number of molecules contained within the CRR, and $\Delta\mu$ is the potential energy barrier per molecule that hinders the cooperative

rearrangement. Thus, the AG theory relates the non-Arrhenius temperature dependence of structural relaxation times to the increasing size of the CRR. The size z^* of the CRR as a function of temperature is directly related to the macroscopic configurational entropy of the supercooled liquid in the AG theory such that

$$z^* = \frac{N_A s_c^*}{S_c} = \frac{N_A k_B ln2}{S_c} \tag{2.5}$$

where N_A is Avogadro's number, s_c^* is the configurational entropy of the smallest possible CRR (which possesses two transition states), and S_c is the macroscopic configurational entropy. The average size of the CRR increases as the supercooled liquid becomes denser, leading to a corresponding decrease in the macroscopic configurational entropy.

Through this theory, it is seen that the precipitous increase in the structural relaxation times and the inherent non-Arrhenius temperature dependence results from a decrease in configurational entropy on approach toward T_g. For liquids of different fragility, the size of the CRR and the corresponding configurational entropy have material specific temperature dependences which are not determined in the AG theory. Yamamuro et al. estimated the temperature dependence of several glass forming liquids by measuring the temperature dependence of the specific heat capacity of these liquids.[28, 29] In this work they found that the size of the CRR z^* for a variety of small molecule glass forming liquids begins from approximately one at temperatures far from T_g and was $z^* \approx 4–8$ at the T_g of these materials.[28, 29] What is surprising about this result is the AG theory predicts that only a very subtle increase in the cooperativity length scale in a glass forming liquid is required to produce the enormous experimentally observed changes in structural relaxation times.

2.1.2. The dynamic crossover

As mentioned previously, the VFT function is often used to fit relaxation data over a broad range of time scales and temperatures. However, the VFT function systematically deviates from the relaxation data measured for many glass forming liquids, indicating that this function only approximately describes the temperature dependence of the structural relaxation process.[30] Further detailed analysis of relaxation data performed by Stickel et al. has shown that in those systems with systematic deviation from single VFT, there is a temperature where the high temperature VFT behavior of structural relaxation transitions to a distinct, low temperature behavior.[31, 32] This is called the dynamic crossover, and it can be seen as the intersection of two straight lines in the so called "Stickel plot" shown in Fig. 2.2.

Goldstein has hypothesized that when the liquid viscosity reaches approximately 1 Pa·s (or $\tau \approx 10^{-8}$ s), molecules in the liquid become so tightly packed that free diffusion becomes hindered, and the molecular transport process as a consequence becomes thermally activated.[33] In the framework of the Mode Coupling Theory (MCT), it is hypothesized that at a certain temperature T_C, the molecular motions in a liquid undergo a kinetic transition from "liquid like" to "solid like" dynamics.[34, 35] MCT describes structural relaxation as a two-step process. On picosecond time scales, molecules execute motions that can be described qualitatively as cage rattling motions. The molecule will escape from its cage of neighbors after a certain waiting time, and this escaping from the cage is the structural relaxation process. The coupling between the fast, cage rattling motions and the cage escape process causes the exponential slowdown of the structural dynamics according to MCT. The structural relaxation time is predicted to have a critical power law dependence on temperature, $\tau_\alpha \propto (T - T_C)^{-\gamma}$, where the relaxation time diverges at the critical temperature, T_c. It has been found that the critical temperatures estimated

in the framework of MCT and the dynamic crossover temperature estimated from the Stickel derivative analysis of relaxation times are found to be very similar in most materials.[36] It should be noted, however, that the diverging relaxation time of MCT is a theoretical construct and does not occur in real glass forming liquids. Although, some authors have suggested that this underlying dynamic transition is connected to the change of the temperature dependence of structural relaxation time which occurs at the dynamic crossover temperature.[37]

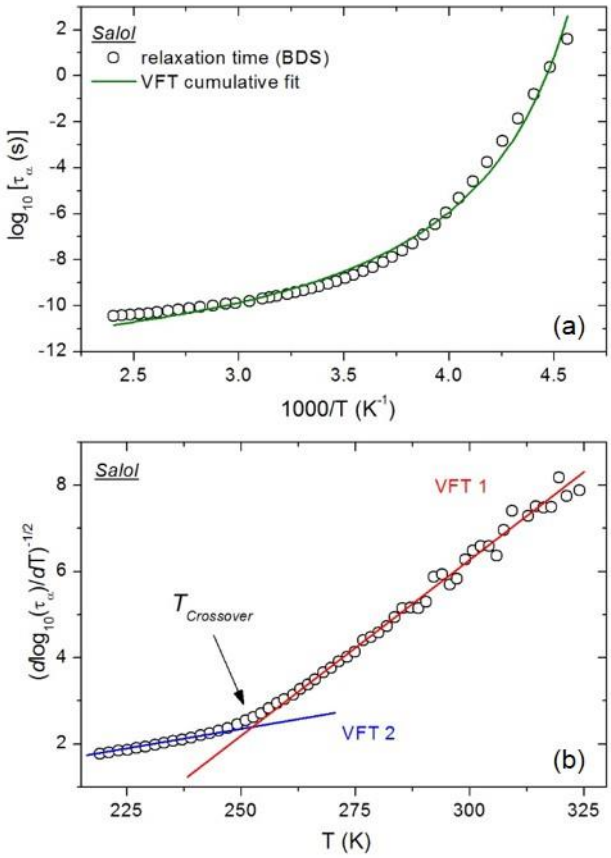

Figure 2.2. (a) Structural relaxation times of the molecular liquid salol measured via broadband dielectric spectroscopy are shown fit with the Vogel-Fulcher-Tammann equation. (b) The "Stickel" derivative of the relaxation times of salol reveals that there are two distinct dynamical regimes which require fitting with different VFT functions. Data taken from ref. [30].

At temperatures near the dynamic crossover temperature, it has been observed that the translational and rotational molecular motions begin to decouple from one another, and it is also at this temperature that secondary relaxation processes (the Johari-Goldstein relaxation) visibly break away from the main structural relaxation process.[38, 39] The dynamic crossover temperature may be just as important as the glass transition temperature because it is interconnected with many important experimental phenomena of supercooled liquids. It is thus critical to develop a thorough understanding of the dynamic crossover for all types of supercooled liquids. Nonetheless, there is still no complete explanation for why the structural dynamics change at this specific temperature for so many supercooled liquids.

2.1.3. Stretched exponential structural relaxation and dynamical heterogeneity

One of the distinctive features of the structural relaxation process in glass forming liquids is that when experimentally measured, it generally occurs with a non-exponential time dependence (or has a broad spectral distribution in frequency).[7, 40] The Kohlrausch-William-Watts (KWW) function[41]

$$\varphi = \exp(-\left(\frac{t}{\tau_{KWW}}\right)^{\beta_{KWW}}) \tag{2.6}$$

where β_{KWW} and τ_{KWW} are the characteristic stretching parameter and relaxation time, is usually employed to model the non-exponentiality when fitting density correlation functions measured via inelastic neutron scattering or orientational correlation functions measured via quasielastic light scattering. In a dilute suspension of non-interacting Brownian particles, these correlation functions which describe the translational and rotational motion of the particles will decay with a purely exponential form (i.e. $\beta_{KWW} = 1$).[42] As will be seen in this dissertation, it is very rare for a supercooled liquid to exhibit non-exponential structural relaxation, although there are some interesting cases where this type of relaxation behavior may occur.

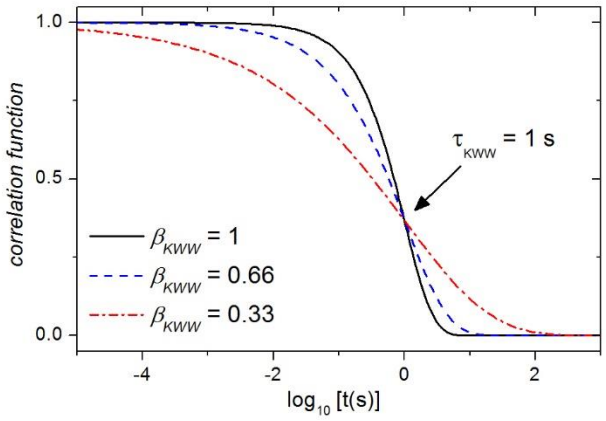

Figure 2.3. Simulated stretched exponential relaxation functions with the same characteristic relaxation time and different degrees of non-exponentiality.

There are two opposing explanations for why the structural relaxation process can appear stretched when measured experimentally, and they are referred to as the homogenous and heterogeneous scenario.[38, 43] In an experiment where measurements of structural relaxation are performed, a large ensemble of molecules is probed, and their individual structural relaxation processes are inherently averaged. The time dependent macroscopic correlation function can be generally written in the heterogeneous scenario as

$$\varphi(t) = \int g(\tau) \exp\left(-\frac{t}{\tau}\right) d\tau \tag{2.7}$$

where $g(\tau)$ is a probability density of individual molecular relaxation times.[44] This interpretation of stretched exponential relaxation implies that all of the molecules participating in a structural relaxation event do so in a purely exponential (i.e. diffusive) fashion, and each molecule executing structural relaxation has its own inherent relaxation time which can be significantly different from that of a neighboring molecule. The measured stretching exponent in the heterogeneous scenario becomes less than one (pure exponential) when the distribution of relaxation times broadens. Thus, it has been proposed that the stretching parameter from

experimentally measured correlation functions may be a quantification of the degree of dynamical heterogeneity in a liquid.

In the homogeneous scenario, on the other hand, all molecules participating in structural relaxation do so in an intrinsically non-exponential fashion, and it occurs on a time scale that is shared by all participating molecules. The nonexponentiality, in this case, may arise from strong intermolecular interactions. These interactions may lead to a hierarchical temporal pathway of the structural relaxation process, wherein molecular motion at times prior to the moment of structural relaxation govern, to some degree, how the present structural relaxation event will occur.[45, 46] This type of non-Markovian dynamical picture leads to nonexponential structural relaxation, and it is similar to the concept of the Mode Coupling Theory.

There has been a significant effort over the last several decades to determine whether the homogenous or heterogeneous scenario is responsible for non-exponential structural relaxation in glass forming liquids. Experiments have shown that structural relaxation may be intrinsically non-exponential to some degree,[47, 48] while considerable dynamical heterogeneity may also exist in the liquid and lead to a deviation from pure exponential behavior.[49, 50] However, the physical reasons behind dynamical heterogeneity and how it affects properties of supercooled liquids are still lacking. Several theoretical and simulation studies have been performed in an attempt to identify and characterize the role that dynamical heterogeneity plays in controlling the viscous slowdown of glass forming liquids. A liquid is dynamically heterogeneous when the molecules of the liquid have a distribution of mobilities, where some of the molecules are essentially immobile on a certain observation time scale, while other molecules are highly mobile on this same time scale. This distribution of mobilities is readily observed in computer simulations of glass forming liquids, and a representative image of dynamical heterogeneity observed in a

simulated liquid, is shown in Fig. 2.4.[46] There are experimental methods such as 4D NMR,[50] non-resonant hole burning spectroscopy,[51] and optical photo bleaching experiments[52, 53] which have shown that a distribution of relaxation times does exist in a glass forming liquid. However, no experimental techniques are currently available to directly probe the dynamical heterogeneity in glass forming liquids.

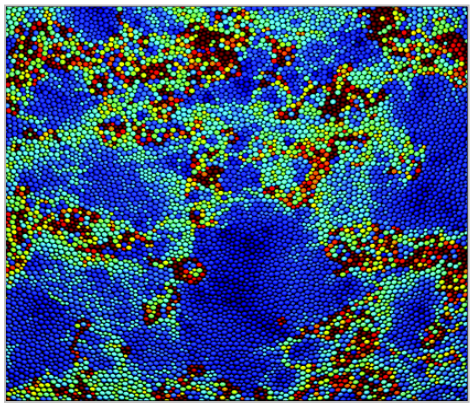

Figure 2.4. Mobility heat-map from a computer simulation of a model supercooled liquid of spherical particles. The blue particles are those which have not moved during a certain time step Δt, while the red particles are those which have moved more than one particle diameter. As is seen, there is a very wide distribution of particle mobilities.[46]

The existence of dynamical heterogeneity in supercooled liquids is often invoked to account for the experimentally observed decoupling of translational and rotational molecular motion in supercooled liquids as the glass transition is approached. This translation-rotation decoupling is also referred to as the violation of Stokes-Einstein (SE) and Debye-Stokes-Einstein (DSE) relations.[38, 54] The Stokes-Einstein (SE) relation connects the translational diffusion of Brownian particles to the viscosity of a surrounding medium

$$D_T = \frac{k_B T}{6\pi\eta r} \tag{2.8}$$

where η is the shear viscosity of the medium and r is the hydrodynamic radius of the diffusing object.[55] The Debye-Stokes-Einstein relation (DSE)[56] similarly describes the relationship between rotational diffusion of Brownian particles and the viscosity of the medium

$$D_R = {\tau_\alpha}^{-1} = \frac{k_B T}{8\pi\eta r^3} \tag{2.9}$$

When the SE and DSE equations are combined, it is readily shown that the above hydrodynamic relations predict that the product $D_T \cdot \tau_\alpha$ is temperature independent.

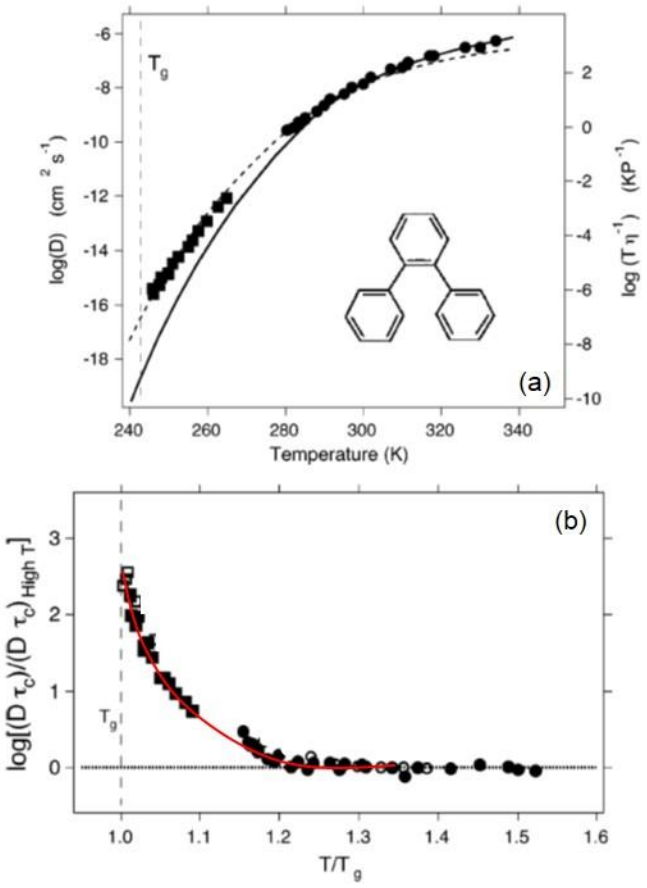

Figure 2.5. (a) Translational diffusion coefficient (solid symbols) and temperature-scaled viscosity (solid line) of the glass forming liquid ortho-terphenyl (OTP) is plotted as a function of temperature. It can be seen that these quantities deviate from one another as T_g is approached. (b) The normalized product $D_T \cdot \tau_\alpha$ for the same measured OTP is shown plotted against T_g-scaled temperature. It can be seen that the molecular dynamics no longer follow the SE/DSE relations near T_g.[57]

The SE and DSE relations have been found to hold at high temperatures above the dynamic crossover temperature T_c, but they breakdown at temperatures close to T_g.[38] For some glass forming liquids (Fig. 2.5), such as ortho-terphenyl, the translational diffusion rate is nearly two orders of magnitude faster than the corresponding structural relaxation time at T_g.[57] Most of the proposed explanations for the violation of the SE and DSE relations, as mentioned previously, account for this unique behavior by attributing it to the dynamical heterogeneity in a supercooled liquid. It is hypothesized that in the high temperature regime, near the normal melting point of the liquid and above, the distribution of structural relaxation times is narrow and the degree of dynamical heterogeneity is small. It is in this regime where the rotational and translational motions in nearly all glass formers are strongly coupled. As the liquid is cooled, dynamical heterogeneity becomes more prominent, and molecules that were once dynamically independent become correlated.

As a result of the increasingly pronounced dynamical heterogeneity, the distribution of structural relaxation times broadens, and the measured diffusion coefficient or structural relaxation time sample this distribution in different ways. The diffusion coefficient can be considered an average over all inverse relaxation times in the liquid $\langle \tau^{-1} \rangle$, while the structural relaxation is an average over all relaxation times in the liquid $\langle \tau \rangle$.[58] The gap between the measured diffusion coefficient, which is heavily weighted by the fast components of the relaxation time distribution, and the measured structural relaxation time, which is heavily weighted by the slow components of the distribution, thus becomes increasingly pronounced as the glass transition is approached specifically because of the effects of dynamical heterogeneity on the relaxation time distribution. The dynamical heterogeneity hypothesis intrinsically connects the width of the relaxation time distribution to the degree of decoupling, i.e. the ratio of

translational and rotational diffusion coefficients. In order to test the dynamical heterogeneity hypothesis, it is necessary to characterize the translational and rotational diffusion coefficients, as well as the relaxation time distribution (i.e. the nonexponentiality parameter). While much research effort has been devoted to classifying and understanding the effects of dynamical heterogeneity on supercooled liquid dynamics, it remains unclear if dynamical heterogeneity is the underlying cause of the unique properties of supercooled liquids, or if it is a generic effect of the subtle changes that the supercooled liquid experiences upon approaching the glass transition.[59]

2.2. Room Temperature Ionic Liquids

2.2.1. Introduction to ionic liquids and their applications

Having discussed the properties and phenomenology of glass forming liquids in general, this next section will be devoted to defining the subset of materials known as room temperature ionic liquids (RTILs or ILs). While not strictly defined, it is generally accepted that RTILs are salts which are liquid at or below 100°C.[1, 14] These materials usually consist of large, asymmetric, and charge delocalized cations that are paired with organic or inorganic anions having significantly different chemical structure and symmetry.[2] Whereas simple molten salts possess a large crystal lattice energy due to the highly symmetrical counter-ion chemical structures, the incompatibility of the chemical structures in ILs frustrates the crystal lattice and dramatically reduces the melting temperature. As an example, the normal melting temperature of sodium chloride is T_m = 801°C,[60] while the normal melting temperature of the prototypical room temperature ionic liquid 1-butyl-3-methylimidazolium bis(trifluoromethylsulfonyl)imide [BMIM][NTF_2] is T_m = -1°C.[61] Not only does the structural complexity lead to lower melting temperatures for these materials, but many ILs are also highly stable in the supercooled liquid

phase with characteristic glass transition temperatures commonly found in the range of 180–220 K. As can be seen in Fig 2.6, the glass transition temperature increases weakly with increasing molecular volume for a wide variety of ionic liquids (the alkali inorganic salts are not room temperature ILs and clearly exhibit different behavior).

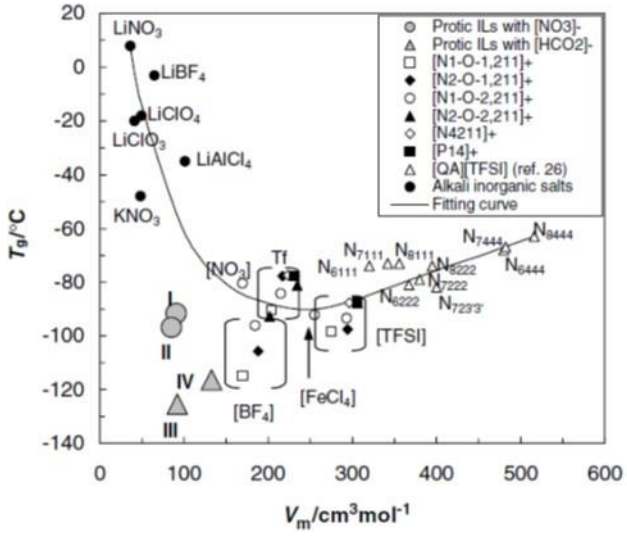

Figure 2.6. The glass transition temperature T_g is shown plotted as a function of molecular volume for a variety of ionic liquids. Excluding the inorganic salts, T_g increases weakly with increasing molecular volume.[62]

The wide variety of counterion pairs that can be formed from the ions shown in Fig. 2.7 represent the subset of ILs known as aprotic ionic liquids (AIL). In the AILs, charge is permanently fixed to the cation via covalent attachment of molecular side groups to form ammonium and phosphonium functionalities (there are other types of AILs such as sulfonium, but those shown in Fig. 2.7 are most common). The anions are usually formed through the deprotonation of "super-acid" molecules such as $HNTF_2$. It is estimated that there are

approximately 10^6 ILs that could be synthesized from all known counterion combinations, and it is because of this diversity that many people have come to refer to ILs as "designer solvents".[3]

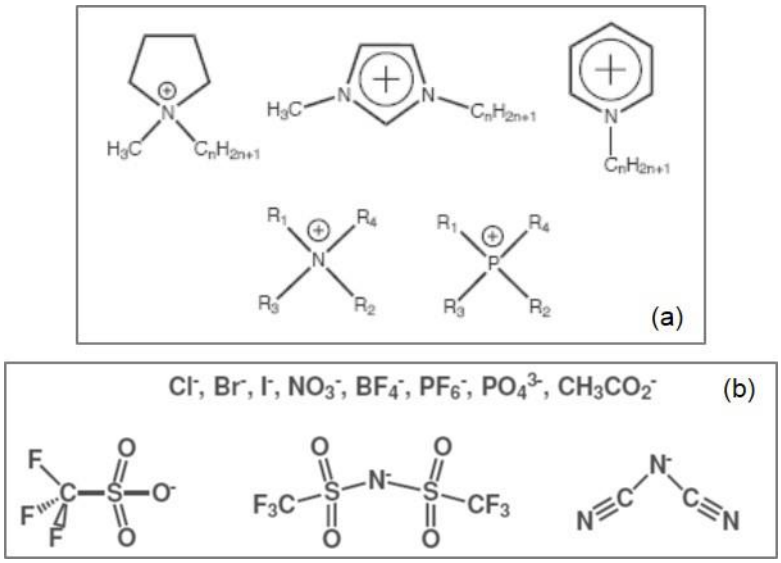

Figure 2.7. Common cations (a) and anions (b) constituting the aprotic ionic liquids.[14]

Aprotic ionic liquids have many unique physical properties which make them important materials for technological applications. Due to their low vapor pressures and high thermal decomposition temperatures, AILs are being explored for use as non-volatile and recyclable "green" reaction media, as heat transfer fluids in solar-thermal energy plants, as novel industrial lubricants, and also in carbon capture and sequestration technologies.[63-66] Furthermore, many AILs have intrinsically high ionic conductivities and can withstand relatively high voltages compared to other electrolytic media, such as water (1.2 V), before electrochemical breakdown occurs.[66, 67] These properties make ILs especially promising candidates for a range of electrochemical applications.

For example, current lithium-ion battery technology employs electrolytes which consist of hazardous salts (e.g. $LiPF_6$) dissolved in volatile and potentially reactive solvents (ethylene carbonate, dimethoxyethane).[63] If the temperature of the battery becomes too high, there is a risk for thermal runaway to occur, in which the electrode and electrolyte undergo exothermic chemical reaction. During this reaction, the pressure inside the battery increases dramatically, and due to the flammability of the electrolyte, the battery may catch fire and explode. This risk could be abated by using ionic liquids in place of the organic solvents because of their low vapor pressure and flammability.[2] Conversely, if the temperature of the battery becomes too low, the electrolyte may become too viscous (or potentially even crystallize) to allow ions to diffuse fast enough to provide the desired power. AILs may be used to extend the usable temperature range of batteries to lower temperatures.

Another important class of ionic liquids are the protic ionic liquids (PIL),[62, 68, 69] which are formed due to the reversible transfer of protons between a Brønsted acid and Brønsted base such that

$$HA + B \rightleftarrows A^- + HB^+ \tag{2.9}$$

Depending on the degree of free energy reduction due to proton transfer, the equilibrium of this reaction may lie far to the right resulting in a highly ionized PIL, or it may lie far to the left resulting in poor ionization and a mixture of neutral and ionized acid/base moieties.[70] Ethylammonium nitrate (EAN), first synthesized by Paul Walden in 1914, is one of the earliest examples of a protic ionic liquid—one in which the equilibrium of eq. 2.9 lies far to the right.[71] As a result of the large degree of ionicity, the boiling point of this PIL is quite high at T_b = 240˚C, and the conductivity is also high with $\sigma_{dc} = 2\times10^{-3}$ S/cm at room temperature.[72]

PILs have an extremely large versatility and an enormous potential for technological applications due to the relative ease of synthesis, as well as the ability to tune the physicochemical properties according to the variability of the proton transfer reaction. Many active pharmaceutical ingredients, for example, are delivered as protic salts, and the ability to control the ionicity by varying the acid and base chemical structures could enhance solubility and cell permeation rates.[73, 74] Another important application of PILs is as the electrolyte of anhydrous polymer membrane fuel cells.[69, 75] Current fuel cell technology employs polymer membranes electrolytes, such as Nafion, which are humidified with water to enhance proton conductivity between the cathode and anode. While the intrinsic proton conductivity of these humidified membranes are high (10^{-2} S/cm), fuel cells must operate at temperatures usually above the boiling point of water.[76] Angell et al. have shown that protic ionic liquids, such as protic ammonium salts and their eutectic mixtures, have intrinsically high proton conductivity and are thermally stable at temperatures above 100°C.[77] Furthermore, these electrolytes have the potential to be used in simpler cell designs and with a wider variety of catalysts than aqueous electrolytes.

2.2.2. Charge and mass transport in ionic liquids

While there are certainly many important technological applications of ILs, it is critical to develop a thorough and predictive understanding of the physicochemical properties of these materials in order to utilize them properly and to their full potential. To this end, numerous studies of the charge and mass transport properties of ILs have been performed in an attempt to establish the chemical structure–physical properties relationships in these materials.[78-81] One of the most well characterized properties of the room temperature ionic liquids is the temperature dependent ionic conductivity σ_{dc}. The conductivity of an electrolyte or ionic liquid is defined as

$$\sigma_{dc} = \sum_i n_i \mu_i q_i \tag{2.10}$$

where the summation is over the distinct populations of charge carriers in the liquid, n_i is the number density of free charge carriers, μ_i is the electrical mobility, and q_i is the electrical charge of the ions.[82] According to the Einstein relation, which relates the electrical mobility to the self-diffusion coefficient, eq. 2.10 can be reformulated such that

$$\sigma_{dc} = \frac{(n_+ D_+ q_+^2 + n_- D_- q_-^2)}{k_B T} \tag{2.11}$$

where $D_{+,-}$ is the self-diffusion coefficient of the positive and negative ions, respectively.[55] In this classical picture, electrical conductivity in ionic liquids is controlled by the Brownian-like translational diffusion of ions.

Tokuda et al. were among the first to systematically study the charge transport properties and the relationship between ionic self-diffusion coefficients and dc conductivity in aprotic ionic liquids.[83-86] In their studies, the self-diffusion coefficients of a series of ionic liquids with the same cation $[BMIM]^+$ and different anions were experimentally determined using pulsed field gradient nuclear magnetic resonance (PFG NMR). The authors found systematic differences in the diffusion coefficients of the studied ionic liquids, as seen in Fig. 2.8, indicating that the chemical structure of the anion plays an important role in governing both cationic and anionic mobility. Interestingly, it was also found that the counterions of a given IL have nearly identical self-diffusion coefficients at all measured temperatures—independent of ionic size.

According to eq 2.11, both the self-diffusion coefficients and the concentration of free ions determine the conductivity of the ionic liquid. Using measurements of dc conductivity in conjunction with the measured diffusion coefficients, Tokuda et al. found that the mole fraction of free ions $f = \frac{n_{free}}{n_{tot}}$ in the family of imidazolium based ILs was lower than unity with f = 0.5–0.7, indicating that a significant degree of long-lived ion association occurs in these ILs.[83-86]

Their studies were some of the first to quantitatively determine the ionicity of a wide variety of ILs, and they explicitly demonstrated that most ILs are not ideal, completely dissociated electrolytes. The exact mechanism of ion association in ILs and the physical/chemical reasons behind it remain poorly understood. Some authors have claimed that counter-ions may form discrete pairs or well defined aggregate clusters, and this limits the mole fraction of free ions.[87] This concept has been challanged based on structural studies of several ionic liquids via XRD and MD simulation,[88, 89] as well as dielectric spectroscopy studies,[90] which suggest instead that the ionic solvation environment in most ionic liquids is relatively symmetrical. There are cases, however, where large hydrophobic side groups may disrupt this symmetry and lead to ionic aggregation.

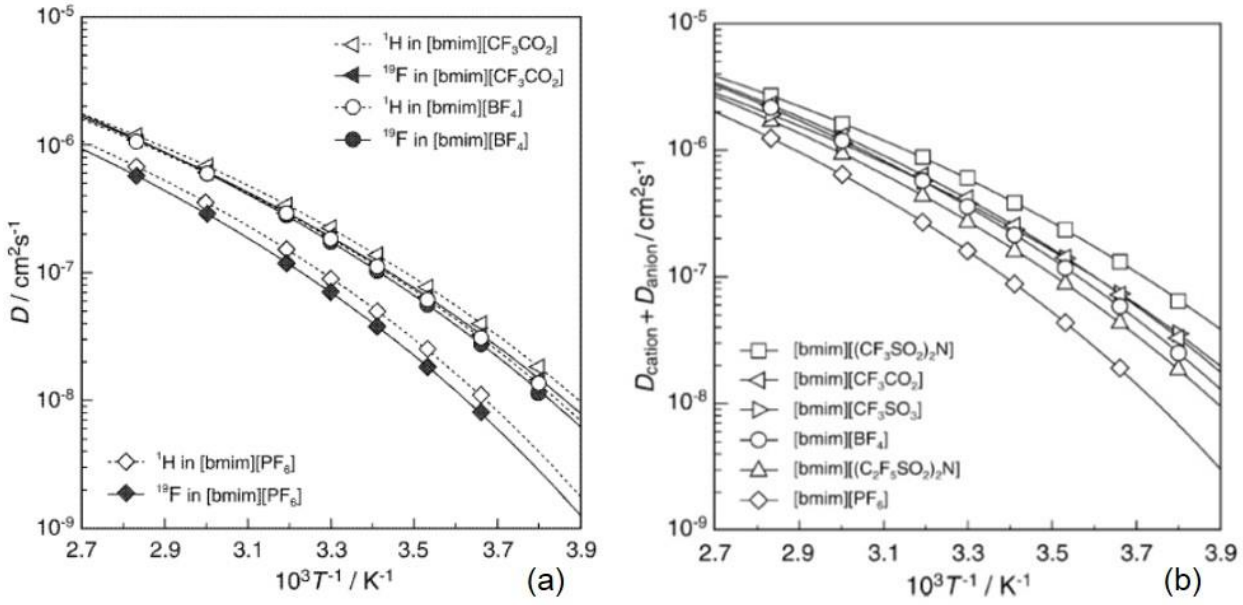

Figure 2.8. Diffusion coefficients for a set of imidazolium based ionic liquids as determined via pulsed field gradient nuclear magnetic resonance (PFG NMR). Pane (a) shows the cationic (^1H) and anionic (^{19}F) diffusion coefficients individually, and pane (b) shows the total diffusion coefficients.[83]

One of the major drawbacks of PFG NMR is that it can only be used to determine diffusions coefficients in the high temperature and highly fluid regime. Since many ILs can be supercooled, it is important to characterize the transport properties of these materials in the highly viscous state as well. To this end, Sangoro et al. have performed several studies of the dielectric and charge transport properties for a wide variety of ionic liquids.[91] In addition to developing a technique to calculate ion diffusion coefficients and free ion concentrations from dielectric relaxation data over a broad temperature range which extends from T_m down to T_g (a method which will be employed throughout this dissertation and described in Ch. 4), the authors also characterized the complex dielectric permittivity of many ionic liquids over a broad frequency range.

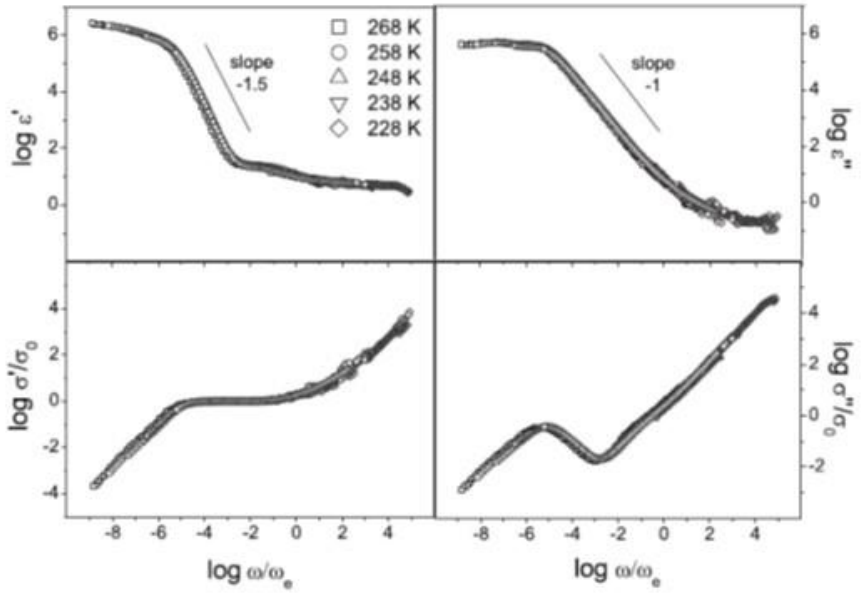

Figure 2.9. Universal scaling of the complex dielectric permittivity and conductivity in the ionic liquid 1-butyl-3-methylimidazolium tetrafluoroborate [BMIM][BF₄].[90]

Through their studies, the authors found that the complex dielectric permittivity measured under different thermal conditions in the same IL, as well as for different species of ILs, exhibited a quasi-universality.[92] This universality was suggested to arise from the fact that the underlying mechanism of charge transport, which they suggest is Brownian-like hopping of ions in a disordered liquid matrix, is identical regardless of the specifics of the ionic liquid chemical structure. Recent studies have shown that this universality is only an approximation, however, and there certainly are different aspects of the charge transport mechanism in these ILs which may be influenced by the ionic chemical structure.[93]

The work of Tokuda et al.[83-86] and Sangoro et al.[90-92] demonstrate that the dominant variable determining the dc conductivity of an ionic liquid is the translational ion mobility (and the corresponding viscosity), while the concentration of free ions plays only a much smaller role. The connection between the conductivity of an ionic melt and the viscosity is not a new idea, however, and it was first proposed by Walden in 1906 that the molar conductivity of a dilute electrolyte is linearly proportional to the viscosity such that $\Lambda \cdot \eta = Const$ ($\Lambda = \sigma_0/n$ is the molar conductivity, n is the number density of ions, and η is the shear viscosity).[94] It has been found that the so-called Walden rule is well obeyed in many neat aprotic ionic liquids in the relatively fluid state.[62] For some aprotic ionic liquids with large aliphatic side groups, however, the calculated Walden product falls well below what would be expected for 100% ion dissociation (the ideal Walden line).[95] These liquids are referred to as sub-ionic, and their less-than ideal ion transport properties may be connected to enhanced ion association, hindered free ion mobility, or a combination of both factors. Many protic ionic liquids have also been found to lie far below the ideal Walden line, and this is generally attributed to incomplete proton transfer between Brønsted acid and Brønsted base.[96] As is seen in Fig. 2.10, however, there are some

liquids which lie above the ideal line, and they are referred to as "super-ionic" or "super-protonic" liquids.

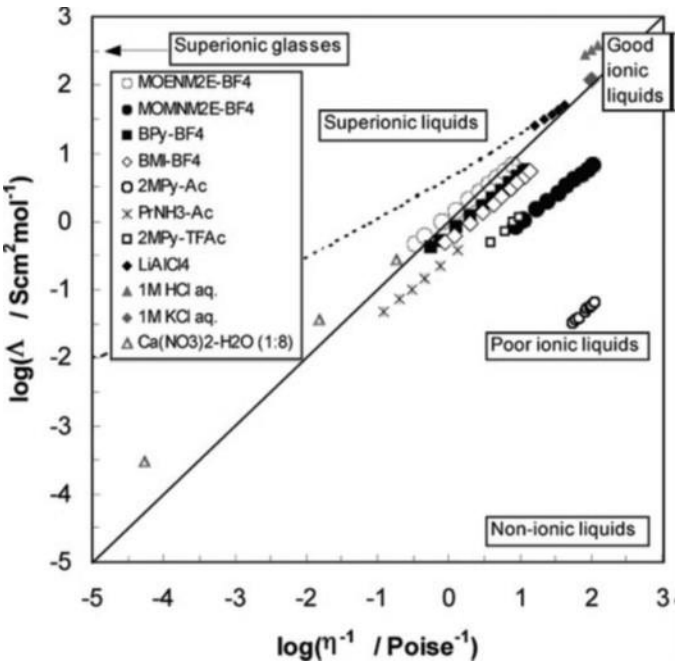

Figure 2.10. "Walden Plot" showing the relationship between molar conductivity and fluidity in a variety of aprotic and protic ionic liquids.[62]

In the classical Walden picture, the translational mobility of ions is directly coupled to the liquid viscosity and molecular reorientation rates via the Stokes-Einstein and Debye-Stokes-Einstein relations. Interestingly, it has been reported based on tracer diffusion measurements[97] and PFG NMR measurements[98] that these classical hydrodynamic relations are not necessarily obeyed in room temperature ionic liquids. This is corroborated by recent studies of several aprotic ionic liquids which have shown that the Walden rule is not obeyed in many ionic liquids near T_g, and instead a fractional Walden rule $\Lambda \cdot \eta^{\gamma} = Const$ must be applied to describe the relationship between viscosity and conductivity.[99] The fractional Walden rule behavior observed

in ionic liquids has been hypothesized to be connected to the amphiphilicity of the ions, which may cause strongly heterogeneous chemical environments to form in the liquid matrix.[14]

It is not necessary, however, for a glass forming liquid to possess chemical heterogeneity to exhibit anomalous diffusion, and this is actually a common phenomenon of supercooled liquid dynamics (as shown for ortho-terphenyl in section 2.1.3.). It has been shown for the ionic melt Ca-K-NO_3 (CKN), for example, that ionic conductivity is enhanced relative to structural relaxation by nearly three orders of magnitude near T_g.[93] Decoupling of ionic conductivity from viscosity has also been observed in the ionic liquid [BMIM][PF_6], although the magnitude of the effect is much smaller than for CKN.[100, 101] Unfortunately, there are exceedingly few detailed experimental studies of structural relaxation in room temperature ionic liquids, and this greatly limits our understanding of the relationship between ion transport and structural dynamics in ionic liquids. It is a primary goal of this dissertation to contribute to the understanding of these properties and the relationship between glassy dynamics and charge transport in ionic liquids.

2.2.3. Structural heterogeneity in ionic liquids

Many of the constituent ions comprising ionic liquids are complex and exhibit pronounced chemical heterogeneity. Aliphatic side groups, for example, are commonly bonded to the highly polar cations to disrupt the molecular symmetry and lower the electrostatic friction between counterions. While this generally reduces the melting point of the ionic liquid and stabilizes it against crystallization in the supercooled liquid state, the presence of hydrophobic alkyl tails in the ionic matrix leads to strongly pronounced compositional and structural heterogeneity.[102]

Ionic liquids have pronounced nanoscale structure as a result of the formation of charge ordered, counterion solvation shells.[103] In addition to this ubiquitous structural feature, it has also

been shown that hydrophobic alkyl side groups self-aggregate into nanoscopic domains, leading to well-ordered mesoscale structures in the liquid matrix.[104] As the length of the alkyl side chains increase beyond n = 4 carbons, these domains become more coherent and well defined, while also growing moderately in size, with a length scale of approximately 1–2 nm.[102, 105] The increasingly pronounced nanophase segregation can be seen in the evolution of the mesoscale pre-peak in the x-ray diffraction pattern of the series of alkyl-imidazolium chloride based ILs (Fig 2.11). Using atomistic MD simulations, Annapureddy et al. demonstrated that this pre-peak in the static structure factor arises from correlations between anions which are separated by the hydrophobic nanodomains.[106, 107] Wang et al., using atomistic MD simulations, showed that these alkyl nanodomains can even execute slow, collective motions at low enough temperatures.[108]

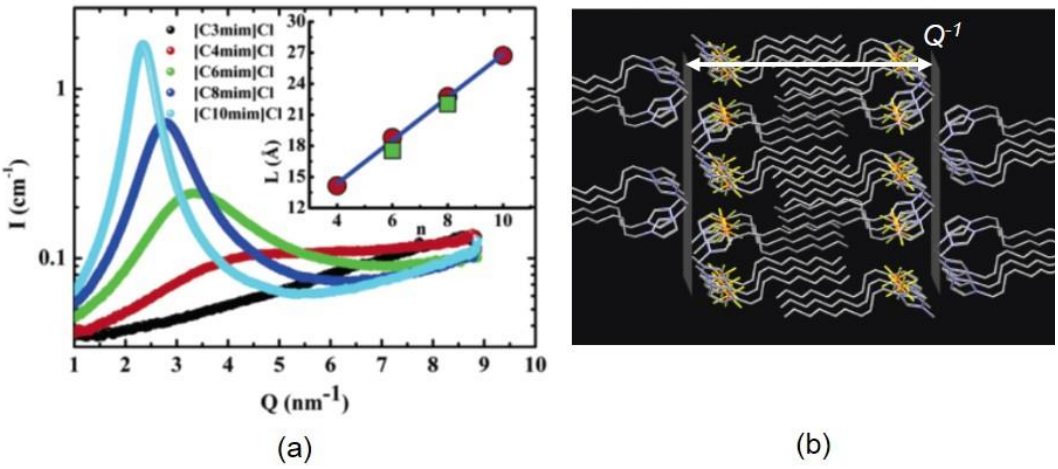

Figure 2.11. (a) The x-ray diffraction pattern of a series of alkylimidazolium based ionic liquids shows a pronounced pre-peak associated with mesoscale structure formation.[102] (b) Classical MD studies of the crystal structure of similar ILs have demonstrated that this pre-peak arises from anion-anion correlations that reflect the length scale l of self-aggregated alkyl chains ($l \approx Q^{-1}$).[107]

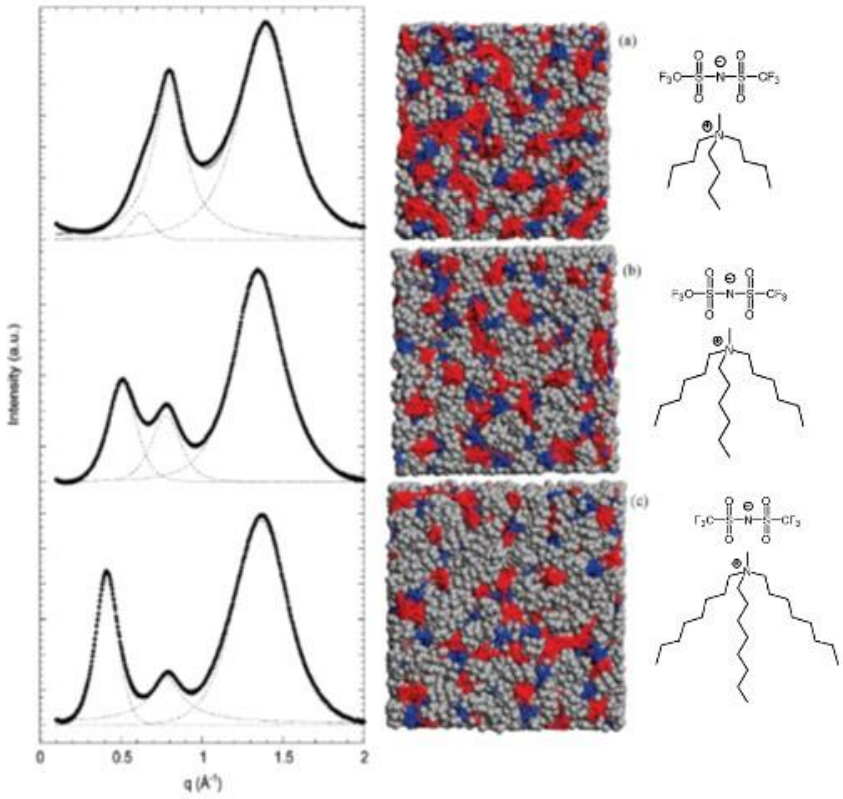

Figure 2.12. X-ray diffraction patterns (left),[109] atomistic MD simulation snapshots (center),[110] and chemical structures (right) are shown for three trialkylmethylammonium bis(trifluoromethylsulfonyl)imide [NXXX1][NTF$_2$] ionic liquids in the liquid state. In addition to the peaks associated with intermolecular ordering (≈ 1.4 Å^{-1}) and charge ordering (≈ 0.8 Å^{-1}), the XRD data exhibit a pre-peak associated with hydrophobically aggregated alkyl domains at ≈ 0.4 Å^{-1}. These alkyl nanodomains are also clearly seen in the MD snapshots (grey = neutral alkyl, red = anion, blue = cation charge center).

The formation of nanophase segregated alkyl-domains is more strongly pronounced in the tetra-alkylammonium and phosphonium based ionic liquids, as seen in Fig 2.12.[111] Similar to the imidazolium based ionic liquids studied by Triolo et al. (Fig 2.11), it has been shown that hydrophobically aggregated nanodomains form in tetra-alkylammonium ILs when the alkyl side chains of the cation become longer than butyl (n = 4).[109] MD simulations of the same series of ammonium ILs have shown that the volume fraction of hydrophobically aggregated domains

begin to percolate the liquid medium when the tails are four carbons long, and they will occupy a majority of the liquid volume when the alkyl tails become sufficiently long ($n \approx 6$).[110]

It is natural to suspect that this strong compositional heterogeneity may have a dramatic impact on the molecular dynamics in these types of ionic liquids. Since the forces in the hydrophobic, alkyl-rich domains are significantly different than in the charge-rich domains, one might expect local molecular diffusion and the rate of chemical reactions in one region to occur on much different timescales than in a region only a few nanometers away. There are, however, exceedingly few experimental studies of the charge transport and structural dynamics in these types of ionic liquids, and the interrelationship between nanophase segregated structures and transport properties of ionic liquids largely remains an unanswered question.

2.3. Ionic Conductivity and the Random Barrier Model

As ions translate through a liquid electrolyte under the influence of an applied electrical field, they not only experience the force of the external field, but they also experience a drag force from counterions moving in the opposing direction. Depending on the concentration of the electrolyte, these ion-ion interactions—which are conceptualized in the Debye-Hückel theory as a test ion traversing a continuum of opposite charge and dielectric constant ε—may significantly decrease the drift velocity of ions and correspondingly reduce the dc conductivity.[112] Using this concept and the hydrodynamic Stokes-Einstein equation, the electrolyte viscosity is seen to be directly connected to the dc conductivity, as was empirically suggested by Paul Walden.

This theoretical construction applies, however, only the steady state conditions in an electrolyte solution, and it is necessary to extend this picture to include time dependent effects. The main approximation of Debye-Hückel theory, i.e. that the counterion solvation environment is a continuum, ignores the fact that this solvent environment takes a certain relaxation time τ in

order to react and rearrange around the moving ion. When an ac external field is applied with oscillation periods much shorter than τ, the ion will move (in response to the field) much more rapidly than the counterion solvation cloud can rearrange. At these frequencies the drag force from the solvation cloud is averaged out, causing the ion to move much faster and the conductivity to increase. On the other hand, at frequencies much lower than τ^{-1}, the solvation cloud is completely in phase with the solvated ion, and the steady state (dc) condition is restored. This relaxation effect, known as the Debye Falkenhagen effect, qualitatively accounts for why the conductivity of an electrolyte increases with increasing frequency.[82, 112]

Despite decades of research, the physical connection between long time ion motion, which is the process behind dc conductivity, and the motion of ions on timescales proportional to or even shorter than the solvent relaxation time τ is not well understood. In an important step toward understanding the ion transport mechanism in disordered materials, Barton, Nakajima and Namikawa discovered that the magnitude of dc conductivity was proportional to the frequency of the characteristic dielectric relaxation peak in a wide variety of glasses, such that

$$\sigma_{DC} = p\varepsilon_0 \Delta\varepsilon \omega_{max} \tag{2.12}$$

where p is a proportionality constant of order one, ε_0 is the vacuum permittivity, $\Delta\varepsilon$ is the dielectric strength, and ω_{max} is the peak frequency.[113] This observation, known as the BNN relation, was a major step forward because it demonstrated that dc and ac conductivity in glasses are due to the same mechanism, and that the dielectric relaxations observed in ionic systems are caused by the translational motion of ions. It has been recently demonstrated that the BNN relation holds for a large variety of room temperature ionic liquids as well.[92]

In order to effectively model the conductivity spectrum in ionic materials, it is necessary to use a theory that treats conduction in a way that, according to the BNN relation, does not

require different ion transport mechanisms for the frequency-dependent ac component and the frequency-independent dc component. To this end, Dyre et al. have developed an analytical model known as the Random Barrier Model (RBM) in which ions in a disordered matrix experience random, spatially varying potential energy barriers which prevent them from hopping to new sites in the matrix.[114-116] The randomness of the potential energy landscape derives from the amorphous nature of liquid or glassy structure. They envision ion hopping as a purely dynamically heterogeneous process, in which a broad distribution of measured relaxation times results from a broad distribution of potential energy barriers. They have analytically determined the form of the frequency dependent conductivity spectrum in the continuous time random walk approximation, such that

$$\sigma^*(\omega) = \sigma_{dc} \frac{\mathrm{i}\omega\tau_e}{ln(1+i\omega\tau_e)} \tag{2.13}$$

In their model, τ_e is the time it takes an ion to surmount the largest free energy barrier and hop to a new site. For all times longer than τ_e, ion motion occurs due to the cumulative result of several distinct ion hopping events, and this is the regime of long-range and long-time dc conductivity.

The RBM has a few important qualities which make it a useful tool when modelling ion conduction in ionic materials. The first is that, in a unifying way, it ascribes both ac and dc conductivity to the same underlying physical process, which is the hopping of ions through the liquid matrix. The second important quality is that it accurately describes the shape of the conductivity spectra that have been experimentally measured in a wide variety of ionic glasses and liquids over a broad frequency range, as seen in Fig. 2.13. The RBM model will be used throughout this dissertation to model the conductivity and permittivity spectra of the room temperature ionic liquids studied herein. The efficacy of this model in describing the dielectric

spectrum of the studied room temperature ionic liquids will be analyzed in detail in the proceeding chapters of this dissertation.

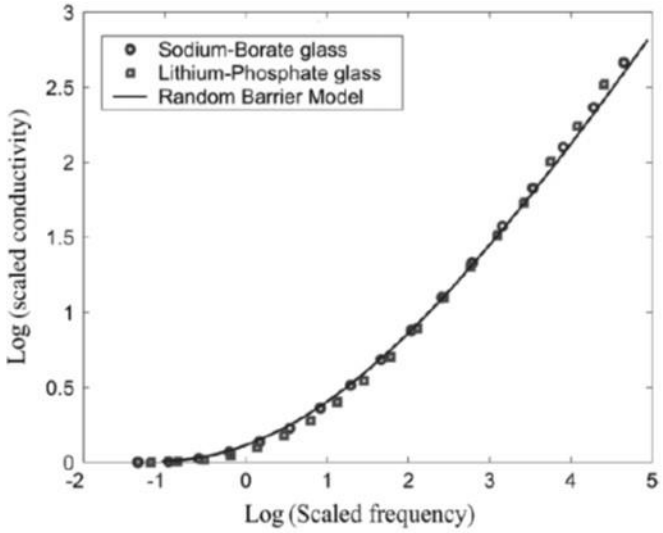

Figure 2.13. Fitting of the Random Barrier Model (eq. 2.13) to the real part of the conductivity spectrum in two glass-forming materials.[117]

3. Experimental Methods

In this section, the theoretical considerations and practical implementation of the experimental techniques employed for these studies will be introduced. Broadband Dielectric Spectroscopy and Quasielastic Light Scattering Spectroscopy were the primary experimental tools used to achieve the research objectives laid out previously, so these two techniques will be discussed in detail. The remaining experimental methods will be discussed only briefly.

3.1. Broadband Dielectric Spectroscopy

Many liquids consist of molecules which, due to their structural asymmetries and electronic charge distributions, possess permanent dipole moments.[118] In the presence of an external electric field, these permanent dipole moments will tend to align along the direction of the field in order to minimize the free energy of the system. This process is called orientational polarization, and the extent to which a field may polarize a dielectric material is determined by the electrical susceptibility of the material under question.[119] The alignment of the permanent dipole moment in the field is necessarily accompanied by a reorientation of the molecule on which the dipole moment resides. Thus, by probing the time dependence of the polarization of dielectric materials due to an external electrical field, one can study ensemble averaged molecular reorientational dynamics. This field of study is known as dielectric spectroscopy. The state of the art dielectric spectroscopy instrumentation currently allows for the study of reorientational dynamics over an extremely large window of time, from nearly picosecond timescales to hours—hence the slightly more ostentatious moniker of *Broadband Dielectric Spectroscopy* (BDS).

3.1.1. Principles of dielectric spectroscopy

The way in which electromagnetic fields interact with a dielectric medium is described by Maxwell's equations,

$$\nabla \times \boldsymbol{E} = -\frac{\partial}{\partial t}\boldsymbol{B} \tag{3.1}$$

$$\nabla \times \boldsymbol{H} = \boldsymbol{j} + \frac{\partial}{\partial t}\boldsymbol{D} \tag{3.2}$$

$$\nabla \cdot \boldsymbol{D} = \rho_f \tag{3.3}$$

$$\nabla \cdot \boldsymbol{B} = 0, \tag{3.4}$$

where $\boldsymbol{E}$ and $\boldsymbol{B}$ are the electric and magnetic field, $\boldsymbol{D}$ is the electric displacement field, $\boldsymbol{H}$ the magnetic induction, $\boldsymbol{j}$ the current density, and ρ_f is the density of free charges in the medium.[120] Throughout this dissertation we will consider only nonmagnetic materials and assume that the magnetic field $\boldsymbol{B}$ and magnetic induction $\boldsymbol{H}$ are equal to zero. When a dielectric material is in the presence of an external electric field $\boldsymbol{E_{ext}}$, the medium polarizes due to a variety of microscopic processes such as electronic polarization, atomic polarization (i.e. vibrational motions), orientational polarization, and charge drift.[121] In a linear, homogenous, and isotropic dielectric medium, the polarization $\boldsymbol{P}$ of the medium, which encompasses all of the above contributions, is proportional to the total electric field in the medium $\boldsymbol{E}$, such that $\boldsymbol{P} = \varepsilon_0 \chi \boldsymbol{E}$, where ε_0 is the permittivity of vacuum and χ is the electric susceptibility. The electric displacement field is equal to the sum of the electric field and polarization, where $\boldsymbol{D} = \varepsilon_0 \boldsymbol{E} + \boldsymbol{P}$. The dielectric permittivity ε (or dielectric constant) of the medium is defined such that $\boldsymbol{D} = \varepsilon \varepsilon_0 \boldsymbol{E}$, and it follows that $\varepsilon = \chi + 1$.

Similar to the relation connecting the electric displacement $\boldsymbol{D}$ to the electric field $\boldsymbol{E}$, Ohm's Law defines the relation between the current density and the electric field through the conductivity σ, such that $\boldsymbol{j} = \sigma \boldsymbol{E}$. If the electric field is periodic in time $\boldsymbol{E} = \boldsymbol{E_0}\exp(-i\omega t)$,

where ω is the angular frequency, one can connect the conductivity and permittivity using eq. (3.2), Ohm's Law, and the relation between displacement and electrical field. Combining these relations, we see that

$$\sigma^* \boldsymbol{E} = -\varepsilon^* \varepsilon_0 \frac{\partial}{\partial t} \boldsymbol{E} = -\varepsilon^* \varepsilon_0 (-i\omega) \boldsymbol{E} \tag{3.5}$$

which leads to the equation $\sigma^*(\omega) = i\omega\varepsilon_0\varepsilon^*(\omega)$. Thus, the real part of the permittivity is proportional to the imaginary part of the conductivity, and vice versa. In this dissertation, experimental measurements of both the complex conductivity and complex permittivity will be routinely presented, and it should be noted that while these two functions may appear quite differently from one another, they still reflect the same underlying properties of the material under study.

The polarization $\boldsymbol{P}$ of a dielectric medium under an applied static electric field is related to the contributions of the constituent molecular permanent dipole moments, such that

$$\boldsymbol{P} = \frac{1}{V} \sum_i \boldsymbol{\mu}_i + \boldsymbol{P}_\infty = n\langle \boldsymbol{\mu} \rangle + \boldsymbol{P}_\infty \tag{3.6}$$

where $\boldsymbol{\mu}$ is the molecular dipole moment, $\boldsymbol{P}_\infty$ is the polarization due to all processes other than dipole orientational polarization (which occur very rapidly relative to orientational polarization), and n is the number density of permanent dipoles. The mean dipole moment ‹$\boldsymbol{\mu}$› can be calculated according to Boltzmann statistics, such that $\langle \boldsymbol{\mu} \rangle = \frac{\mu^2}{3kT} \boldsymbol{E}$, and it follows that $\boldsymbol{P} = \frac{n\mu^2}{3kT} \boldsymbol{E} + \varepsilon_0 \chi_\infty \boldsymbol{E} = \varepsilon_0 \chi \boldsymbol{E}$. According to the relation between susceptibility and permittivity, we find that the dielectric strength $\Delta\varepsilon$ associated with the alignment of dipoles in an applied field is $\Delta\varepsilon = \varepsilon_s - \varepsilon_\infty = \frac{n\mu^2}{3\varepsilon_0 kT}$.[119] This equation is useful to qualitatively understand that the macroscopic properties of the dielectric medium are connected to the molecular dipole moments. In a real dielectric medium, however, dipole-dipole interactions and local field screening effects

(fields induced by the dipoles themselves) have an important contribution to the measured dielectric constant, but these effects are not taken into account in the above equation.

In a molecular liquid, the polarization response to an applied electric field approaches the steady state with a complex functional form, and this time dependent process is called dielectric relaxation. Figure 3.1 shows a qualitative sketch of the polarization response to an applied step-like electric field. In this case, the permittivity is a frequency dependent complex number $\varepsilon^*(\omega) = \varepsilon'(\omega) - i\varepsilon''(\omega)$, where ε′ and ε″ are the real and imaginary parts of the permittivity, respectively. From a qualitative standpoint, ε′ represents the amount of energy that can be reversibly stored in the dielectric medium, while ε″ represents the energy that is dissipated by the medium as it becomes polarized.

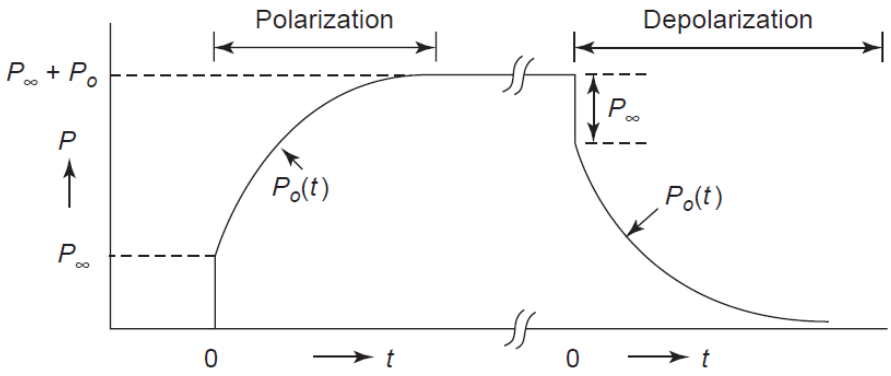

Figure 3.1. Time dependent polarization response of a dielectric medium to a step-like applied electric field.[121]

The response of a dielectric medium to an applied field can be treated in the framework of linear response theory if the applied field is small. For a step change in the applied field like the one seen in Fig. 3.1, the time dependent permittivity (related to orientational polarization) can be straightforwardly calculated, where $\varepsilon(t) = (P(t) - P_\infty)/E(t)\varepsilon_0$. If a sinusoidal field is applied

to the medium, the complex dielectric permittivity is related to the polarization in a manner similar to the static case described previously, where $\varepsilon^*(\omega) = \frac{\boldsymbol{P}(\omega)}{\varepsilon_0 \boldsymbol{E}(\omega)} + 1$.

According to the Fluctuation-Dissipation theorem, the polarization response of a dielectric medium to an infinitesimal applied electric field is related to the autocorrelation function of the transient polarization fluctuations in the absence of an applied field,

$$\varphi(t) = \frac{\langle \Delta P(0) \Delta P(t) \rangle}{\langle \Delta P^2 \rangle} \tag{3.7}$$

where *ΔP(t)* are the spontaneous fluctuations of the polarization (or dielectric constant) about the mean value.[122] The spontaneous polarization fluctuations are related to the complex permittivity spectrum[123]

$$\frac{\varepsilon^*(\omega) - \varepsilon_\infty}{\Delta\varepsilon} = \int_0^\infty \exp(-i\omega t) \left(-\frac{d}{dt} \varphi(t) \right) dt \tag{3.8}$$

It is on the basis of the Fluctuation-Dissipation theorem that we can use the response of a system to a small perturbation to probe the equilibrium fluctuations in the same system, and vice versa.

The simplest model of dielectric relaxation is the case of rotational diffusion of an isolated dipole moment in a viscous medium.[56, 124] In this model, the rate of change of the polarization is proportional to the magnitude of the polarization

$$\frac{dP(t)}{dt} = -\frac{1}{\tau} P(t) \tag{3.9}$$

where $1/\tau$ is the characteristic rotational diffusion rate of the dipole moment. Solving this integral equation for *P(t)* and plugging the result into eq. (3.7), the polarization auto correlation function associated with this reorientational diffusion process is $\varphi(t) = \exp(-\frac{t}{\tau})$. Using this result in eq. (3.8), the complex dielectric function can be analytically determined, such that

$$\varepsilon^*(\omega) = \varepsilon_\infty + \frac{\Delta\varepsilon}{1 + i\omega\tau} \tag{3.10}$$

This model for calculating the complex dielectric spectrum of a rotating dipole moment in an applied field is known as the Debye Model, and the real and imaginary parts of this spectrum are shown in Fig. 3.2. Most real dielectric materials do not exhibit a "Debye-like" relaxation spectrum, but instead have much more complicated spectral shapes which will be discussed in the next section.

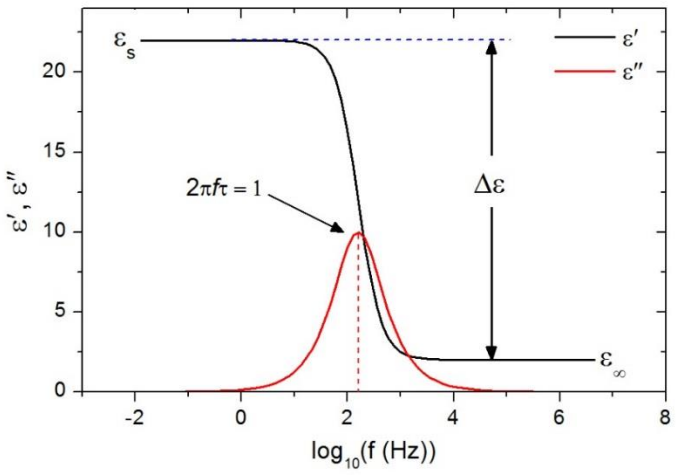

Figure 3.2. Real (ε') and imaginary (ε") parts of the dielectric permittivity corresponding to a Debye Relaxation. In this simulated curve, Δε = 20, ε∞ = 2, and τ = 0.01 s.

3.1.2. Analyzing dielectric spectra of molecular liquids

As mentioned in the previous section, a dielectric medium will polarize in an applied electric field due to processes such as electronic distortions, atomic vibrations, molecular reorientational motions, and charge migration. The characteristic time scales associated with these processes are vastly different (from fractions of picoseconds up to hours), and their contributions to the dielectric spectrum will appear in the corresponding frequency windows. While the timescale is certainly one of the most important parts of the dielectric spectrum, the spectral shape often provides important additional information about the microscopic nature of

the relaxation process being probed. In order to extract this information, we will employ a series of functions which are used to model the dielectric spectrum in molecular liquids. Since this dissertation is concerned primarily with reorientational processes, we will focus on the model functions which describe this type of dielectric relaxation.

The Debye Model is the basis for our understanding of reorientational processes in dielectric spectroscopy. When an isolated dipole executes Brownian rotational diffusion in a viscous medium, the complex dielectric spectrum has the form described by eq. (3.10). In the ε'' representation, the peak in the spectrum is a Lorentzian function with area $\Delta\varepsilon$ and center τ^{-1}. It is rare to observe a Debye like relaxation process for most molecular liquids, however.[125] Usually, the spectrum associated with the dipolar reorientation process is significantly broadened (primarily on the high frequency side of the maximum), and there are three major model functions (known as the Cole-Cole, Cole-Davidson, and Havriliak-Negami functions) which have been derived to fit the dielectric spectrum of these materials.[119] These model functions are all phenomenological generalizations of the Debye Model, and qualitative insight into the relaxation time distribution function can be gained from using these fits. There is, however, no direct link between non-Debye relaxation and a heterogeneous distribution of relaxation times in the liquid. As was mentioned in the literature review section, intrinsic spectral broadening can result from intermolecular interactions and non-Markovian diffusion processes such as those described by Mode Coupling Theory.

The first step toward the generalization of the Debye model was made by Cole and Cole (CC function),[126] where they described a symmetrically broadened relaxation peak with the function

$$\varepsilon_{CC}^{*}(\omega) = \varepsilon_{\infty} + \frac{\Delta\varepsilon}{1+(i\omega\tau_{CC})^{\alpha}} \tag{3.11}$$

where $0 < \alpha \leq 1$. Since this function lead to symmetric broadening, the peak maximum occurs at $\omega_{max} = 1/\tau_{CC}$. In many cases the CC function is used to model the so-called β-relaxations, which are generally associated with fast, intramolecular side group fluctuations. The second generalization is the Cole-Davidson function (CD function),[127] which describes an asymmetrically broadened relaxation peak, such that

$$\varepsilon_{CD}^{*}(\omega) = \varepsilon_{\infty} + \frac{\Delta\varepsilon}{(1+i\omega\tau_{CD})^{\beta}} \tag{3.12}$$

where $0 < \beta \leq 1$. At frequencies smaller than the corresponding peak maximum, the CD function retains the spectral shape of the Debye model, and the frequency $\omega = \tau_{CD}^{-1}$ is the smallest relaxation rate in the liquid. The peak maximum of the CD occurs at $\omega_{max} = \frac{1}{\tau_{CD}} tan\left(\frac{\pi}{2\beta+2}\right)$. This function is used to model the so-called α-relaxation process of many small molecule glass-forming liquids. As discussed in the literature review, the exact nature of the α-relaxation process in molecular liquids is not well understood, but it is generally accepted that it reflects the collective reorientational motion of whole molecules (or polymer segments). The final generalization was introduced by Havriliak and Negami (HN function),[128] and it is a combination of the CC and CD functions. The HN function includes both symmetric and asymmetric broadening

$$\varepsilon_{HN}^{*}(\omega) = \varepsilon_{\infty} + \frac{\Delta\varepsilon}{(1+(i\omega\tau_{HN})^{\alpha})^{\beta}} \tag{3.13}$$

where α and β are defined as for the CC and CD functions. The HN function describes the segmental relaxation process of many polymeric liquids well. The peak relaxation frequency of the HN function occurs at $\omega_{max} = \frac{1}{\tau_{HN}}\left(\sin(\frac{\alpha\pi}{2+2\beta})\right)^{1/\alpha}\left(\sin(\frac{\alpha\beta\pi}{2+2\beta})\right)^{-1/\alpha}$. The effects on the spectral shape of the exponents α and β are depicted in Fig. 3.3.

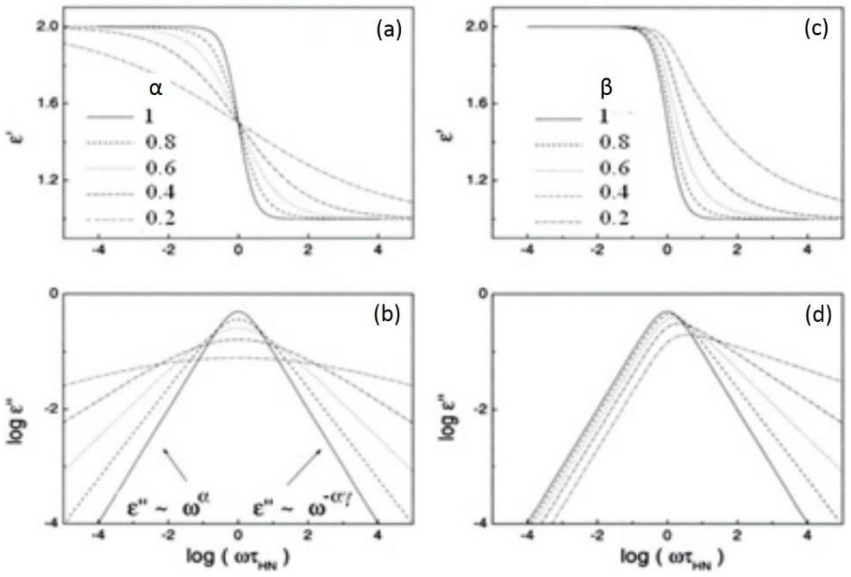

Figure 3.3. Real (ε') and imaginary (ε") parts of the Cole-Cole (CC) (a,b) and the Cole-Davidson (CD) (c,d) function are shown for different values of α and β. The Havriliak-Negami (HN) function combines the symmetric and asymmetric aspects of the CC and CD functions.[119]

In addition to dipolar reorientations, the migration of ions through a dielectric medium will also contribute to the complex permittivity spectrum. While the way to model such a process is still a matter of rigorous debate, the Random Barrier Model (which was discussed in the literature review section) accurately describes the permittivity spectrum of many ion conducting liquids, such as the molten eutectic salt Calcium-Potassium-Nitrate (CKN).[59] This function has a significantly different spectral shape than the previous three, where

$$\varepsilon^*_{RBM}(\omega) = \varepsilon_\infty + \frac{\Delta\varepsilon}{ln(1+i\omega\tau_{RBM})} \tag{3.14}$$

The detailed application of these functions to dielectric spectra will be demonstrated in Ch. 4, and eq. (3.14) will be used throughout the course of this dissertation to model ion motion in room temperature ionic liquids.

3.1.3. Measurement and instrumentation details

All broadband dielectric spectroscopy measurements were carried out using the Novocontrol Concept 80 system. This device was used to measure the complex dielectric function $\varepsilon^*(\omega)$ of the materials studied for this dissertation in the frequency window 10^{-2}–10^{7} Hz. The measurement scheme which is employed by the Concept 80 system is shown in Fig. 3.4, and it is seen in the schematic that the material under study is treated as the dielectric medium of a test parallel plate capacitor.

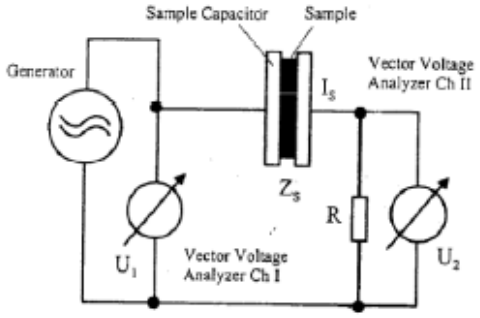

Figure 3.4. Schematic for the measurements of the complex dielectric permittivity of liquid samples using the Novocontrol Concept 80 system.[119]

The quantity that is physically measured by the device is the complex impedance $Z^*(\omega)$ of the sample capacitor. First, the device generates a monochromatic sinusoidal voltage across the sample and the current I_s through the sample is determined by measuring the voltage drop across the test resistance R. In general, the current $I_s(\omega)$ will be shifted in phase φ relative to the voltage $U_s(\omega)$, such that $Z_S^*(\omega) = \frac{U_S^*(\omega)}{I_S^*(\omega)} = \left|\frac{U_S}{I_S}\right| e^{i\varphi} = \left(\frac{U_1^*(\omega)}{U_2^*(\omega)} - 1\right) R$. Since the complex capacitance is related to the complex impedance and complex permittivity of the capacitor medium (our sample), we find that $\varepsilon_S^*(\omega) = \frac{1}{i\omega R C_0 \left(\frac{U_1^*(\omega)}{U_2^*(\omega)} - 1\right)}$, where C_0 is the empty sample cell capacitance. For

all measurements reported herein, the sample cell was a stainless steel parallel plate capacitor with plate diameter 20 mm. The plate spacing was maintained with small Teflon spacer posts at approximately 0.1–0.2 mm for all measurements.

The test samples were loaded by injecting the sample liquid into the empty capacitor with a needle until the entire sample volume was filled. The liquid sample remained mounted throughout measurement via the capillary force exerted by the stainless steel electrodes. While the liquid volume may have changed slightly during measurements due to thermal expansion, this effect is small enough to neglect for most cases. The filled test capacitor was then placed into the measurement circuit as shown in Fig. 3.4, and was mounted in a cryostat under dry nitrogen atmosphere. The sample temperature was controlled with the Novocontrol Quatro system, where the heating and cooling was performed with temperature regulated nitrogen gas, with temperature stability of ±0.1 K.

3.2. Quasielastic Light Scattering Spectroscopy

Quasielastic light scattering (QELS) techniques are complimentary to dielectric spectroscopy, and are very similar in many respects. The time window that can be probed by QELS techniques is similar to BDS—from fractions of picoseconds to hours. Whereas dielectric spectroscopy measures the polarization response of permanent molecular dipoles to a time varying applied electric field, QELS probes the equilibrium fluctuations of an ensemble of optically polarizable molecules. When a monochromatic electric field (of optical wavelengths) impinges upon a medium, fluctuations of the local optical properties will cause interference between the locally scattered waves, resulting in a diffraction (or speckle) pattern (elastic scattering).[129] This is identical to x-ray or neutron diffraction, except the wave-vectors involved in light scattering experiments are very small. If these local optical properties vary with time due

to molecular vibrations, the frequency of the scattered light will be shifted relative to the incident light. When the local optical properties fluctuate due to reorientational or diffusive molecular motions, the elastic line becomes broadened. By analyzing this part of the light scattering spectrum we can characterize microscopic molecular dynamics.[42, 130, 131] It should be noted that quasielastic light scattering measurements are especially important in the study of room temperature ionic liquids. For normal dipolar fluids, the molecular reorientation process is well resolved by dielectric spectroscopy. In ion-conducting fluids, however, the molecular reorientation process is not clearly observable in the dielectric spectrum due to strong contributions from ion motion. In order to develop the connection between ionic translational and rotational motions, it is essential to study ionic liquids with both dielectric and QELS techniques.

3.2.1. Principles of quasielastic light scattering spectroscopy

When a monochromatic electric field $\boldsymbol{E_i}(r,t) = \boldsymbol{n_i} E_0 e^{i(\boldsymbol{k_i}\cdot\boldsymbol{r}-\omega_i t)}$, where $\boldsymbol{n_i}$ is the polarization vector, E_0 is the field amplitude, $\boldsymbol{k_i}$ is the incident wave vector, and ω_i is the angular frequency, impinges on a medium, this field exerts a force on the electron clouds of the molecules comprising the medium. The field consequently induces molecular dipole moments which oscillate with the same frequency as the incident field, and these oscillating dipoles subsequently radiate light. This type of interaction of electromagnetic radiation with a molecule is called scattering.[42] If the medium is optically homogenous and there are no fluctuations of the local dielectric constant (at optical frequencies), light scattered from one sub-region of the medium will, due to interference, exactly cancel out the light from a corresponding sub-region. This will result in no net scattered light at any point far from the medium (other than in the forward direction).

If, on the other hand, the medium is not optically homogenous and has a local dielectric constant $\boldsymbol{\varepsilon}(\boldsymbol{r},t) = \varepsilon_0\boldsymbol{I} + \delta\boldsymbol{\varepsilon}(\boldsymbol{r},t)$, then the amplitudes of the scattered fields from different sub-regions will certainly be different and this will result in scattered light with frequency and wave-vector corresponding to the orientations and positions of the molecules in the medium. The scattered field at a distance *R* in this case will be

$$E_s(R,t) = \frac{-k_f^2 E_0}{4\pi R\varepsilon_0} e^{i(k_f R - \omega_i t)} \delta\varepsilon_{if}(\boldsymbol{q},t) \tag{3.15}$$

where $k_f = \frac{2\pi n}{\lambda_f}$ is the wave vector of the scattered light, and $\delta\varepsilon_{if}(\boldsymbol{q},t) = \boldsymbol{n}_f \cdot \delta\boldsymbol{\varepsilon}(\boldsymbol{q},t) \cdot \boldsymbol{n}_i$ is the component of the dielectric constant fluctuation tensor along the initial and final polarization directions. In most QELS experiments the magnitude of k_i and k_f are approximately equal, which allows one to straightforwardly calculate the magnitude of the wave vector $\boldsymbol{q} = \boldsymbol{k}_i - \boldsymbol{k}_f$ such that $q = \frac{4\pi n}{\lambda_i}\sin(\frac{\theta}{2})$, where θ is the angle between the initial and final wave vectors, as shown in Fig. 3.5. When the above condition is satisfied, the scattered electric field results from dielectric constant fluctuations with wave vector $\boldsymbol{q}$.

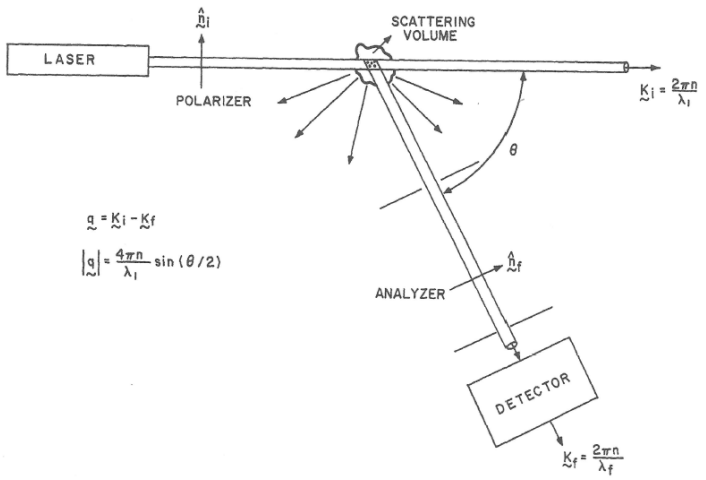

Figure 3.5. Diagram of the Quasielastic Light Scattering (QELS) experiment.[42]

Molecular rotations and translations will modulate the scattered electric field at the detector as a function of time, and the characteristic rates associated with these motions can be obtained from the electric field time correlation function

$$g^1(t) = \langle E_S^*(R,0)E_S(R,t)\rangle = \frac{k_f^4|E_0|^2}{16\pi^2R^2\varepsilon_0^2}\langle \delta\varepsilon_{if}(\boldsymbol{q},0)\delta\varepsilon_{if}(\boldsymbol{q},t)\rangle e^{-i\omega_i t} \tag{3.16}$$

In a typical light scattering experiment we measure the spectral density of scattered light using interferometry and dispersion techniques (these will be described in the next section). According to the Wiener-Khintchine theorem,[132] the time correlation function of the scattered electric field is related to the spectral density of scattered light, such that

$$I_{if}(\boldsymbol{q},\omega,R) = \frac{A}{2\pi}\int_{-\infty}^{+\infty} dt\langle \delta\varepsilon_{if}(\boldsymbol{q},0)\delta\varepsilon_{if}(\boldsymbol{q},t)\rangle\, e^{-i(\omega_i-\omega_f)t} \tag{3.17}$$

where A is the prefactor of eq. (3.16) and $\omega = \omega_i - \omega_f$ is the frequency shift between the incident and scattered light. Thus by measuring the spectrum of scattered light, we can obtain information about the local dielectric constant fluctuations caused by molecular motion.

There are two approaches to understanding the spectrum of scattered light from small molecule liquids—the dielectric continuum approach described above as well as a microscopic molecular approach.[42] The continuum approach is a reasonable approximation for the light scattering mechanism because optical wavelengths are much larger than molecular sizes, which should result in an averaging of local properties. While it is useful to consider the spectrum of scattered light in terms of local dielectric constant fluctuations when deriving eqs. (3.15-3.17), it is very helpful to consider the way these fluctuations are connected to local molecular properties in order to develop an intuitive understanding of the scattering mechanism. When a monochromatic field is incident upon a single molecule with polarizability tensor $\boldsymbol{\alpha}$, this field induces an oscillating dipole which subsequently radiates light (as described previously). Similar

to the previous arguments, the scattered field from this molecule will be proportional to $(\boldsymbol{n}_f \cdot \boldsymbol{\alpha}(t) \cdot \boldsymbol{n}_i) e^{i\boldsymbol{q}\cdot\boldsymbol{r}(t)}$, where ***r(t)*** is the position of the molecular center of mass at time *t*. In a condensed medium of molecules which are weakly electronically coupled to one another, the scattered field will result from a superposition of contributions from all molecules in the scattering volume, and the spectral density, similar to eq. (3.17), will be

$$I_{if}(\boldsymbol{q},\omega) = \frac{A}{2\pi}\int_{-\infty}^{+\infty} dt \langle \delta\alpha_{if}(\boldsymbol{q},0)\delta\alpha_{if}(\boldsymbol{q},t)\rangle\, e^{-i\omega t} \tag{3.18}$$

where $\alpha_{if}(\boldsymbol{q},t) = \boldsymbol{n}_f \cdot \boldsymbol{\alpha}(\boldsymbol{q},t) \cdot \boldsymbol{n}_i$.

Having established how the spectral density of scattered light is related to the local fluctuations in the optical properties of a medium, we will now look at two model systems which will provide a background for understanding the light scattering spectrum of neat molecular liquids. The first and most simple model system to consider is a liquid consisting of spherical and optically isotropic molecules which undergo Brownian motion.[42] When light impinges on a spherically symmetric molecule, the symmetry of the polarizability tensor $\boldsymbol{\alpha}$ dictates that the induced dipole is parallel to the applied field such that $\boldsymbol{\mu} = \alpha \boldsymbol{E}$. In this case the fluctuations of the polarizability tensor along the initial and final polarization directions $\delta\alpha_{if}(\boldsymbol{q},t)$ reduce to

$$\delta\alpha_{if}(\boldsymbol{q},t) = \left(\boldsymbol{n_i} \cdot \boldsymbol{n}_f\right)\alpha \int_V d^3r\, \delta\rho(\boldsymbol{r},t) e^{i\boldsymbol{q}\cdot\boldsymbol{r}} = \alpha(\delta\rho(\boldsymbol{q},t)) \tag{3.19}$$

where $\delta\rho(\boldsymbol{q},t)$ are the spontaneous density fluctuations with wavevector $\boldsymbol{q}$ at time *t*. Plugging this result into eq. (3.18) we see that the light scattering intensity of spherical and optically isotropic particles is proportional to the self-intermediate scattering function $F_s(\boldsymbol{q},t)$

$$I_{VV}(\boldsymbol{q},\omega) = \frac{A}{2\pi}\alpha^2 \int_{-\infty}^{+\infty} dt \langle \delta\rho(\boldsymbol{q},0)\delta\rho(\boldsymbol{q},t)\rangle\, e^{-i\omega t} = I_0 \int_{-\infty}^{+\infty} dt F_s(\boldsymbol{q},t)\, e^{-i\omega t} \tag{3.20}$$

where the subscript *VV* denotes that both the initial and final polarization vectors are oriented in the vertical (*y*) direction while the incident and scattered wavevectors lie in the *xz* plane. This is

referred to as *polarized* scattering. As is seen from eq. (3.19), when the incident and final polarizations are orthogonal to each other such that we measure *VH* or *HV* scattering, there will be no scattered light. This geometry will be important in the discussion of the next model system, and it is referred to as *depolarized* scattering.

For Brownian diffusion, the self-intermediate scattering function can be calculated such that $F_s(\boldsymbol{q}, t) = \exp(-q^2 Dt) = \exp(-\frac{t}{\tau_q})$, where *D* is the translational diffusion coefficient. $F_s(\boldsymbol{q},t)$ is proportional to the electric field correlation function, and it follows that the spectral density of scattered light will be a Lorentzian function centered on the incident light frequency with full width at half maximum (FWHM) equal to τ_q^{-1}. This result is similar to the results obtained for the Debye Model presented in the previous section on dielectric spectroscopy. Thus we can measure the translational self-diffusion coefficient in the medium by measuring the light scattering spectrum from spherical, isotropic molecules (or particles).

The next model to be considered is a system of cylindrically symmetrical and optically anisotropic molecules undergoing diffusive motions. The light scattering spectrum will now consist of a contribution from both translational as well as rotational diffusion of the molecules.[42] Generalizing the results for spherical, isotropic molecules, the intensity of scattered light from optically anisotropic molecules is proportional to

$$I_{if}(\boldsymbol{q}, t) = A\langle\alpha_{if}(0)\alpha_{if}(t)\rangle\langle\delta\rho(\boldsymbol{q}, 0)\delta\rho(\boldsymbol{q}, t)\rangle = A\langle\alpha_{if}(0)\alpha_{if}(t)\rangle F_s(\boldsymbol{q}, t) \quad (3.21)$$

From eq. (3.21) we see that the light scattering spectrum will consist of a contribution from reorientational motions, which are contained in the polarizability correlation function, as well as density fluctuations or translational motions. Because there is no wave vector dependence in the polarizability correlation function, this part of the spectrum provides information on purely local motions, allowing us to probe single molecule rotational dynamics.

We now will consider a cylindrically symmetrical molecule with polarizability along the axis of the cylinder $\alpha_{\parallel}$ different from the polarizability in the radial directions $\alpha_{\perp}$. In the coordinate system shown in Fig. 3.6, the polarized and depolarized components of the light scattering spectrum are proportional to the polarizability tensor components such that

$$I_{VV}(\boldsymbol{q},t) = A\langle\alpha_{zz}(0)\alpha_{zz}(t)\rangle F_s(\boldsymbol{q},t) \tag{3.22a}$$

$$I_{VH}(\boldsymbol{q},t) = A\langle\alpha_{yz}(0)\alpha_{yz}(t)\rangle F_s(\boldsymbol{q},t) \tag{3.22b}$$

In order to calculate $\alpha_{zz}(t)$ and $\alpha_{yz}(t)$, it is necessary to express the molecule-fixed polarizability tensor in the laboratory frame. The projection of this tensor into the laboratory frame yields the polarizability tensor components

$$\alpha_{zz} = \alpha_{\parallel}\cos^2\theta + \alpha_{\perp}\sin^2\theta = \alpha + \left(\frac{16\pi}{45}\right)^{\frac{1}{2}}\beta Y_{2,0}(\theta,\varphi) \tag{3.23a}$$

$$\alpha_{yz} = (\alpha_{\parallel} - \alpha_{\perp})\sin\theta\cos\theta\sin\varphi = i\left(\frac{2\pi}{15}\right)^{\frac{1}{2}}\beta[Y_{2,1}(\theta,\varphi) + Y_{2,-1}(\theta,\varphi)] \tag{3.23b}$$

where $Y_{lm}(\theta,\varphi)$ are the spherical harmonics, $\alpha = \alpha_{\parallel} + 2\alpha_{\perp}$ is called the isotropic part of the polarizability tensor since that part of eq. (3.23a) is independent of molecular orientation, and $\beta = \alpha_{\parallel} - \alpha_{\perp}$ is the optical anisotropy. The scattering from cylindrically symmetric particles reduces to the spherically symmetric case above when $\alpha_{\parallel} = \alpha_{\perp}$. Plugging eqs. (3.23) into eqs. (3.22) we see that the polarized and depolarized components of the scattering intensity are proportional to

$$I_{VV}(\boldsymbol{q},t) = A[\alpha^2 + \left(\frac{16\pi}{45}\right)\beta^2 F_{2,0}^2(\theta,\varphi)]F_s(\boldsymbol{q},t) \tag{3.24a}$$

$$I_{VH}(\boldsymbol{q},t) = A\frac{2\pi}{15}\beta^2[F_{1,1}^2(t) + F_{1,-1}^2(t) + F_{-1,1}^2(t) + F_{-1,-1}^2(t)]F_s(\boldsymbol{q},t) \tag{3.24b}$$

where $F_{m,m'}^{l}(t) = \langle Y^*{}_{l,m}(\theta,\varphi,0)Y_{l,m'}(\theta,\varphi,t)\rangle$ are the orientational time correlation functions.

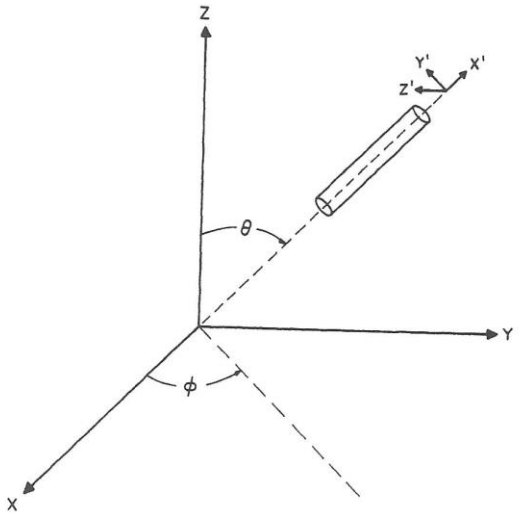

Figure 3.6. Geometry of a cylindrically symmetrical molecule in the molecular frame (primed) and laboratory frame (unprimed).[42]

The Debye model[56] for rotational diffusion is once again applied to obtain the orientational correlation functions needed to calculate the scattering intensities in eqs. (3.24). In this model, the orientational correlation functions can be shown to be

$$F^{l}_{m,m'}(t) = \frac{1}{4\pi}\exp(-\frac{l(l+1)t}{\tau_{rot}}) \tag{3.25}$$

This result is nearly identical to that of the dielectric spectroscopy section, except that $l = 2$ for QELS measurements, and $l = 1$ for dielectric spectroscopy measurements.[133] Using eq. 3.25 in eqs. (3.24), we find that the light scattering intensities are proportional to

$$I_{VV}(\boldsymbol{q}, t) = A[\alpha^2 + \left(\frac{4}{45}\right)\beta^2\exp(-\frac{6t}{\tau_{rot}})]\exp(-q^2Dt) \tag{3.26a}$$

$$I_{VH}(\boldsymbol{q}, t) = A[\left(\frac{1}{15}\right)\beta^2\exp(-\frac{6t}{\tau_{rot}})]\exp(-q^2Dt) \tag{3.26b}$$

The translational diffusion term usually decays much more slowly that the rotational diffusion term and does not contribute to the depolarized spectrum eq. (3.26b). This is because the wave

vectors probed in the scattering experiment are very small, resulting in a slow decay of the translational term, regardless of the magnitude of the translational diffusion coefficient.

Thus, measuring the depolarized light scattering spectrum of optically anisotropic molecules allows one to characterize the average molecular reorientation rate in the liquid. Since this dissertation presents measurements of the characteristic reorientation rates of various ionic liquids, any mention of light scattering will likely be concerned with depolarized scattering only. It should also be noted that the exact polarizability of a molecule is usually quite complicated, and it is not straightforward to calculate the scattering functions from molecular liquids. However, most molecules have some degree of optical anisotropy, and the above models elucidate how this general property allows one to characterize molecular reorientational dynamics. Furthermore, these models only apply for dilute systems without collective molecular effects, which will certainly add to the complexity of the spectrum.

3.2.2. Analyzing light scattering spectra of molecular liquids

The analysis of light scattering data are in principle identical to the methods presented for the analysis of dielectric spectra. The main difference is that in addition to frequency domain measurements of the spectral density of scattered light (which is related to the frequency dependent permittivity measured by dielectric spectroscopy), we also measure the electric field time correlation function $g^1(t)$ which is related to the spectral density through the Fourier transform. Similar to the analysis of permittivity spectra of dielectric measurements, it is often useful to analyze light scattering spectra in the susceptibility representation. According to the Fluctuation-Dissipation theorem, the imaginary part of the light scattering susceptibility is proportional to the spectral density such that $\chi''(\omega) = \frac{I(\omega)}{[n(\omega,T)+1]}$, where $n(\omega,T) = (e^{\frac{\hbar\omega}{kT}} - 1)^{-1}$ is the Bose-Einstein occupation factor.[122] For the temperatures and frequencies probed by QELS,

this factor reduces to the classical approximation such that $\chi''(\omega) = \frac{\hbar\omega}{kT} I(\omega)$. In this representation, the CC, CD, and HN functions can all be applied to light scattering data as they are for dielectric spectroscopy.

In the photon correlation spectroscopy technique, the electric field time correlation function $g^1(t)$ can be measured, and thus time domain data is obtained. If the molecular motion that is probed by the experiment is Brownian diffusion (rotations or translations), the correlation function decays exponentially, such that $g^1(t) = \exp(-\frac{t}{\tau})$. Analogous to the spectral broadening observed in dielectric spectra of molecular liquids, QELS data in the time domain rarely decay exponentially, and instead the correlation functions follow a stretched exponential form, such that $g^1(t) = \exp(-(\frac{t}{\tau})^{\beta})$, where β is called the stretching parameter. This function is known as the Kohlrausch-William-Watts (KWW) function.[41] The exact molecular reasons for this spectral shape are not known, and there are several potential explanations as discussed in the literature review section.

3.2.3. Measurement and instrumentation details

There are three experimental techniques that are applied in this dissertation to characterize the light scattering spectrum over timescales spanning sub-picoseconds to seconds. Two of these techniques—interferometry and dispersion—are used to measure the light scattering spectral density in the frequency window from 500 MHz up to 10 THz (10^{-9}–10^{-13} s). They work by filtering the scattered light so that individual frequency increments of the spectrum can be measured independently. The third method is known as photon correlation spectroscopy, and it is used in the time domain to characterize dynamics slower than 10^{-8} s. This method directly records all of the scattering intensity as a function of time, and a hardware correlator is

used to calculate the intensity correlation function (which is related to the field correlation function).

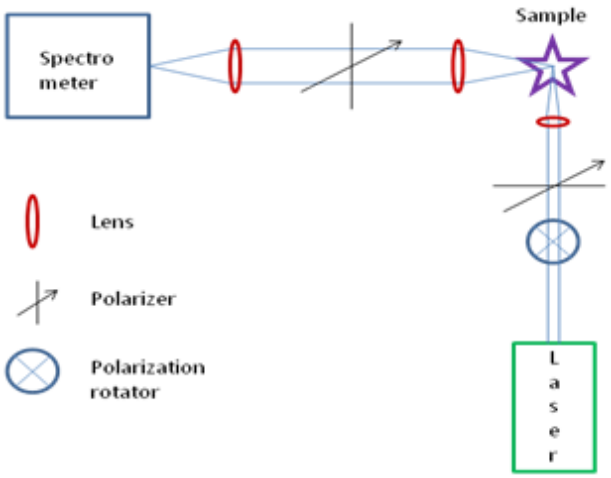

Figure 3.7. Diagram of the QELS measurement illustrating the 90° scattering geometry.[134]

The external optical system used for these three techniques, are essentially the same, and is illustrated in Fig. 3.7. A monochromatic laser source (λ = 532 nm (green) or 647 nm (red)) is first passed through a polarizer such that vertically (or horizontally) polarized light is selected. This light is focused onto the sample which is contained inside a cryostat with optically transparent windows allowing for various scattering angles to be probed. The scattered light is collected by a lens and passes through another polarizer, allowing for the measurement of either polarized or depolarized scattered light. Finally, this scattered, analyzed light is focused onto the entrance of the detector and recorded. The cryostats used were the Janis ST-100, with temperature range 100–375 K and stability ±0.1 K, and the Oxford Optistat, with temperature range 100–475 K and stability ±0.1 K. The lasers used were the Coherent Verdi (532 nm) with max power = 2 W, as well as the Lexel (647 nm) with max power = 300 mW.

In the interferometry technique, the scattered light is passed into a Fabry-Perot interferometer cavity, which consists of two mirrors in which the inner surfaces are highly reflective (≈ 98%). The light that enters then reflects multiple times inside the cavity, and the only waves that can pass the interferometer are those whose wavelengths are half integer multiple of the mirror spacing, such that $m\left(\frac{\lambda}{2}\right) = L$. The frequency spacing between the adjacent cavity modes (m and m+1) is called the free spectral range and is $\Delta\nu = \frac{c}{2nL}$, where c is the speed of light and n is the refractive index of the cavity medium (air). This frequency spacing is normally much wider than a typical Lorentzian spectrum resulting from molecular rotation and diffusion.

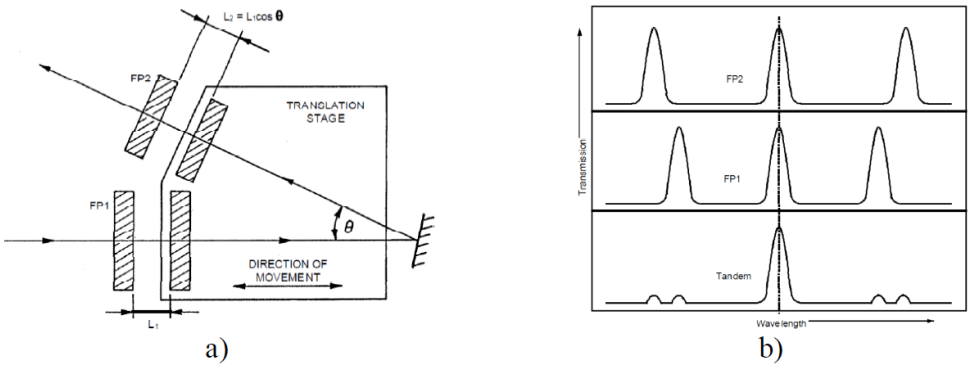

Figure 3.8. (a) Schematic of the Tandem Fabry Perot (FP) interferometer. (b) Illustration comparing the spectrum obtained from a single FP interferometer vs. the tandem FP setup.[135]

A Tandem Fabry-Perot interferometer (TFPI–Sandercock model) extends the free spectral range beyond that of a single Fabry-Perot. In the Tandem Fabry-Perot system, two interferometers are used in series, and their mirror spacings L_1 and L_2 are slightly offset from one another, where $m\left(\frac{\lambda}{2}\right) = L_1$ and $n\left(\frac{\lambda}{2}\right) = L_2$. The mirror spacings are selected so that they simultaneously pass

the first order mode, but now the second order mode cannot be passed by the first FP and vice-versa. However, the interferometer does pass the 20th order mode, and optical-bandpass filters are used to suppress contributions of this mode from the spectrum. This results in a considerably extended FSR as illustrated by Fig. 3.8. The mirrors are then scanned through small distances using piezo-motors, and the intensity of the scattered light that passes through the TFPI is recorded at each different mirror spacing, corresponding to a specific wavelength or frequency increment. The Tandem Fabry-Perot interferometer was used in this dissertation to measure the light scattering spectral density over a frequency window from 0.5–350 GHz.

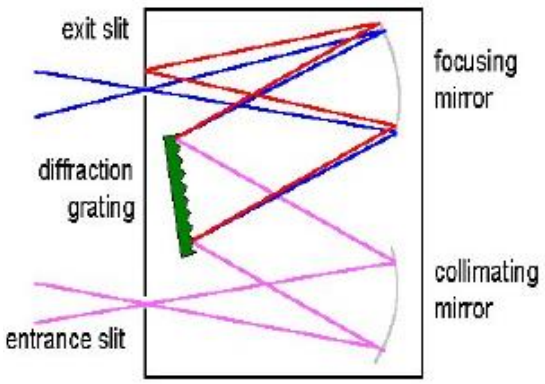

Figure 3.9. Schematic of the light dispersion filter used in the Jobin Yvon T64000 spectrometer.[134]

The second technique used to measure the light scattering spectral density in the frequency domain is the diffraction grating, or light dispersion, method. In this technique, scattered light from the sample is passed to the spectrometer and collimated onto a diffraction grating. Light of differing wavelengths will be dispersed by this grating at different angles, and when it arrives at the second collimating mirror, it will be focused by this mirror onto different positions in the spectrometer. If we have a small slit at the exit leading to a single pixel detector,

only light of one wavelength will reach the detector. By changing the angle of the diffraction grating in the spectrometer, we can scan light of different wavelengths across the detector and measure the spectrum. Alternatively, the spectrometer used in this study (Jobin Yvon T64000) employs a CCD detector which allows for the simultaneous recording of several frequency increments of the spectrum. This spectral technique was used to measure the light scattering spectral density over a frequency window from 200–10000 GHz.

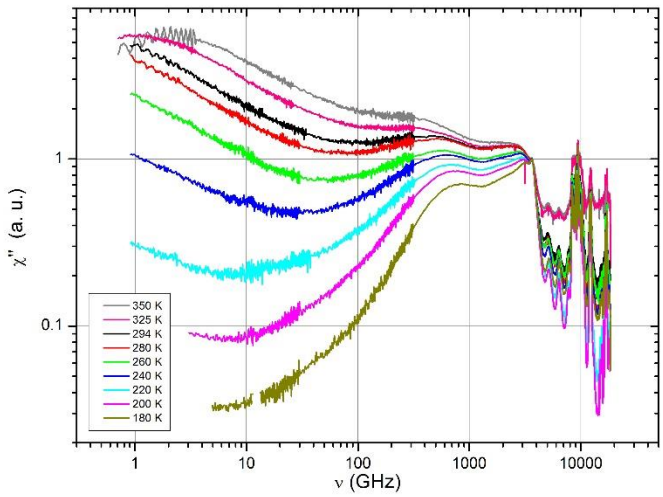

Figure 3.10. Depolarized dynamic light scattering susceptibility spectra of the ionic liquid [BMIM][NTF$_2$] recorded at various temperatures. The spectra were obtained by compiling the spectral densities measured using the Jobin Yvon T64000 and the Tandem Fabry Perot Interferometer. Below 10 GHz the molecular reorientation process is observed as a peak (at high temperatures) which moves out of the window at low temperatures. Between 100–3000 GHz, intermolecular librational modes are observed, and intramolecular optical vibrations are observed above 3000 GHz.[93]

The photon correlation spectroscopy (PCS) technique is different from the first two methods described above in that the detector records the whole unfiltered band of scattered light as a function of time. In this technique, scattered light from the sample is focused onto the

entrance of a point photodiode detector through a fiber optic coupling device. As described above, molecular translations and rotations will modulate the scattered intensity in time, and the temporal pattern of these fluctuations reflect the timescales of these motions. The electrical signal from the photodiode (which is proportional to the measured intensity) is then passed to the hardware autocorrelation device (ALV-7004 fast digital correlator) which computes the Intensity Autocorrelation Function (ICF) $g^2(t) = \frac{\langle I(o)I(t)\rangle}{\langle I^2\rangle}$, where *I(t)* is the measured intensity at time *t*. The intensity auto correlation function is related to the electric field autocorrelation function through the Siegert-relation such that $g^2(t) = 1 + \gamma|g^1(t)|^2$, where γ is a correction factor known as the coherence factor. PCS was used to measure the field correlation function in the time window 10^{-9}–100 s.

3.3. Other Measurement Techniques

3.3.1. Rheology

Viscosity is the measure of the resistance of a fluid to strain under the presence of an applied stress.[136] The shear viscosity of a liquid is a bulk property, similar to the dc conductivity (or resistivity), and the classical theories of diffusion and ion conduction directly link the molecular translational diffusion rate and dc conductivity to the shear viscosity of the liquid medium. In order to gain a deeper understanding of the motion of molecules and ions in viscous media, it is often useful to combine measurements of molecular reorientation and translation obtained via dielectric spectroscopy and light scattering with shear viscosity measurements.[137]

The shear viscosity of the ionic liquids studied in this dissertation was measured using the creep compliance technique, where compliance is defined as the ratio of strain to stress (eq. 3.27). In creep compliance measurements, a liquid sample (which is initially at equilibrium) is

placed under a constant, small applied shear stress at time t = 0 s. The sample will begin to strain, and this strain will increase as t increases. Part of this strain is recoverable, and when the stress is removed, the material will elastically recover this portion of the strain. At long times the strain becomes irreversible, and this irreversible part is directly connected to the shear viscosity

$$J(t) = \frac{\gamma(t)}{\sigma_0} = J_R(t) + t/\eta \quad (3.27)$$

where $J(t)$ is the creep compliance, $J_R(t)$ is the recoverable creep compliance, and η is the shear viscosity.[136] All rheology (shear compliance) measurements were performed with an AR2000ex rheometer (TA instruments) using 25 mm parallel plates with the sample mounted between the plates. All samples were in nitrogen atmosphere with temperature controlled using dry nitrogen gas.

3.3.2. Differential scanning calorimetry

Differential scanning calorimetry (DSC) measures heat flow upon a temperature change of an investigated material, allowing one to characterize the specific heat capacity of the material. DSC is used to characterize thermal transitions in materials such as crystallization, melting, and the glass transition.[138] Upon crystallization (melting), the quantity of heat flowing out of (into) the sample changes sharply, and the temperature where this change occurs can be straightforwardly determined. Similarly, when a supercooled liquid is cooled through the glass transition temperature (T_g), it falls out of equilibrium which results in a step-like reduction in the heat flow as it is cooled through T_g. DSC was used to measure the calorimetric glass transition temperature of the ionic liquids presented in this dissertation.

In DSC, the sample and the reference are heated (cooled) such that the temperature of each is kept identical. The reference was an empty aluminum sample container. As the temperature of the sample and reference are varied, a different amount of heat is required to keep

the sample and reference at the same temperature, and this differential heat is recorded as a function of temperature. For this dissertation, the sample and reference were heated and cooled at a constant rate of 5-10 K/min, and since the heating/cooling rate is constant, the rate of heat flow from the sample can be measured as a function of temperature. All DSC measurements were performed in nitrogen atmosphere using a Q1000 differential scanning calorimeter (TA instruments).

4. Dynamics and Charge Transport in Imidazolium based ILs

4.1. Introduction

Understanding the physicochemical properties of room temperature ionic liquids (ILs) has become an active area of chemical physics research in the past decade due to their many potential technological applications. In particular, ILs have been shown to be potentially useful materials for electrochemical applications due to the large electrochemical window and relatively high electrical conductivity.[1, 2, 139, 140] As a result, significant research effort has been focused on characterizing the charge transport properties in ILs.

Several experimental studies have been performed to measure the ion diffusion coefficients and conductivity in several types of ILs upon variation of the cation and anion chemical structures. Many of these studies, however, characterized the charge transport in these materials only at high temperatures and in the highly fluid state.[83-86] In an effort to expand on this work, further studies were performed to characterize the charge transport properties in various ionic liquids over a broad temperature range, from above the melting point down to the glass transition temperature. In the works of Sangoro et al., a method to characterize ion diffusion rate and free ion concentration via dielectric spectroscopy was proposed, and successfully applied to several ionic liquids.[80, 81, 90, 92] While, these authors systematically studied the electrical conductivity and ion diffusion rate for many ILs, they did not analyze the influence of chemical structure on the free ion concentration in these materials.

While the charge transport properties are more thoroughly studied, there are only very few experimental studies of the reorientational structural dynamics in ionic liquids.[87, 100, 141, 142] Since many of these ionic liquids can be supercooled through a glass transition, it is important to understand whether or not these ionic liquids exhibit the phenomenology of other supercooled

molecular liquids, such as nonexponential structural relaxation, decoupling of translational and rotational motions, and the presence of the dynamic crossover temperature T_c. It is essential to characterize the reorientational motion (structural relaxation) as well as translational motion of ions in order to develop the complete picture of how ion transport occurs in these materials.

In this chapter, experimental studies of the charge transport properties and reorientational structural dynamics are presented for a series of three imidazolium based room temperature ionic liquids. The dielectric spectroscopy and dynamic light scattering data analysis techniques as applied to ionic liquids are presented in detail in this chapter, and will be referred to in the following chapters. It has been found that the chemical structure of the anion has a significant effect on the ionic conductivity in these imidazolium based ionic liquids. As the anion size and asymmetry increases, the ion diffusion coefficients increase while the corresponding glass transition temperatures decrease. The free ion concentration has been found to exhibit minor differences upon variation of the anion, indicating that the primary effect of the chemical structure is to change the ion mobility in these liquids. Turning to the analysis of the reorientational structural dynamics, many interesting differences have been observed when comparing ionic liquids to neutral molecular liquids. These ionic liquids exhibit no dynamic crossover, no change in the spectral shape of the structural relaxation process, and very weak decoupling of translational and rotational degrees of freedom—phenomena which are nearly ubiquitously observed in molecular liquids. These observations suggest that ionic liquids, while exhibiting the general characteristics of supercooled liquids, have important differences that may be the result of their unique interionic interaction mechanisms.

4.2. Experimental Details

1-butyl-3-methylimidazolium trifluoroacetate [BMIM][TFA] (M_W = 252.23 g/mol, ρ_m = 1.22 g/cm^3)[86], 1-butyl-3-methylimidazolium hexafluorophosphate [BMIM][PF_6] (M_W = 284.18 g/mol, ρ_m = 1.38 g/ cm^3)[143], and 1-butyl-3-methylimidazolium bis(trifluoromethylsulfonyl)imide [BMIM][NTF_2] (M_W = 419.4 g/mol, ρ_m = 1.44 g/cm^3)[144] were purchased from Sigma-Aldrich chemical company and used as received. The mass densities reported above are from the literature, and were recorded at T = 295 K. The chemical structures of these ionic liquids are shown below in Fig. 4.1. Before performing measurements, the liquid samples were passed through 220 nm PVDF filters into cleaned, dried mL sized cylindrical glass vials. The filled vials were then placed into a vacuum oven at T = 350 K and P = 1 mbar for 24 h to remove residual impurities and dissolved gasses. For these samples, treatment in the vacuum oven was necessary to prevent crystallization during the course of the BDS and DLS measurements.

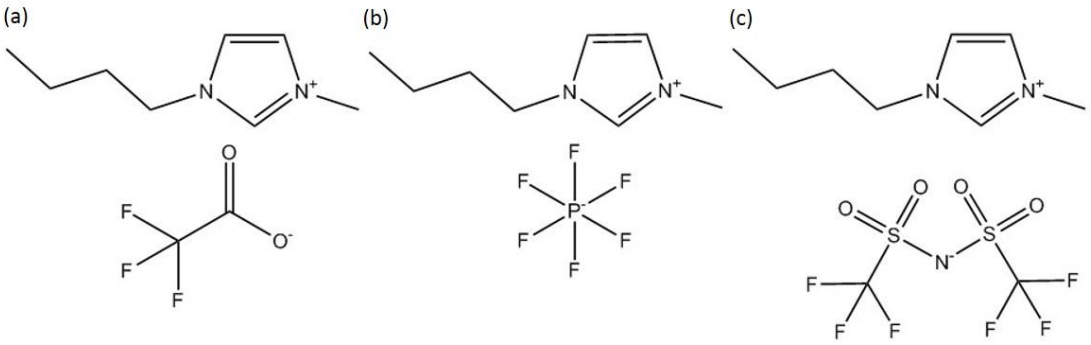

Figure 4.1. Chemical structures of the imidazolium-based ionic liquids: (a) 1-butyl-3-methylimidazolium trifluoroacetate [BMIM][TFA], (b) 1-butyl-3-methylimidazolium hexafluorophosphate [BMIM][PF_6], (c) 1-butyl-3-methylimidazolium bis(trifluoromethylsulfonyl)imide [BMIM][NTF_2].

Depolarized dynamic light scattering (DDLS) spectra were measured to characterize the structural relaxation/molecular reorientation process (α process) of the three imidazolium-based ILs over thirteen decades in time, from 10^{-11} s through 100 s. For these liquids, this corresponds to temperatures ranging from 375 K down to approximately 180 K, i.e. from above the melting point down to the glass transition temperature T_g. To characterize the α process at short timescales (10^{-11} s through 10^{-9} s), frequency domain measurements were performed in the backscattering geometry, with laser wavelength λ = 532 nm and laser power P = 100 mW, using the Jobin Yvon T64000 triple monochromator spectrometer and the tandem Fabry-Perot interferometer (Sandercock Model) at three different free spectral ranges (10 GHz, 50 GHz, 375 GHz). By combining these two techniques, hereto referred as Brillouin-Raman (BR) spectroscopy, the depolarized light scattering spectral density was measured in the frequency window 0.5 GHz – 10 THz. To characterize the α process at longer time scales (10^{-7} s through 100 s), depolarized photon correlation spectroscopy measurements (PCS) were performed in right angle geometry, with laser wavelength λ = 647 nm and laser power P = 100 mW. The scattered light was collected with a single mode optical fiber, split between two avalanche photodiode detectors, and cross correlated using the ALV-7004/FAST multi-tau digital correlator. Frequency domain measurements were performed with the sample mounted in a Janis ST-100 optical cryostat with temperature stability of ± 0.1 K. Time domain measurements were performed with the sample mounted in an Oxford Optistat cryostat with temperature stability of ± 0.1 K.

Broadband dielectric spectroscopy (BDS) was used to characterize the dc conductivity, as well as the ionic and dipolar relaxation processes in these liquids over a similar range of temperatures as measured with DDLS. These measurements were performed using the

Novocontrol Concept 80 system in the frequency window 10^{-2} Hz – 1 MHz. The samples were mounted between parallel stainless steel plates, diameter d = 15 mm and plate spacing l = 0.2 mm. The Novocontrol Quatro temperature control unit was used to heat and cool the sample with temperature stability of ± 0.1 K.

4.3. Results and Discussion

4.3.1. Quasielastic light scattering data analysis

Figure 4.2 presents the DDLS spectra of [BMIM][TFA] measured at several temperatures via BR frequency domain measurements and PCS time domain measurements. The spectral features observed in [BMIM][PF_6] and [BMIM][NTF_2] are nearly identical to those seen in Fig. 4.2., and they are not shown for the sake of brevity. All data analysis techniques presented below for the representative IL [BMIM][TFA] were applied to the other two ILs in an identical manner.

The α process, which reflects collective molecular reorientations, is seen as a peak in the BR spectrum (Fig. 4.2(a)) that moves out of the frequency window (to lower frequencies) as the temperature decreases. Since the cation $[BMIM]^+$ has a larger optical polarizability than the anion due to the delocalization of the electrons on the imidazolium ring (it is also more anisotropic due to the planar shape of the imidazolium ring), the α process in the depolarized light scattering spectrum likely reflects the collective reorientation of cations in the matrix.[145] At temperatures where the peak of the α process is visible in the BR spectrum (Fig. 4.2(a)), the LS data were fit using the imaginary part of the Cole-Davidson function,

$$\chi''(\nu) = \Delta\chi[\cos(\operatorname{atan}(2\pi\nu\tau_{CD}))^{\beta_{CD}}]\sin[\beta_{CD} \cdot \operatorname{atan}(2\pi\nu\tau_{CD})], \quad (4.1)$$

where $\Delta\chi$ is the polarizability amplitude (analogous to the dielectric strength), τ_{CD} is the characteristic relaxation time, and β_{CD} is the characteristic non-exponentiality parameter. τ_{CD} was converted to the most probable relaxation time (corresponding to the peak maximum) such that

$\tau_\alpha = \frac{\tau_{CD}}{tan\left(\frac{\pi}{2\beta_{CD}+2}\right)}$.[119] While an analytical connection between the shape parameters β_{CD} and β_{KWW} does not exist, Lindsay and Patterson[123] showed that there is an empirical connection between the CD and KWW functions such that

$$\beta_{KWW} = \begin{cases} 0.97\beta_{CD} + 0.144\,; & [0.2 \leq \beta_{CD} < 0.6] \\ 0.683\beta_{CD} + 0.316\,; & [0.6 \leq \beta_{CD} \leq 1] \end{cases} \quad (4.2)$$

The shape parameter β_{KWW} was calculated via eq. 4.2, using the values of β_{CD} determined from the frequency domain measurements.

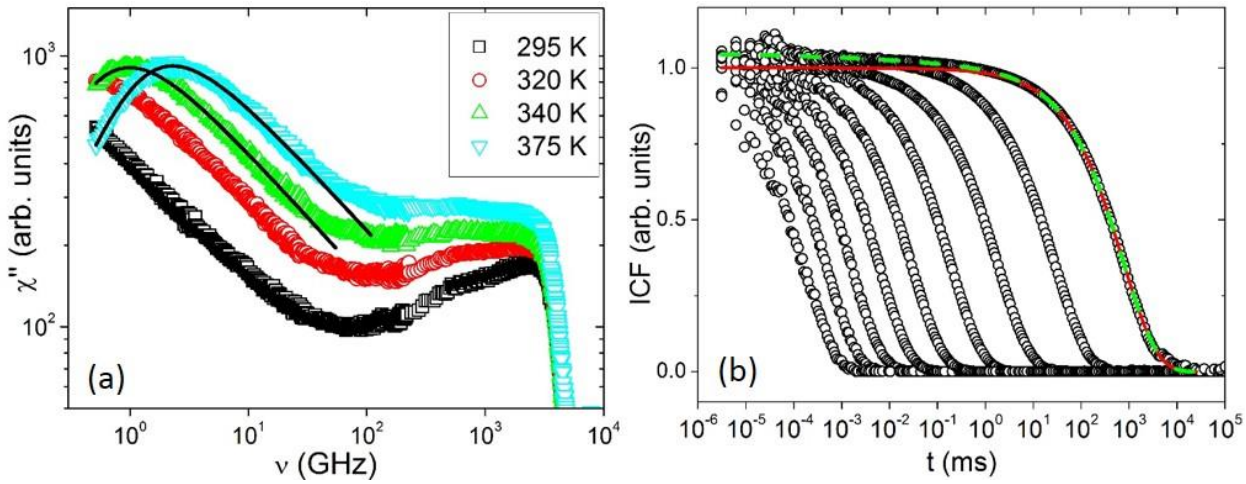

Figure 4.2. (a) Depolarized light scattering susceptibility spectra are shown at several temperatures for the IL [BMIM][TFA]. The black lines are fits of the α relaxation peak using the Cole-Davidson function. (b) Normalized intensity correlation functions (ICF) of [BMIM][TFA] measured at several temperatures. The data measured at 190 K are shown fit to a single KWW relaxation function (red line) as well as to a superposition of two KWW functions (green dashed line) accounting for the α relaxation and the excess wing.[146]

As the IL is cooled toward the calorimetric glass transition temperature T_g, the molecular reorientational motions slow down precipitously, and they are no longer observable using the BR frequency domain technique. At temperatures where these motions occur with a characteristic time between 10^{-7}–100 s, which is deep in the supercooled liquid regime, PCS time domain

measurements are used to characterize the structural dynamics and α process. The α process is observed in the time domain as a stretched exponential decay of the intensity correlation function (ICF), as seen in Fig. 4.2(b). At temperatures very close to the glass transition, the ICF also shows a very slight decay in addition to the α process. This spectral feature is known as the excess wing, and it is commonly observed in the dielectric and light scattering spectra of glass forming liquids.[147-150]

The molecular origin of the excess wing is not known, and it is currently the subject of active research in the field. Some authors have suggested that the excess wing is related to single molecule rotational motions, while the α process is the signature of truly cooperative and collective molecular motions.[151] Another interpretation is in the framework of the dynamical heterogeneity hypothesis, which suggests that the excess wing is the spectral signature of highly mobile molecules, while the α process represents the slower sub ensemble of molecules.[152] Whatever the case, it is interesting, although not surprising, that the ionic liquids also show a signature of the excess wing, and it demonstrates further that the excess wing is a common feature of molecular relaxation in glass forming materials.

The intensity correlation functions shown in Fig 4.2(b) were fit with a superposition of two KWW functions,

$$ICF = g^2(t) - 1 = \gamma |g^1(t)|^2 = \gamma \left| a_1 \exp\left(-\left(\frac{t}{\tau_1}\right)^{\beta_1}\right) + a_2 \exp\left(-\left(\frac{t}{\tau_2}\right)^{\beta_2}\right)\right|^2 \quad (4.3)$$

where γ is the coherence factor of the optical system, a_1 and a_2 are the relative relaxation strengths, τ_1 and τ_2 are the characteristic relaxation times, and β_1 and β_2 are the non-exponentiality (KWW) parameters of the α relaxation (1) and excess wing (2).[42, 130] The characteristic α relaxation times τ_1 were converted to the most probable relaxation times τ_α by

numerically simulating the one-sided sine Fourier transform of the best fit KWW relaxation function,[123] where

$$\chi''(\omega) = \int_0^\infty \sin(\omega t) \cdot (-\frac{d}{dt} g_1(t)) dt \quad (4.4)$$

The fitting function, as opposed to the experimental data, is converted to the susceptibility representation for ease of calculation, and no information is lost in the process. Once the correlation function is converted to the susceptibility representation, the most probable (peak) relaxation time can be straightforwardly determined. The structural relaxation times τ_α as well as the characteristic stretching parameters for the three [BMIM] based ILs were determined from the fits of the PCS data using eq. 4.3.

4.3.2. Broadband dielectric spectroscopy data analysis

Figure 4.3 presents the dielectric spectra of [BMIM][TFA] recorded at several temperatures in the supercooled liquid regime. Once again, the spectra of the other two ionic liquids presented in this section are very similar and are not shown for the sake of brevity. The real part of the conductivity spectrum σ' (Fig. 4.3(a)) for all ionic liquids studied exhibits three main spectral features: (i) at low frequency the conductivity is strongly frequency dependent due to the accumulation of ions at the electrode interface (electrode polarization effect), (ii) at intermediate frequencies the conductivity becomes frequency independent due to the drift current of ions in the liquid matrix (dc conductivity), and (iii) at high frequencies the conductivity once again becomes frequency dependent as a result of the ion-hopping process (ac conductivity).[119] These three regions have corresponding analogs in the real and imaginary parts of the permittivity and conductivity, as seen in Fig. 4.3. Throughout this dissertation, our analysis will only focus on the spectral regions at frequencies faster than the electrode polarization effect.

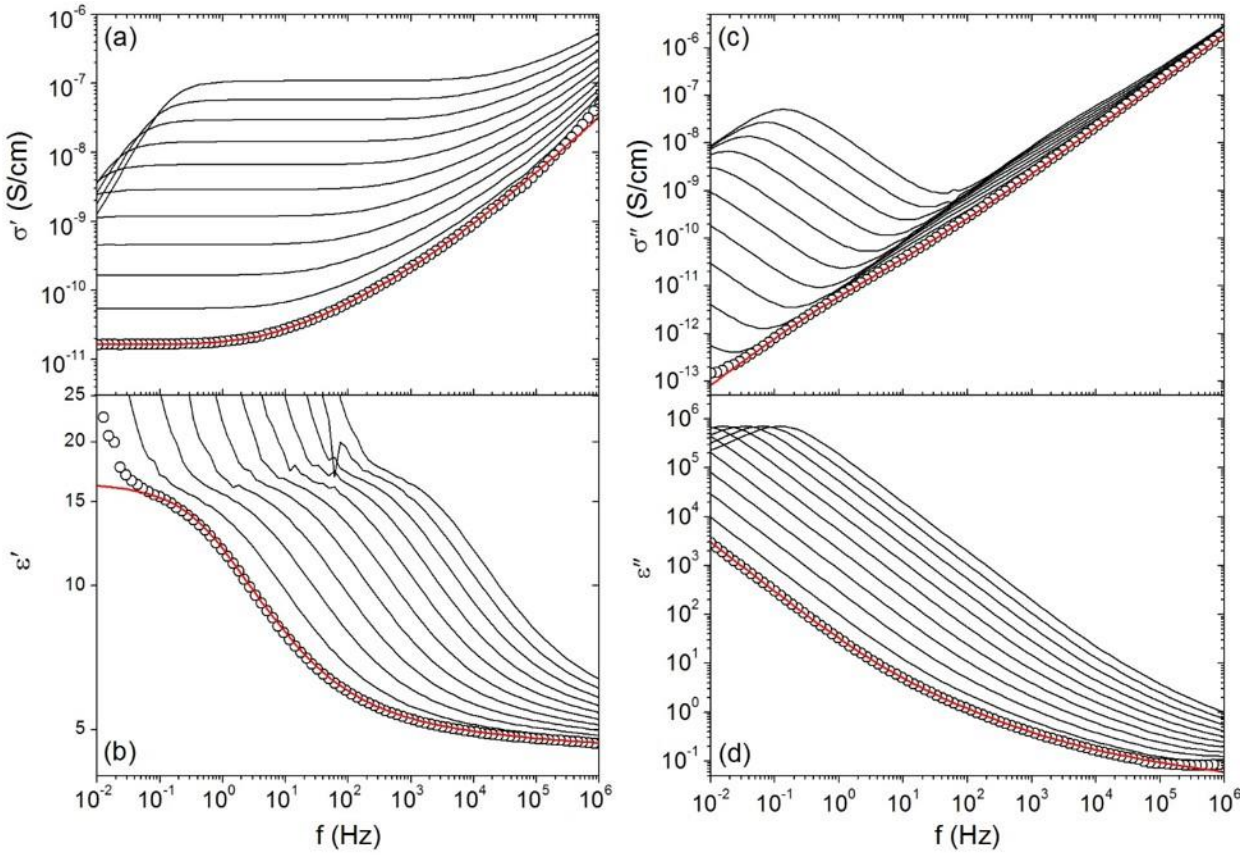

Figure 4.3. Real (a,b) and imaginary (c,d) parts of the complex conductivity σ and permittivity ε* spectrum of [BMIM][TFA] are shown at several temperatures in the supercooled liquids regime. The red line is a fit to the data using the combined Random Barrier Model and Havriliak Negami function (Eq. 4.6).*

The complex dielectric function (ε^* or σ^*) contains the information necessary to characterize the charge transport properties in ionic liquids. The most important and pertinent information that we are interested in extracting is twofold: what is the intrinsic dc conductivity as a function of temperature and what is the characteristic ion-hopping rate in these materials? Similar to the analysis of the quasielastic light scattering data, the spectral shape, as well as the presence of additional relaxation processes, will also aid in unravelling the charge transport mechanism in ILs. The main tool we will use to model the dielectric spectra and determine the

characteristic ion hopping rate in ionic liquids is known as the Random Barrier Model (RBM) of ion conduction in amorphous materials.

As discussed in the literature review section, the RBM makes few assumptions in order to analytically determine the complex dielectric function associated with the ion hopping process in amorphous materials. There are other analysis techniques and empirical models for ion conduction, but the RBM is the only theoretical framework which provides a physical insight into the dielectric spectrum in these materials.[114, 116, 117] In the RBM, ion motion occurs as a sequential, Brownian-like hopping process through a spatially heterogeneous energy landscape. Each ion is located in a different site in the liquid, and in order to hop to the next site, these ions must overcome an energy barrier which is completely uncorrelated to any of the corresponding sites. When the ion hops from its original position to the next site, the counter-ion solvation cloud undergoes rearrangement in order to re-solvate the new ion configuration. This solvent reorganization results in the fluctuation of a virtual dipole moment, analogous to the reorientational polarization process in dipolar liquids. As a consequence, the motion of ions exhibits a step like frequency dependence of the real part of the dielectric permittivity, as is seen in Fig. 4.3(b) for [BMIM][TFA].

The complex dielectric function associated with ion motion in the framework of the RBM has been solved analytically in the continuous time random walk approximation,

$$i\omega\varepsilon_0\varepsilon^*(\omega) = \sigma^*(\omega) = \sigma_0\left(\frac{i\omega\tau_e}{\ln(1+i\omega\tau_e)}\right) \tag{4.5}$$

where σ_0 is the plateau (dc) conductivity and τ_e is the characteristic ion hopping rate.[116] It has been demonstrated that the RBM (Eq. 4.5) fits the dielectric spectrum of many room temperature ionic liquids with minor deviations.[81] Furthermore, it was recently demonstrated that for the ionic melt Calcium-Potassium-Nitrate (CKN), a homogenous melt whose ions possess negligible

permanent dipole moments, the RBM model almost identically reproduces the dielectric spectrum.[59] In the three imidazolium ILs presented in this chapter, the RBM successfully describes the high frequency tail of the ion hopping process, but a sizeable part of the dielectric spectrum is left unaccounted for, as seen in Fig. 4.4. To account for this discrepancy, we have phenomenologically added an additional relaxation process to the model in order to completely fit the spectrum. The fitting function used to model the dielectric spectrum of the ILs presented in this dissertation is

$$i\omega\varepsilon_0\varepsilon^*(\omega) = \sigma^*(\omega) = \sigma_0\left(\frac{i\omega\tau_e}{\ln(1+i\omega\tau_e)}\right) + i\omega\varepsilon_0\left(\varepsilon_\infty + \frac{\Delta\varepsilon_{\mathrm{HN}}}{(1+(i\omega\tau_{HN})^\alpha)^\beta}\right) \quad (4.6)$$

where the first additive contribution is the Random Barrier Model and the second additive contribution is the Havriliak Negami (HN) Function. For the ILs presented in this chapter, the second relaxation function was always found to have a Cole-Cole spectral shape (i.e. $\alpha = 1$).

While the origin of this additional Cole-Cole relaxation is not known, there are several potential sources for its presence in the spectrum. A natural hypothesis is that it may arise from the rotational motion of permanent dipole moments which lie on these ionized molecules. From a qualitative standpoint, the molecular structures presented in Fig. 4.1 all have highly electronegative components of the ions, and these components of the molecules may give rise to permanent dipole moments. Because of the ionic and dipolar nature of these liquids, it is straightforward to expect that they would have a dielectric spectrum composed of an ion hopping process that is coupled to the ion rotation process. Another possibility for this dielectric relaxation is the existence of nanophase segregation of the apolar alkyl tails on the imidazolium cations from the charged parts of the liquid matrix.[153] These domains are insulating, and have dramatically different dielectric properties when compare to the ion rich domains. As a consequence of this, the interface between the ionic and neutral parts of the system may become

polarized due to the accumulation of space charges, and this effect is called Maxwell-Wagner-Sillars (MWS) polarization.[119] The exact manner in which this process might contribute to the spectrum will be explored in more detail in Ch. 5.

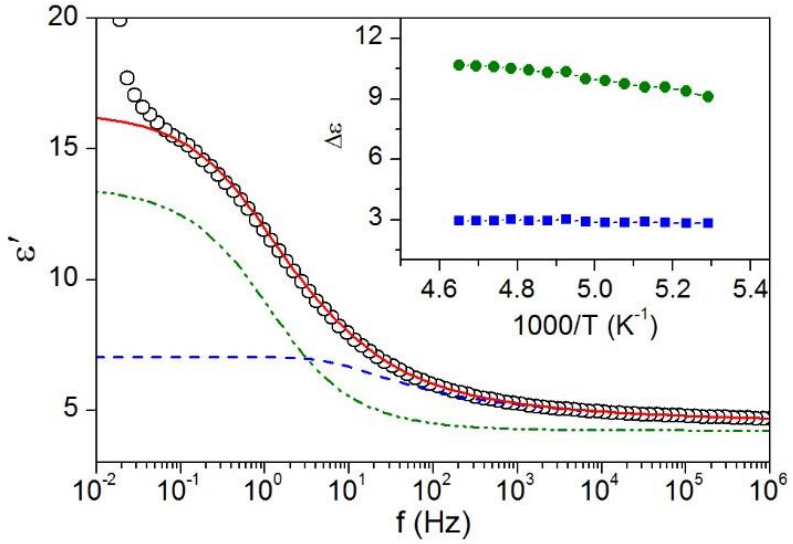

Figure 4.4. The detailed fitting of the real permittivity of [BMIM][TFA] using eq. 4.6 is shown at one temperature. The dashed blue line is the contribution from the Random Barrier Model, the green dashed-dotted line is the contribution from the Cole-Cole relaxation, and the red line is the cumulative fit. The inset presents the dielectric strength of the RBM and CC process as a function of inverse temperature.

As can be seen in the inset of Fig. 4.4, the dielectric strength of the CC process in [BMIM][TFA] decreases slightly in the temperature range measured via dielectric spectroscopy, and this is unusual for a reorientational relaxation process in a dipolar fluid.[119] This might indicate that anti-ferroelectric like ordering of the ionic dipole moments becomes enhanced with decreasing temperature. The dielectric strength of the CC relaxation in the other [BMIM] ionic liquids was also found to exhibit similar temperature dependence, and the absolute values of the CC dielectric strength ($\Delta\varepsilon \approx 9$-$11$) were observed to be similar for the three ILs. The spectral

shapes of the CC processes were found to be nearly identical, with $\alpha_{cc} = 0.75$ for [BMIM][TFA], $\alpha_{cc} = 0.70$ for [BMIM][NTF_2], and $\alpha_{cc} = 0.73$ for [BMIM][PF_6]. Additionally the spectral shape was found to be temperature independent over the studied temperature range in these ILs, as has been observed for several other ionic liquids. While it is still not possible to precisely determine the origin of the CC relaxation with the above experimental facts, the data suggest that the CC relaxation is not related to the details of the anion chemical structure. Since the spectral shape and amplitude of the CC relaxation is invariant for these three ILs, it is instead probable that this contribution to the dielectric function and the ion transport process is specifically connected to the properties of the [BMIM] cation, or it may be related to properties on a more coarse-grained scale.

4.3.3. Conductivity, ion diffusion rate, and free ion concentration in [BMIM] ILs

The first goal of this section will be to understand how the anion structure influences the conductivity in imidazolium ILs. The second goal is to understand how the chemical structure of the anions affects the diffusion coefficients and number density of free ions. The number density of "free" ions can be thought of as the amount of ions that are simultaneously breaking out of their solvation environments and transporting charge through the liquid matrix. Of course, the remaining ions are not free, and they may be in paired states, or their net charge may be counterbalanced by a symmetrical counterion solvation shell. This second counterion solvation structure is most likely the mechanism of ion neutralization in these ILs. Looking at the dielectric spectrum, it is clear that there is no dielectric relaxation associated with ion pairs. The effective dipole moment of an ion pair and the corresponding dielectric strength would be much larger than what is observed in the dielectric spectrum of the imidazolium ILs (Fig. 4.3) (the dielectric strength for discrete ion pairs spaced a distance of 4 Å would be approximately $\Delta\varepsilon \approx 20\text{-}25$), and

this indicates that the ion–solvation shell structure has some degree of symmetry.[90] Secondly, x-ray diffraction measurements and MD simulations both suggest that discrete ion pairs do not exist in the liquid structure of many types of ILs.[88]

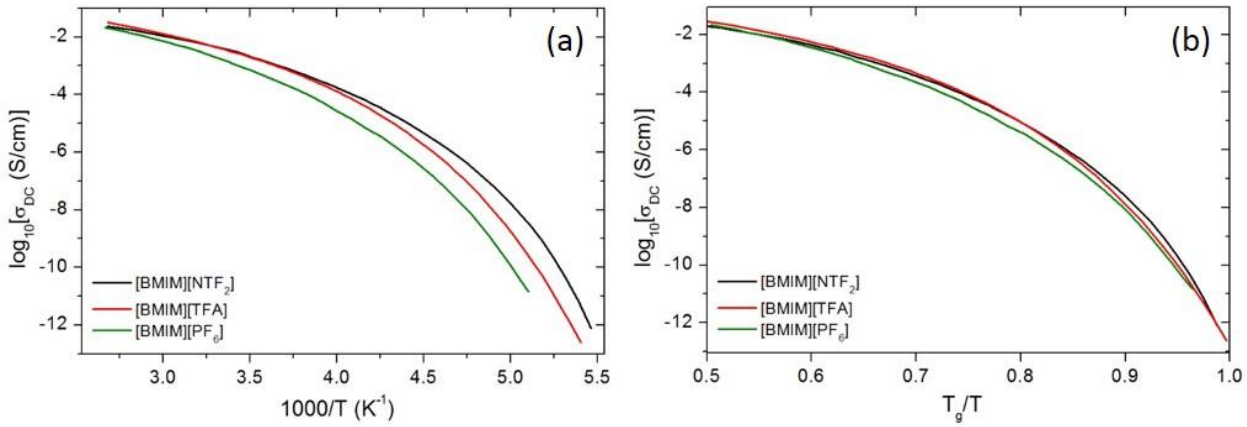

Figure 4.5. (a) DC conductivity of the three imidazolium based ionic liquids is shown plotted against inverse temperature. (b) When the temperature axis is scaled by T_g, it can be seen that these ILs have slightly different approaches toward T_g, i.e. different dynamic fragility.

Figure 4.5(a) presents the dc conductivity σ_0 (or σ_{DC}) as a function of inverse temperature for the three [BMIM] ionic liquids studied in this chapter. The conductivities at high temperature are all very similar with values exceeding 0.01 S/cm at 350 K. As these materials are supercooled toward their respective glass transition temperatures, the dc conductivities decrease, analogously to the slowing of the molecular reorientation rates observed in the QELS measurements. The major differences between the conductivities of these ILs are observed at low temperature, where it is seen that the conductivity of [BMIM][NTF_2] becomes increasingly larger than the other two ILs at any given temperature. At the lowest measured temperatures, the conductivity of [BMIM][NTF_2] is larger than that of [BMIM][PF_6] by more than three orders of

magnitude. The natural question to ask is are these differences in conductivity due to a difference in the ion mobilities, free ion concentration, or a combination of both of these factors? Furthermore, are these changes related to the chemical structure of the ions?

The calorimetric glass transition temperatures T_g for these ionic liquids were measured via Differential Scanning Calorimetry and are as follows: T_g = 191 K for [BMIM][PF_6], T_g = 186 K for [BMIM][TFA], and T_g = 181 K for [BMIM][NTF_2]. By comparing the glass transition temperatures, we can qualitatively characterize the relative molecular or ionic mobility in these materials. A liquid with a lower T_g will tend to have a higher mobility at any given temperature when compared to a liquid with a higher T_g.[4] It is possible to directly compare the relative conductivities of these three ILs by plotting the dc conductivities on the normalized T_g/T x-axis (the so-called Angell plot). This type of plot focuses more on the curvature of a dynamical quantity (such as conductivity, relaxation time, or diffusion coefficient) approaching T_g, i.e. the dynamic fragility $m = \left.\frac{dlog_{10}(X)}{d(\frac{Tg}{T})}\right|_{T=T_g}$.[25] It can be seen in Fig. 4.5(b) that relative to their calorimetric glass transition temperatures, the dc conductivities are very similar with only slightly different curvatures in their approach toward T_g. It is evident that the major effect of changing the anion in these imidazolium based ILs is to modify their respective glass transition temperatures, and thus their ionic mobilities at any given temperature.

In addition to the ILs presented herein, we will provide a more detailed assessment of the influence of the anion chemical structure on T_g (and thus the dc conductivity) by referring to measurements of T_g in [BMIM] based ILs from the literature. It can be seen in table 4.1 that the molecular weight plays a role in determining T_g—as the size of the anion increases, the glass transition temperature seems to decrease.[62] This is straightfowardly understood because the

charge distribution on the anion becomes more spread out, and the distance between counterions increases with increasing ion size which results in a reduction in the cohesive energy and the electrostatic friction between counterions.[154] This reduction in counterion friction allows for higher ion mobility at any given temperature. However, it is also seen in Table 4.1 that this trend is not strictly observed. For [BMIM][NO_3] the ion size is similar to the halide based ionic liquids, yet the glass transition temperature is nearly 30 K lower. This break in the trend is likely due to the fact that the $[NO_3]^-$ ion is asymmetrical, resulting in a more loosely formed counterion coordination structure, less electrostatic friction, and relatively higher mobility (lower glass transition temperature).

Table 4-1. Glass transition temperature, molecular weight, and assessment of the symmetry of the anion for a series of 1-butyl-3-methylimidazolium based ionic liquids.[155-157]

Ionic Liquid Chemical Name	Glass Transition Temperature T_g (K)	Molecular Weight M_W (g/mol)	Spherical Symmetry? (Y/N)
1-butyl-3-methylimidazolium chloride [BMIM][Cl]	225	174.7	Y
1-butyl-3-methylimidazolium bromide [BMIM][Br]	221	219.1	Y
1-butyl-3-methylimidazolium iodide [BMIM][I]	215	266.1	Y
1-butyl-3-methylimidazolium nitrate [BMIM][NO_3]	188	203.2	N
1-butyl-3-methylimidazolium tetrafluoroborate [BMIM][BF_4]	186	226.0	Y
1-butyl-3-methylimidazolium hexafluorophosphate [BMIM][PF_6]	191	284.18	Y
1-butyl-3-methylimidazolium trifluoroacetate [BMIM][TFA]	186	252.23	N
1-butyl-3-methylimidazolium bis(trifluoromethylsulfonyl)imide [BMIM][NTF_2]	181	419.4	N

Having determined how the anion chemical structure influences the dc conductivity in [BMIM] based ILs, we now turn to the question of how it separately influences ion mobility and free ion concentration. Conductivity is defined according to the Einstein relation such that

$$\sigma_0 = \frac{(n_+ D_+ q_+^2 + n_- D_- q_-^2)}{kT} \tag{4.7}$$

where k is Boltzmann's constant, $n_{+,-}$ is the number density, $D_{+,-}$ is the diffusion coefficient, and $q_{+,-}$ is the charge of positive and negative ions in the liquid.[55] In order to have a complete picture of the ion transport properties in these ILs, it is necessary to characterize n and D. Based on the assumption that the constituent ions undergo Brownian motion, and that the average rate of transport of a free, charge carrying ion is equivalent to the average rate of transport of a counterbalanced ion, it is possible to calculate the characteristic ion diffusion rate D and free ion concentration n_{free} from analysis of the dielectric spectrum in ionic liquids. This method has been shown to provide values of D and n_{free} which quantitatively agree with measurements by other experimental techniques.[80, 81] Through our studies, we have also verified the applicability of this technique in calculating ion diffusion rates and free ion concentrations.[93, 146]

Assuming ions undergo Brownian motion, the ion diffusion coefficient may be calculated such that $D = \frac{\lambda^2}{2\tau_e}$, where τ_e is the characteristic ion hopping rate determined from analysis of the dielectric spectrum using the RBM, and λ is the temperature independent characteristic ion hopping distance. The parameter λ cannot be measured directly, and it is instead determined by quantitatively comparing the diffusion coefficients calculated from the dielectric spectroscopy technique to those measured by Pulsed Field Gradient Nuclear Magnetic Resonance (PFG NMR)—the process of which will be demonstrated below. It has been shown experimentally that the diffusion coefficients of cations and anions are nearly identical ($D_+ \approx D_- = D$)[83], and since n_+

$= n_- = n$, and $q_+ = -q_- = e$ (the elementary charge), we arrive at the expression connecting free ion concentration, dc conductivity, and ion hopping rate

$$\sigma_0 = \frac{2ne^2D}{k_BT} = \frac{ne^2\lambda^2}{k_BT\tau_e} \tag{4.8}$$

Having measured σ_0 and τ_e, the first step in this process is to guess a value of λ (approximately 1 Å), and then calculate the free ion concentration via eq. 4.8. This quantity is shown in fig. 4.6 for the three [BMIM] ionic liquids plotted as a function of inverse temperature.

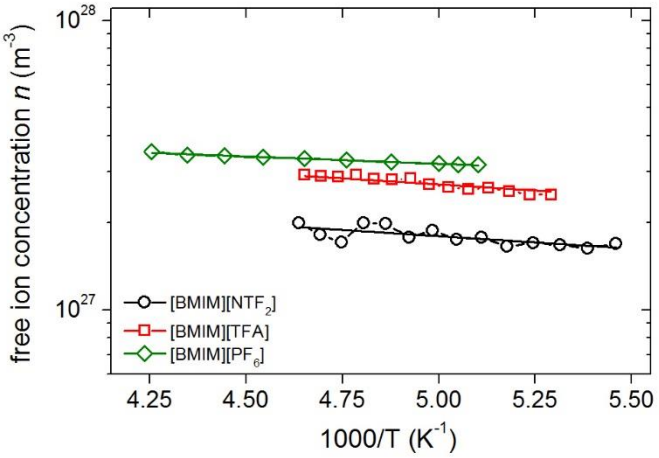

Figure 4.6. Free ion concentration n determined from analysis of the dielectric spectra for the [BMIM] based ionic liquids is plotted against inverse temperature. It is seen that this quantity varies only weakly with temperature for all three ILs.

It can be seen in Fig. 4.6 that the free ion concentration follows an Arrhenius temperature dependence $n = n_0 \exp(-\frac{E_A}{kT})$ over the measured temperature range, and the activation energy E_A is independent of the choice of the parameter λ. It instead depends on the temperature dependent product of σ_0 and τ_e, and the value of λ will merely shift the data up or down on the *y*-axis of Fig. 4.6. The free ion concentration activation energies for these three ionic liquids are observed to be very similar, indicating the specifics of the anion chemical structure play only a minor role in the

ion solvation environment. The activation energies E_A and infinite temperature ion concentrations n_0 are as follows: E_A/k_b = 120 K, $n_0 = 5.75 \cdot 10^{27}$ m^{-3} for [BMIM][PF_6], E_A/k_b = 190 K, $n_0 = 7.10 \cdot 10^{27}$ m^{-3} for [BMIM][TFA], and E_A/k_b = 200 K, $n_0 = 4.83 \cdot 10^{27}$ m^{-3} for [BMIM][NTF_2].

With the activation energy determined from the Arrhenius fitting of the free ion concentration, the functional form of n is inserted back into eq. 4.8 in order to calculate D over the entire temperature range for which the dc conductivity was measured. Thus we are assuming that the activation energy of ion association is identical at all temperature where the IL is in the liquid/supercooled liquid state, which has not been explicitly verified. This assumption is made because the ion hopping rate can only be characterized at lower temperatures, while the dc conductivity can be measured over a very wide temperature range. The calculated D is then compared to the independently measured D (by PFG NMR), and in an iterative manner, the parameter λ is adjusted and the above steps are applied until the calculated BDS diffusion coefficients overlap with the diffusion coefficients measured directly via PFG NMR. The hopping length λ, the free ion concentration n, and diffusion coefficient D have been successfully characterized once the diffusion data are observed to overlap with minimum error. The final results of the so-calculated diffusion coefficients of the three [BMIM] ILs are shown as a function of inverse temperature in Fig. 4.7(a), and the final results for the so-calculated free ion concentration are shown in Fig. 4.6. It is necessary to use this iterative BDS technique because measurements of diffusivity via PFG NMR are restricted to higher temperatures where the IL is in the highly fluid state, and there are no other straightforward experimental techniques to measure self-diffusion coefficients in such a broad temperature range. The values of the ion hopping length λ are as follows: λ = 0.64 Å for [BMIM][TFA], λ = 0.91 Å for [BMIM][PF_6], and

λ = 1.10 Å for [BMIM][NTF_2]. The hopping length λ correlates with molecular weight and volume in these three ILs, as has been observed previously for other types of ILs.[158]

The measured diffusion coefficients in these three ILs exhibit nearly identical trends as observed for the anion chemical structure dependence of the dc conductivity. This implies, once again, that the vast majority of the effect of changing the anion chemical structure is to change the glass transition temperature and the free ion mobility. The diffusion coefficients also differ slightly relative to T_g (Fig. 4.7(b)), indicating that the kinetic pathway toward vitrification and the dynamic fragility *m*, are only slightly influenced by the anion chemical structure.

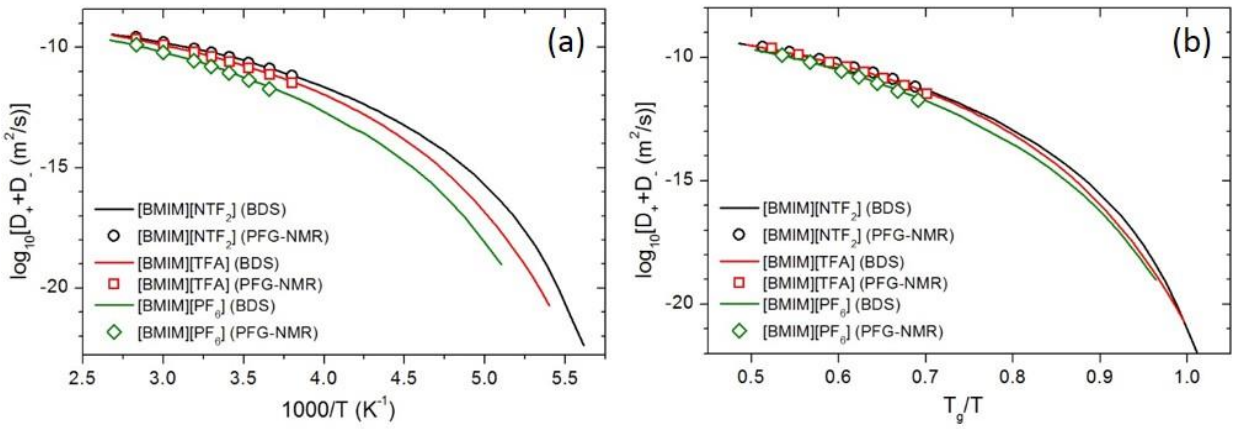

Figure 4.7. (a) Total diffusion coefficient plotted against inverse temperature for the three [BMIM] ionic liquids. (b) Normalized by T_g, it is seen that the diffusivity of these ILs show only minor differences, much like the results obtained for the dc conductivity.

The free ion concentration has been found to vary only weakly among the three different ionic liquids, with [BMIM][PF_6] having the largest free ion concentration and [BMIM][NTF_2] having the lowest free ion concentration—approximately 1.5 times lower than [BMIM][PF_6]. There is no apparent correlation between the free ion concentration and anion chemical structure/molecular size. In addition to the effects of ion association, the free ion concentration

also includes the effects of density and molecular weight on the amount of free ions in the liquid. For a less dense, higher molecular weight ionic liquid, there will simply be a smaller concentration of total ions in the liquid. From a technological standpoint, the free ion concentration is the most relevant quantity to increase conductivity, whereas the mole fraction of free ions provides a more thorough picture of how ions are associating, independent of the ion size and structure. The room temperature (295 K) mass densities of these ILs were taken from the literature (as reported in the experimental section) in order to calculate the number density of total ions, $n_{tot} = 2\rho_m M_W N_A$, where ρ_m is the mass density, M_W is the molecular weight, N_A is Avogadro's number, and the factor of two accounts for the fact that there are two counter ions per ionic liquid molecule. The free ion concentration at 295 K for each IL was calculated using the Arrhenius fitting of the free ion concentration data seen in Fig. 4.6. The mole fraction of free ions at 295 K were then calculated such that $f_{free\ ions} = \frac{n_{free}}{n_{tot}}$, and the values are as follows: f_{free} = 0.56±0.05 for [BMIM][TFA], f_{free} = 0.66±0.05 for [BMIM][PF_6], and f_{free} = 0.57±0.05 for [BMIM][NTF_2].

It is very interesting that the majority of ions in these three [BMIM] ionic liquids are "free" at any given instant in time. This suggests that the interactions between counterions are very weak and well solvated, which is also apparent in the low activation energy of the free ion concentration. It is also interesting that the anion chemical structure does not significantly alter the mole fraction of free ions in these [BMIM] based ionic liquids. Although the molecular sizes are not dramatically different, this result suggests that either the ion association/solvation environment is significantly more dependent on the details of the chemical structure of only the cation, or the ion solvation environment depends much more on the coarse-grained electrostatic interaction between ions. The second of these explanations is in line with independent x-ray

diffraction studies of numerous kinds of ionic liquids, where it has been demonstrated that the static structure factors of ionic liquids show very similar features despite dramatically different ionic chemical structures.[89, 159, 160] While our current study does not conclusively answer this question, it certainly narrows the possibilities to two very different scenarios, and provides corroborative evidence to the coarse-grained picture of the ionic liquid solvation environment scenario. Of course there are exceptions to this picture, as we will see in the next chapter.

4.3.4. Translation-rotation decoupling, dynamic crossover, and non-exponential relaxation

Having characterized the charge transport characteristics in the [BMIM] based ionic liquids presented above, we now will analyze the influence of the anion chemical structure on the glassy dynamics in these ILs. The temperature dependence of ion diffusion (translational motion) measured via BDS and structural α relaxation times (rotational motion) measured via DLS are strongly non-Arrhenius for these three [BMIM] based ionic liquids (Figs. 4.7, 4.8), as is characteristic of most glass forming liquids. To quantify the degree of deviation from Arrhenius temperature dependence, the fragility *m* is commonly used and is defined as

$$m = \left. \frac{d \log \tau_\alpha}{d\frac{T_g}{T}} \right|_{T=Tg} \tag{4.9}$$

where T_g is the dynamic glass transition temperature.[25] Defining T_g as the temperature at which the α- relaxation time is 100 s, we have calculated the fragility and dynamic T_g for each RTIL (for [bmim][PF_6], m = 75 and T_g = 191 K; for [bmim][TFA], m = 80 and T_g = 186 K; for [bmim][NTf_2], m = 95 and T_g = 181 K). The dynamic glass transition temperatures were found to agree well with the calorimetric glass transition temperatures. As can be seen, an increase in anion size and asymmetry ([PF_6] < [TFA] < [NTf_2]) leads to an increase in fragility. As the ion size and asymmetry increase, the molecular packing becomes increasingly frustrated, which

generally leads to more fragile type of thermal activation of molecular motion in the liquid.[161, 162] According to the Generalized Entropy Theory, the fragility of a liquid is dependent on how efficiently molecules can pack together in the liquid structure.[163] As the packing efficiency is decreased, the molecular motion becomes frustrated which results in precipitously slower molecular motion. Our results on ionic liquids fit well with this picture. What is unique about this result is that for these three ionic liquids, fragility *m* is anti-correlated with the glass transition temperature T_g. It has been suggested through analysis of numerous small molecule and polymeric liquids that *m* should be correlated with T_g.[26] Ionic liquids clearly provide a counter example to this correlation.

It can be seen in Fig. 4.8 that the ionic diffusion process for all three ILs has slightly weaker temperature dependence than the α relaxation process measured via DLS. This phenomenon of enhanced diffusion, or decoupling of diffusion from structural relaxation has been observed in numerous other glass forming liquids.[38] The Debye-Stokes-Einstein (DSE) and Stokes-Einstein (SE) relations predict that in simple liquids, translational and rotational diffusion times are proportional to one another, and the proportionality constant is independent of temperature (the ratio $R = D \cdot \tau_\alpha$ should be constant with temperature). This ratio has been shown to hold at high temperatures, from above the melting point down to the dynamic crossover temperature T_C for many glass forming liquids.[38] It has been demonstrated for numerous glass forming liquids, however, that *R* changes dramatically as T_g is approached. To account for the temperature dependence of *R*, a fractional SE-DSE relation was proposed in which *R* depends on the structural relaxation time via a power law, i.e. $R = D \cdot \tau_\alpha \propto {\tau_\alpha}^{\varepsilon}$, where ε characterizes the degree to which the diffusion and structural relaxation are decoupled from one another.[164] For the van der Waals glass forming liquid trisnaphthylbenzene (TNB), *R* changes by nearly two

orders of magnitude from high temperature to T_g, with $\varepsilon \approx 0.15$, and for ortho-terphenyl (OTP), R changes by slightly more than two orders of magnitude, with $\varepsilon \approx 0.25$.[54]

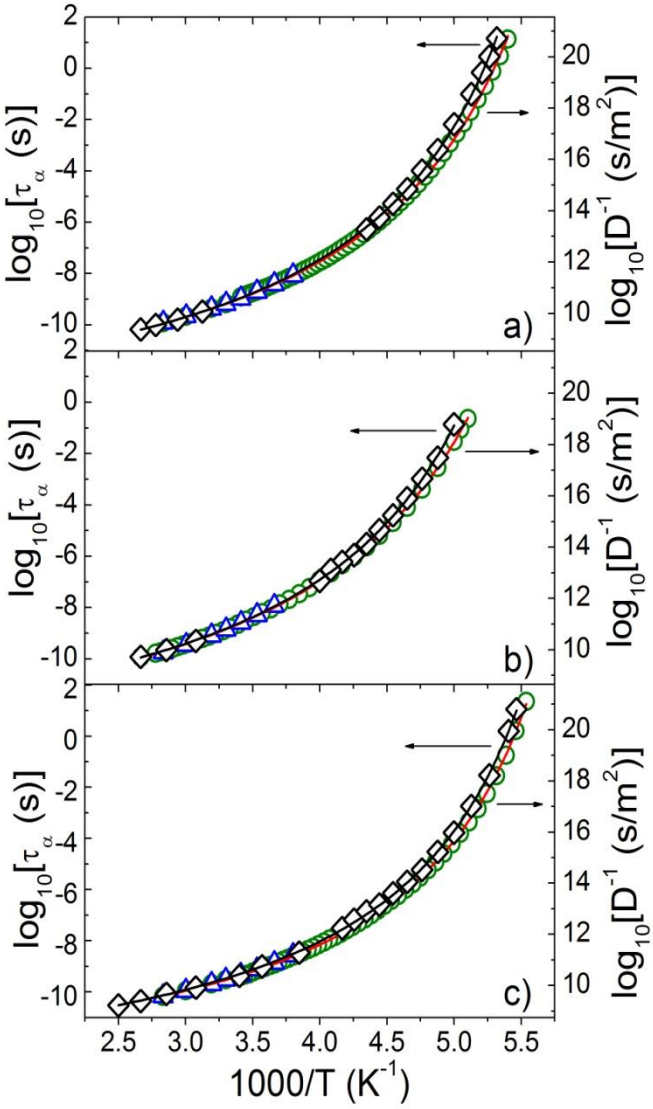

Figure 4.8. Structural relaxation times (black diamonds), BDS diffusion coefficients (open circles), and PFG NMR diffusion coefficients from literature (open triangles) are plotted against inverse temperature for (a) [BMIM][TFA], (b) [BMIM][PF_6], and (c) [BMIM][NTF_2]. The black and red lines are Vogel-Fulcher-Tammann fits to the structural relaxation times and diffusion coefficients, respectively.[146]

The ratio *R* characterizing the decoupling of the diffusion and structural relaxation times for the three [BMIM] based ILs has been analyzed in terms of the fractional DSE relation (Fig. 4.9). It is seen that the ratio *R* changes with relaxation time nearly identically for the three RTILs, and clearly there is no effect of the anion chemical structure on the relationship between translational and rotational motion in these ionic liquids. With *R* changing by less than one order of magnitude from high temperature down to T_g, the decoupling exponent ε is approximately 0.10 ± 0.01 for the three ILs. It has recently been proposed that the decoupling exponent should correlate to the fragility index *m* of the structural relaxation process.[165] Clearly, the fragility independent decoupling in these ILs does not follow this expectation. Perhaps most interesting is that the strength of decoupling, as characterized by ε, is unexpectedly weak for these ILs when compared to other glass forming liquids of similar fragility, such as OTP (*m* = 80) and Ca-K-(NO_3) (*m* = 100), where the decoupling exponents are approximately 0.25 and 0.35, respectively.[57, 93]

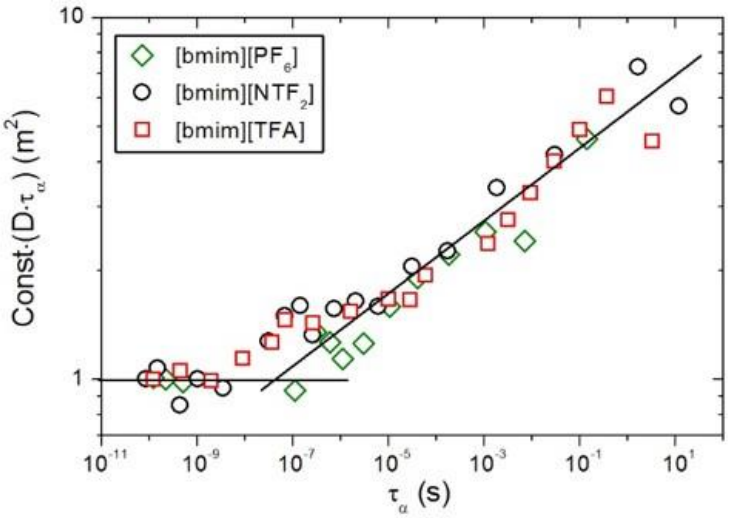

Figure 4.9. Decoupling ratio for the [BMIM] ionic liquids plotted against structural relaxation time. It is seen that all ILs exhibit an identical functional form and depart from the high temperature/fast relaxation time constant value in the vicinity of 10^{-8} s.

The pronounced change in the quantity *R* is thought to stem directly from the effects of dynamical heterogeneity in glass formers.[166] It is hypothesized that regions of varying molecular mobility first form then begin to grow as a supercooled liquid is cooled toward T_g. These regions consist of dynamically correlated molecules, some of which are essentially frozen compared to the average mobility, while some consist of highly mobile molecules. The structural relaxation time, when measured with depolarized light scattering, is an average of all sampled relaxation times $\langle\tau\rangle$, while the diffusion coefficient is an average of all sampled inverse relaxation times $\langle\tau^{-1}\rangle$. Thus, the measured α relaxation time is weighted by the slow components of a hypothetical distribution of relaxation times, while the measured diffusion coefficient is weighted by fast components of the distribution.

According to the barrier hopping theory of Schweizer *et al.*, dynamical heterogeneity becomes increasingly prominent and the relaxation time distribution widens, leading to an increase in the difference between $\langle\tau\rangle$ and $\langle\tau^{-1}\rangle$ as a glass forming liquid is cooled toward T_g.[58] One of the conclusions of this theory is that temperature dependent decoupling of the structural relaxation time and diffusion coefficient is caused by a temperature dependent increase in the distribution of relaxation times, i.e. a temperature dependent stretching parameter, β_{KWW}. This conclusion is challenged, however, by experimental studies of the glass formers OTP,[167] TNB,[168] and Ca-K-(NO_3).[169] The decoupling is quite pronounced in these liquids even though they exhibit temperature independent stretching of the α relaxation process close to the T_g.

As can be seen from Fig. 4.10, all three RTILs also have temperature independent stretching of the α relaxation process with $\beta_{\mathrm{KWW}} = 0.62\pm0.02$ for [BMIM][TFA], $\beta_{\mathrm{KWW}} = 0.61\pm0.02$ for [BMIM][NTF_2], and $\beta_{\mathrm{KWW}} = 0.55\pm0.02$ for [BMIM][NTF_2]. These examples conclusively show that there is no direct connection between the temperature

dependence of the stretching of the α relaxation process and the temperature dependence of translational-rotational decoupling in glass forming liquids, contrary to the Barrier Hopping Theory. It is very interesting that the observed temperature dependence of β_{KWW} in OTP and Ca-K-(NO_3) occurs primarily before the decoupling of diffusion and structural relaxation sets in, and not alongside the decoupling phenomenon. This result suggests that temperature dependent stretching of the structural relaxation process might be a precursor to strong decoupling of translational and rotational degrees of freedom. The phenomenon of decoupling is not well understood, and these results suggest that rotational and translational degrees of freedom may be correlated in strongly interacting molecular liquids such as ionic liquids.

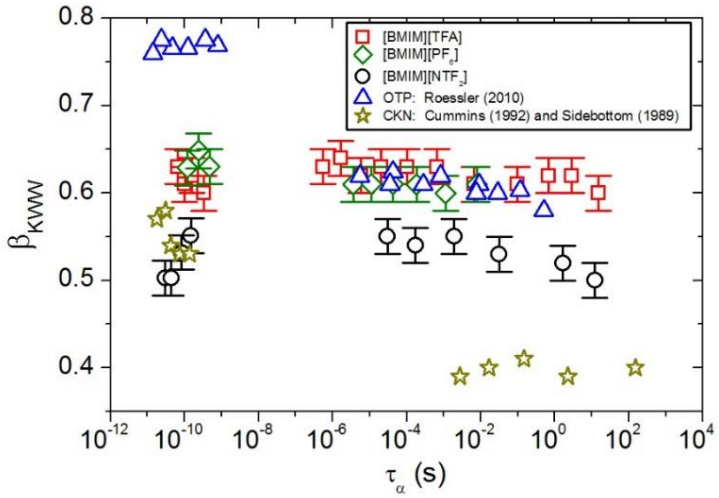

Figure 4.10. The stretching (nonexponentiality) parameter β_{KWW} is constant over the entire studied range of temperatures and relaxation times for the three [BMIM] ionic liquids. This unique feature distinguishes these liquids from other glass formers which can be clearly seen to exhibit a change in β_{KWW} in the vicinity of 10^{-7} s.[146, 169-171]

Commonly associated with translation-rotation decoupling and the onset of dynamical heterogeneity is the existence of two distinct dynamical regions in which the structural relaxation time of a glass forming liquid exhibits different temperature dependences. As described in the

literature review chapter, it has been shown that in each of these two distinct regions, different Vogel-Fulcher-Tammann (VFT) functions are required to describe the experimental data. Stickel, et al. proposed a derivative analysis technique that can identify the existence of a change in temperature dependence of the structural relaxation time.[31, 172] In Stickel's derivative analysis, the quantity $Z = (\frac{-dlog_{10}(X)}{dT})^{-0.5}$ is calculated, where *X* is the characteristic dynamic quantity under question (relaxation time or inverse diffusion coefficient). If the relaxation times follow a VFT temperature dependence, then *Z* will appear as a straight line in temperature. In the case of most glass forming liquids, the temperature dependence of a relaxation process usually changes from one VFT behavior to another at some dynamic crossover temperature, T_B. This temperature can be determined by locating the intersection of two straight lines of different slope when analyzed with this derivative technique. It has been shown that for those liquids with a clear signature of a Stickel crossover, one VFT equation cannot accurately describe the temperature dependence of relaxation times.[172]

The DLS α relaxation times and diffusion rates have been analyzed with this derivate technique. From the inset of Fig. 4.11, it is seen that there is no indication of a change in VFT temperature dependence of the α relaxation time in any of the three ILs. In order to more clearly show this, the α relaxation times were fit using single VFT functions over the entire temperature range (Fig. 4.11). The residuals of these least squares VFT fits oscillate randomly about zero for all three ILs. The temperature dependence of the structural relaxation time in these ILs is much different than other glass formers of similar fragility, such as OTP, salol, propylene carbonate, and Ca-K-(NO_3), which all exhibit a dynamic crossover in the temperature dependence of their relaxation times.[172] While this figure is not presented, the Stickel derivative analysis of the diffusion coefficients in these ILs also show no dynamic crossover temperature.

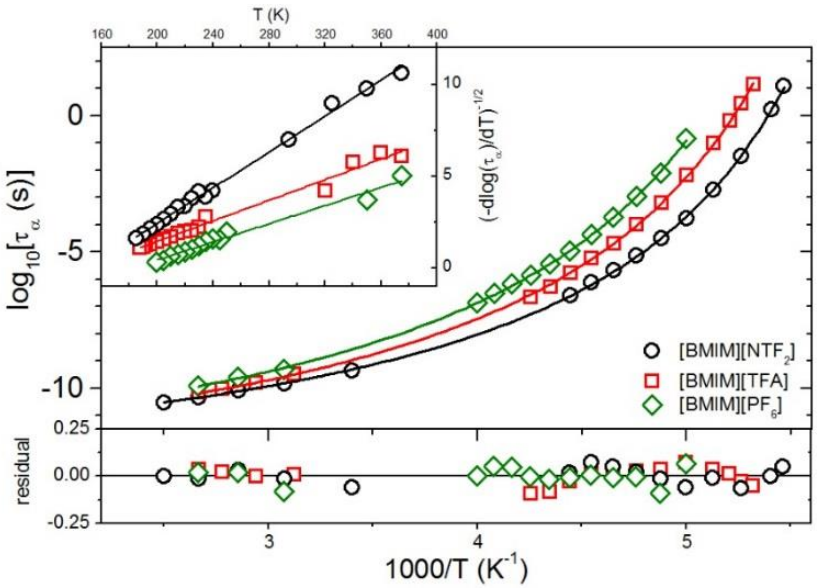

Figure 4.11. Relaxation times determined from dynamic light scattering for the three ILs are shown plotted against inverse temperature in the main pane. The solid lines are VFT fits to the experimental data, and it is seen in the residual inset that the data are fit with minimal error. The upper inset illustrates the Stickel derivative of the relaxation time data, once again illustrating the single VFT temperature dependnece of relaxation times in these ILs.[146]

It has been shown above that the structural relaxation process decouples from the diffusion process in the three [BMIM] based ILs presented herein. This is expected because numerous fragile glass-formers show decoupling of translational and rotational motions as the temperature decreases toward T_g. However, it is also clear that the strength of decoupling is significantly lower than is expected when compared to systems of similar fragility. As stated above, these ILs have a decoupling parameter ε equal to 0.10 ± 0.01 for the three systems, while OTP (fragility $m \approx 80$), for example, has been shown to exhibit a decoupling parameter ε approximately equal to 0.25.[57] This is a very significant difference, but it can be rationalized by considering the following. In these ILs, intermolecular interactions strongly influence the

molecular dynamics, and clearly, the most significant interaction between the ions comprising these liquids is the electrostatic interaction. However, the electrostatic interactions must not solely responsible for the weak decoupling in ILs because the ionic glass former Ca-K-(NO_3) exhibits exceptionally strong decoupling of translational and rotational motions ($\varepsilon \approx 0.35$).

The other important intermolecular interaction inherent to these three ILs is their propensity to form hydrogen bonds between cations and anions.[173] This hydrogen bonding provides a directional interaction between molecules and can serve as a link between the translational and rotational degrees of freedom. We hypothesize that as structural relaxation occurs, the cation will execute reorientational motions that orient it preferentially toward a new hydrogen bonding site. The cation will simultaneously translate by small steps through the liquid as it progressively makes and breaks hydrogen bonds with other molecules through the reorientation process. These rotational steps would occur in large angle jumps since there are only certain molecular moieties which might participate in hydrogen bonding. Indeed, it has been suggested in some recent studies that ion rotation occurs via a jump diffusion mechanism.[174] Based on this qualitative hypothesis we speculate that the strong influence of the hydrogen bond in the molecular motion of these RTILs is responsible for the unusually weak decoupling of translational and rotational motion near T_g. Following this hypothesis, it is also possible to explain the absence of decoupling in other liquids such as the network oxide SiO_2 because the intermolecular interactions present for the case of SiO_2 are purely covalent, and thus strongly directional in nature. We suspect that decoupling of translational and rotational motion would also be highly suppressed in other nonionic, hydrogen bonded liquids such as glycerol and propylene glycol.

As seen in Fig. 4.10, the stretching parameter β_{KWW} is temperature independent for all three ILs (Fig. 4.10), from significantly above the melting point down to the glass transition temperature. One interpretation of the nonexponentiality of the α relaxation process is that it is a result of intermolecular interactions and many body effects on the molecular dynamics.[137] This interpretation (the Coupling Model) states that the strength of the intermolecular interaction can qualitatively be determined by observing how stretched the α process is, with a smaller β_{KWW} (more stretched relaxation) indicating stronger intermolecular interaction. However, the Coupling Model predicts that near some crossover temperature, the liquid should transition from a state of nearly independent molecular motion at high temperature to a state of stronger intermolecular interactions, and thus cooperativity, at low temperature. As is seen in Fig. 4.9, both OTP and Ca-K-(NO_3) exhibit this transition, while the three ILs clearly do not exhibit any change in β_{KWW}. Considering the [BMIM] IL results in the framework of the Coupling Model, it follows that the intermolecular interactions that control structural relaxation at low temperatures persist well above the melting point in these three ILs.

Another explanation for the nonexponentiality of the structural relaxation process is that molecular dynamics are heterogeneous.[38] In this interpretation these results would mean that there is no change in the distribution of relaxation times or the dynamical heterogeneity profile in these ILs in the entire temperature range. Regardless of the interpretation of the stretching, it is alluring to relate the temperature dependence of β_{KWW} and the magnitude of decoupling when comparing the behavior of the RTILs, OTP, and Ca-K-(NO_3). Due to this observation, we speculate that the absence of temperature dependence of the stretching parameter β_{KWW} may be directly connected to the experimentally observed weak decoupling of diffusion and structural relaxation in these imidazolium based ILs.

4.4. Conclusions

In this chapter we have characterized the charge transport properties and reorientational relaxation dynamics in a series of 1-butyl-3-methylimidazolium ionic liquids. It has been shown that the efficiency of long range ion conduction in this set of ionic liquids is strongly dependent on the anion chemical structure. For smaller anions with more symmetrical chemical structures (such as the halides), the glass transition temperatures were shown to be significantly higher than the larger, asymmetrical anions (such as $[NTF_2]^-$). By analyzing the dielectric spectrum of these ionic liquids, it was determined that larger ion diffusion coefficients were mainly responsible for the increased ionic conductivity, and those liquids with lower glass transition temperatures consequently had relatively higher ion diffusivity. There was no clear correlation between anion chemical structure and free ion concentration in these materials, and it was demonstrated that these ionic liquids all have a majority of ions (approximately 60%) participating in conduction at room temperature. Our results suggests that ion association in these types of ILs is relatively weak and is primarily controlled by the coarse-grained nature of the screened electrostatic interaction between counterions. These results also suggest that local molecular friction and the structural relaxation process is the most important mechanism behind conduction in ionic liquids.

Having characterized the influence of anion chemical structure on the ion conduction properties in these materials, we next proceeded to analyze the structural dynamics in [BMIM] ILs and how they are influenced by the anion chemical structure. We have found that the fragility, i.e. the steepness of the temperature dependence of structural relaxation time, becomes significantly larger as the anion size and asymmetry increases. This observation was rationalized according to the Generalized Entropy Theory, which suggests that fragility is directly connected to the efficiency of molecular packing in liquids. It was also found that these ionic liquids show

dynamical characteristics which are unusual and significantly different from those of most molecular glass-forming liquids. The decoupling of translational and rotational motions, a currently unexplained phenomenon in glass transition research, was found to be unusually weak in these ILs, and furthermore it was observed to occur identically regardless of the anion chemical structure. Secondly, these ILs were found to exhibit no apparent dynamic crossover in the structural relaxation times (or self-diffusion). Finally, the spectral shape of the structural relaxation process was found to be temperature independent in these ionic liquids from above the melting point down to the glass transition temperature. These three experimental observations all illustrate that the dynamics of these types of ionic liquids show very interesting differences when compared to other molecular glass forming liquids. We have hypothesized that these phenomena are interrelated and may be a result of the directional character of the inter-ionic hydrogen bonding properties in these liquids.

5. Dynamics and Charge Transport in Ammonium Based ILs

5.1. Introduction

In the previous chapter, the influence of the anion chemical structure on the dynamics and charge transport properties was explored for a homologous series of imidazolium based room temperature ionic liquids. While the calorimetric glass transition temperatures of these liquids were found to systematically change with increasing anionic size and asymmetry, the relaxation spectra measured via dynamic light scattering and dielectric spectroscopy were demonstrated to show minimal variation with changing chemical structure. Additionally, the free ion concentrations exhibited minimal differences upon changing chemical structure. These experimental results indicated that the microscopic dynamics in the [BMIM] based ionic liquids are very similar, and they are primarily influenced by the screened coulomb interaction between counterions, as well as the specifics of the cation chemical structure. In order to understand the influence of the cation chemical structure on the physicochemical properties of room temperature ionic liquids in more detail, the structural dynamics and charge transport properties of a homologous series of tetra-alkylammonium bis(trifluoromethylsulfonyl)imide [Nxxxx][NTF_2] based ionic liquids will be explored in this chapter.

There have been several recent experimental and simulation studies which have investigated how variations in the chemical structure of the cations of room temperature ionic liquids lead to the formation of nanostructure and self-assembled nanodomains.[109, 110, 160] It is well known that molten salts exhibit a strong degree of mesoscale ordering of the counterions as a result of ion solvation.[14] For many ionic liquids and molten salts, the mesoscale structure associated with charge ordering is surprisingly similar and not strongly affected by counterion chemical structure.[160] In addition to this charge ordering, it has been shown that an even longer

length scale structural order occurs in room temperature ionic liquids with long aliphatic side groups. As a result of the amphiphilicity of these types of ILs, the neutral, aliphatic side groups tend to segregate from the charged parts of the ions, forming hydrophobically aggregated domain structures with length scales of 1–2 nm.[102] This type of mesoscale structural order is strongly pronounced in the tetra-alkylammonium based ionic liquids.[110]

While the effects of nanophase segregation and hydrophobic aggregation have been well studied for a large variety of room temperature ionic liquids, there have been no systematic studies which have focused on how these phenomena influence the structural dynamics and charge transport properties in tetra-alkylammonium based ionic liquids. In this chapter we present measurements of the structural dynamics and charge transport properties in a series of three ammonium based ionic liquids with varying alkyl chain length and volume fraction. We have found that the structural dynamics in these ammonium based ILs are highly complex, and this complexity is directly connected to the presence of hydrophobically aggregated alkyl domains. When the alkyl groups occupy a majority of the liquid volume, the reorientational motion of alkyl segments within the hydrophobically aggregated domains controls the microscopic mechanism behind viscous flow and structural relaxation.

In addition to the structural dynamics, we have also found that the charge transport properties of the ammonium ILs are strongly affected by nanophase segregation. As the volume fraction of neutral alkyl moieties increases in the liquid matrix, the presence of hydrophobic aggregation leads to a systematic reduction in the characteristic ion diffusion rate, while also causing a relatively large reduction of free ion concentration and enhanced ion association in these materials. Our results demonstrate that nanophase segregation strongly influences the structural dynamics and charge transport mechanism of ammonium ionic liquids with large

aliphatic moieties. Furthermore, our studies more generally show that the amphiphilic nature of ionic liquid cations can strongly impact the physicochemical properties of these materials.

5.2. Experimental details

Tributylmethylammonium bis(trifluoromethylsulfonyl)imide [N4441][NTF_2] (M_W = 480.5 g/mol, ρ_M = 1.27 g/cm^3),[109] triethyloctylammonium bis(trifluoromethylsulfonyl)imide [N2228][NTF_2] (M_W = 494.6 g/mol, ρ_M = 1.25 g/cm^3),[175] and trioctylmethylammonium bis(trifluoromethylsulfonyl)imide [N8881][NTF_2] (M_W = 648.9 g/mol, ρ_M = 1.10 g/cm^3)[109] were purchased from Iolitec USA and used as received. The chemical structures of these ionic liquids are shown in Fig. 5.1. As can be seen, the elemental composition of the cation and anion were held constant, while only the length and symmetry of the alkyl chains were varied. The liquid samples were filtered through 220 nm PVDF filters into cleaned and dried target vials. Following filtration, the samples were placed in a vacuum oven at T = 75°C and P = 1 mbar for 24 hours to remove residual impurities. After vacuum drying, the samples were flushed with dry nitrogen and were quickly sealed.

The calorimetric glass transition temperatures of these ILs were measured on cooling at 5 K/min using a Q1000 differential scanning calorimeter (TA instruments) and are as follows: T_g = 200 ± 2 K for [N4441][NTF_2], T_g = 192 ± 2 K for [N2228][NTF_2], and T_g = 186 ± 2 K for [N8881][NTF_2]. The glass transition temperatures are seen to decrease as the molecular weight of the IL increases, similar to the trend observed for the imidazolium based ionic liquids studied in the previous chapter.

Broadband dielectric spectroscopy (BDS) was used to characterize the charge transport and dipolar relaxations of over a temperature range from 400 K down to 180 K. The measurements were performed using the Novocontrol Alpha-A dielectric analyzer in the

frequency window 10^{-1} Hz to 10 MHz. The liquid sample was mounted between parallel 15 mm diameter stainless steel plates with small Teflon spacer posts used to maintain a plate distance of 0.1 mm. The temperature of the sample was controlled using a Novocontrol Quattro temperature control unit with stability of ± 0.1 K.

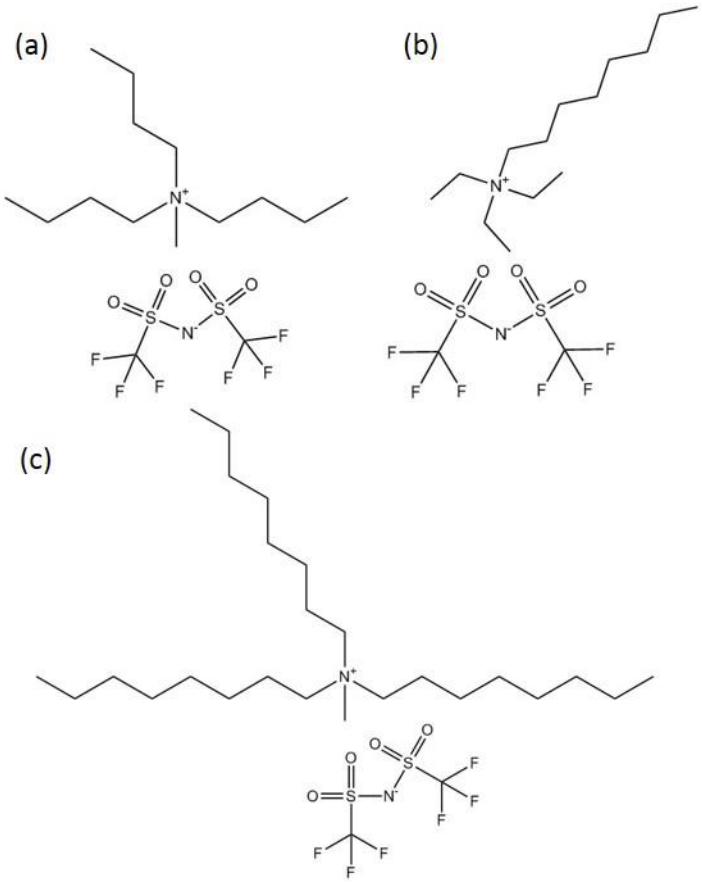

Figure 5.1. Chemical structures of the three ionic liquids studied in this chapter: (a) tributylmethylammonium bis(trifluoromethylsulfonyl)imide [N4441][NTF$_2$], (b) triethyloctylammonium bis(trifluoromethylsulfonyl)imide [N2228][NTF$_2$], and (c) trioctylmethylammonium bis(trifluoromethylsulfonyl)imide [N8881][NTF$_2$].

Depolarized dynamic light scattering (DDLS) measurements were performed to characterize the structural dynamics of the ammonium based ILs in a broad temperature (250 K

down to T_g) and time window (10^{-7} s through 100 s). The measurements were carried out using photon correlation spectroscopy (PCS) in right angle geometry, with laser wavelength = 647 nm and laser power = 200 mW. The vertically polarized incident beam was focused onto the sample mounted in an Oxford Optistat cryostat (temperature stability of ± 0.1 K), and horizontally polarized scattered light was collected with a single mode optical fiber, split between two avalanche photodiode detectors, and cross correlated using the ALV-7004/FAST multi-tau digital correlator.

Rheological creep compliance measurements were performed on the AR2000ex rheometer (TA instruments) using 25 mm plates to measure the shear viscosity of the [N8881][NTF_2] ionic liquid. The temperature of the sample was controlled in an environmental test chamber with liquid nitrogen as the gas source. At each measurement temperature, a constant small stress was applied until a steady state strain was achieved. The zero-shear viscosity was then extracted from the material response at the long time limit. In addition to creep measurements, dynamic mechanical measurements were carried out on the [N8881][NTF_2] IL to obtain the mechanical spectrum in the frequency domain near Tg. Parallel plates of small diameter (4 mm) were used to minimize the contribution of instrument compliance.

Pulsed Field Gradient Nuclear Magnetic Resonance (PFG NMR) measurements were performed using a 400 MHz NMR spectrometer with a home-built gradient device to obtain the self-diffusion coefficients of [N8881][NTF_2] IL at selected temperatures. These measurements were carried out by our collaborators at the University of Leipzig, Germany.

5.3. Results and Discussion

5.3.1. Structural dynamics of ammonium ILs—evidence for nanophase segregation

Figure 5.2 presents the normalized intensity correlation functions $g^2(t)$-1 (ICF) and the corresponding field correlation functions $g^1(t)$ (FCF) at selected temperatures for [N4441][NTF_2] (a,b) and [N2228][NTF_2] (c,d) measured by DDLS.

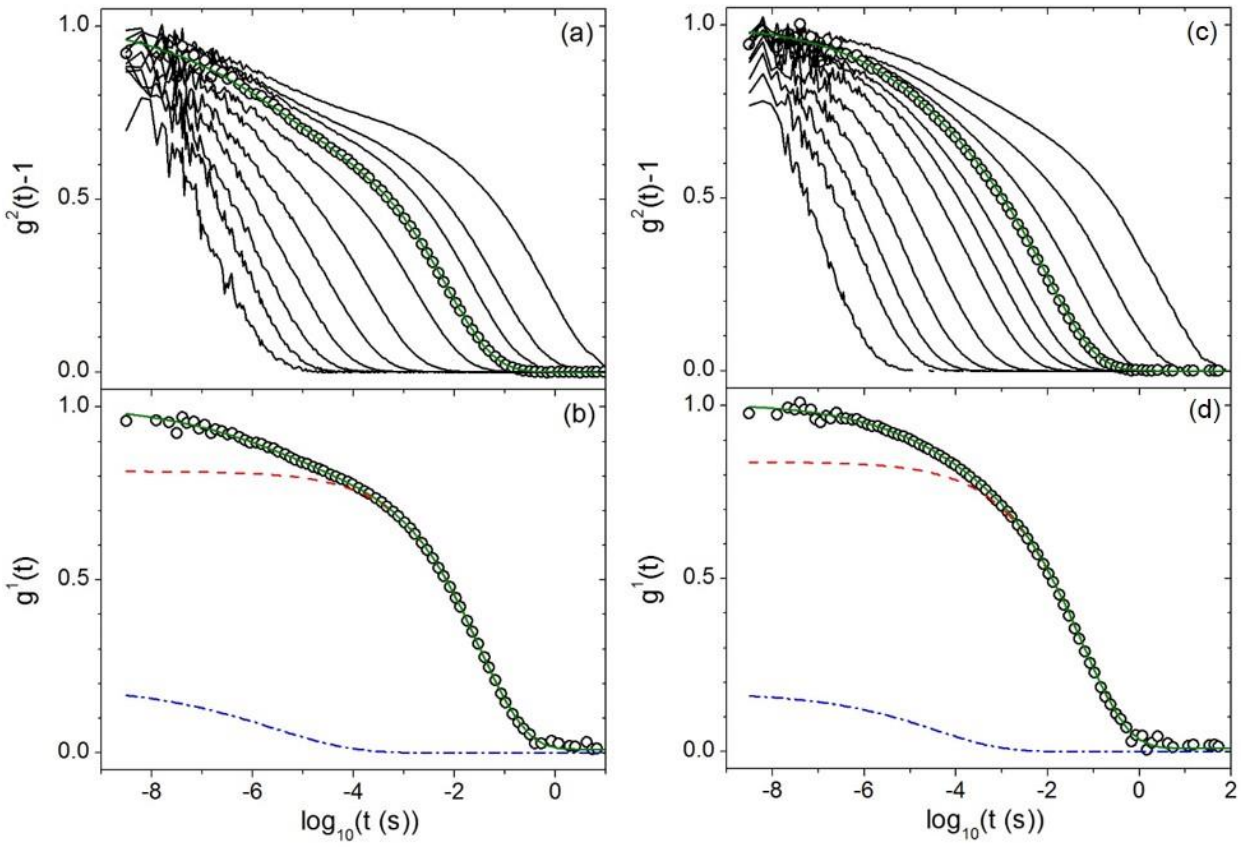

Figure 5.2. Intensity correlation functions measured by DDLS in [N4441][NTF_2] (a) and [N2228][NTF_2] (c) are shown for selected temperatures. The green lines are fits to the data using a superposition of two KWW functions (eq. 4.3). The field correlation functions are shown for one selected temperature in [N4441][NTF_2] (b) and [N2228][NTF_2] (d). The green lines are fits using eq. 4.3, the red dashed lines represent the contribution from the slow KWW function (β_{KWW} = 0.42) while the blue dash-dotted lines represent the contribution from the fast, secondary KWW function (β_{KWW} = 0.30).

Figure 5.3 presents the ICF and FCF of [N8881][NTF_2]. The correlation functions of these ammonium based ionic liquids show very interesting differences when compared to the [BMIM] based ionic liquids studied in Ch. 4. The ICF/FCF data of the three ammonium ionic liquids were fit using a superposition of two KWW stretched exponential functions (eq. 4.3). It can be seen that there is a clear two-step decay of the ICF/FCF of these ammonium based ILs at nearly all temperatures, and the faster, secondary relaxation process occupies a sizable minority of the spectral weight in all three ILs. In contrast, the spectrum of the [BMIM] ILs consisted primarily of a single stretched exponential decay and exhibited the excess wing feature only at temperatures close to T_g. As discussed in Ch. 4, the excess wing was found to account for at most a few percent of the decay of the correlation function in the [BMIM] based ILs. The fast, secondary process of the ammonium ILs is clearly not connected to the excess wing because it is observable in the ICF at nearly all temperatures, and most importantly it is seen that it accounts for nearly 20–40 percent of the spectral weight—much larger than what can be attributed to the excess wing.

We will first analyze the similarities and differences between the DDLS spectra of [N4441][NTF_2] and [N2228][NTF_2]. One of the interesting similarities is that the spectral shape of the faster and slower processes are identical for these ILs, with $\beta_{KWW} = 0.3\pm0.02$ for the fast relaxation process and $\beta_{KWW} = 0.42\pm0.02$ for the slow relaxation process. This observation suggests that the molecular relaxation mechanisms in these ionic liquids are very similar to one another. Of course, this result is not entirely surprising because the chemical structures of the counter ions are nearly identical, and only subtle modifications of the alkyl side chains differentiate the two ILs. The degree of nonexponentiality in these ILs is relatively large and not normally found for the structural relaxation process of most glass forming liquids, indicating

either a strongly heterogeneous dynamical environment, highly non-Markovian dynamics (heterogeneous vs. homogenous scenarios), or perhaps both.[38, 44] As with the [BMIM] based ILs, we found that the nonexponentiality parameters were independent of temperature over the studied temperature range.

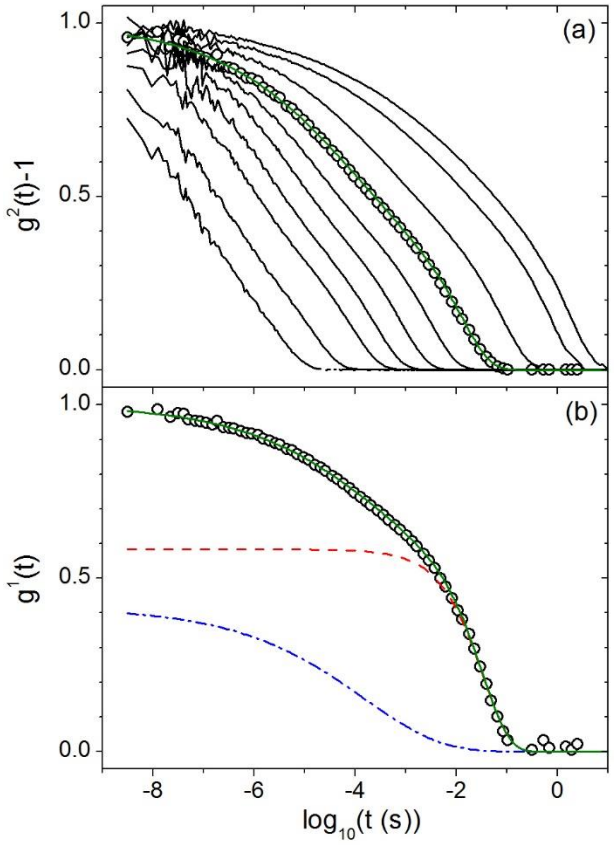

Figure 5.3. Intensity correlation functions (a) measured at selected temperatures, and the field correlation function measured at one temperature in [N8881][NTF$_2$]. The green line is the fit of the data using the superposition of two KWW functions (eq. 4.3), the red dashed line represents the contribution of the slow KWW function (β_{KWW} = 0.85), and the blue dash dotted line represents the contribution of the fast KWW function (β_{KWW} = 0.30).[176]

Secondly, it is seen that the spectral weight of the faster relaxation process is very similar for the two ILs, with the fast relaxation process accounting for approximately 20 percent of the

decay of the field correlation function. There is one notable difference between the spectra of these two ILs, however. It is evident from Fig. 5.2 that relative to the slower relaxation process, the fast process has significantly different temperature dependence in the [N4441] IL when compared to the [N2228] IL. Additionally, the timescales of the fast process in [N2228][NTF_2] are considerably closer to those of the slow process at all measured temperatures.

The DDLS spectra of [N8881][NTF_2], shown in Fig. 5.3, are even more distinct from the spectra of the [BMIM] based ionic liquids studied in Ch. 4, and they also show unique differences when compared to the [N4441] and [N2228] ionic liquids presented in Fig. 5.2. It is immediately evident that the fast relaxation process of [N8881][NTF_2] occupies much more spectral weight than in the shorter chained ammonium ILs. Furthermore, the timescales of the faster relaxation process are considerably closer to those of the slow process—separated now only by a few decades in time. It can be seen in Fig. 5.3 that the overall spectral shape remains similar as the temperature is decreased toward T_g, indicating that the fast and slow processes in the [N8881] ionic liquid have similar temperature dependences in the studied temperature range. This is unlike the other ammonium ILs shown in Fig. 5.2 which show considerable changes in the overall spectral shape with decreasing temperature. Looking at the spectral shapes of the individual relaxation processes of [N8881][NTF_2], the fast relaxation process was found to have a temperature independent stretching parameter $\beta_{KWW} = 0.3\pm0.02$, identical to what was observed for the first two ammonium ILs. Once again, this suggests that the fast relaxation process in all three of these ILs may be of similar origin. The slower process, on the other hand, was found to decay nearly exponentially with a temperature independent stretching parameter $\beta_{KWW} = 0.85\pm0.02$. The corresponding relaxation times of the fast and slow relaxation processes in these three ionic liquids are shown as a function of inverse temperature in Fig. 5.4.

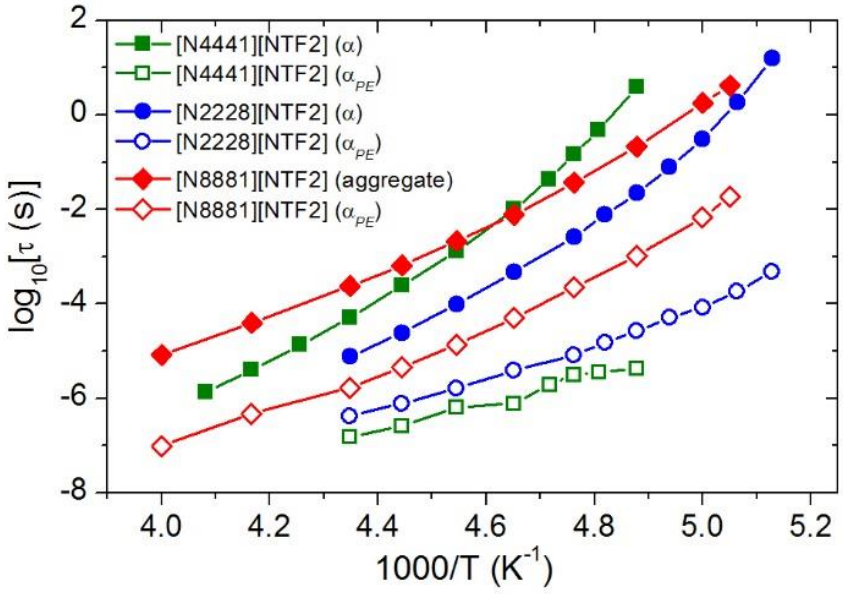

Figure 5.4. Primary and secondary relaxation times measured via DDLS are shown as a function of inversed temperature for the three alkylammonium ILs. The subscript "PE" denotes that this relaxation process is associated with alkyl group motion, while the label "aggregate" denotes that this relaxation is associated with mesoscale moieties, as will be demonstrated in the text.

As seen in Fig. 5.4, the temperature dependence of the relaxation times in these ammonium ionic liquids change strongly with only slight variation of chemical structure, especially when compared to the [BMIM] ionic liquids presented in the previous chapter. The most intriguing aspect of the dynamics in these liquids is not the variation of the glass transition temperature with changing alkyl chain lengths/symmetry, however. It is instead the presence of the clear two-step decay of the correlation function that is observed regardless of the alkyl chain length/volume fraction. So what is the origin of this secondary, fast relaxation process? In order to answer this, we will enumerate the important experimental observations regarding this process.

The first intriguing fact about this relaxation process is that as the number of alkyl units and the length of an alkyl tail increases on the ammonium cation, the fast relaxation process becomes slower and more Vogel-Fulcher-Tammann (VFT) like, i.e. an apparent increase in the dynamic fragility *m* is observed. The temperature dependence of the fast relaxation process in [N4441][NTF_2] can be seen to have an apparently Arrhenius functional form, while the fast relaxation in the [N2228] and [N8881] ILs show clear VFT temperature dependences. VFT temperature dependence of relaxation times are generally only observed for the structural α process, and the non-Arrhenius temperature dependence associated with the VFT function is usually attributed to cooperativity of molecular motion.[137] For many glass forming liquids, a secondary relaxation process can be observed in the dielectric or quasielastic light scattering spectrum, but it is usually very weak in amplitude relative to the structural relaxation process, and it tends to exhibit an Arrhenius temperature dependence.[177] Thus, the fact that the secondary relaxation process in these ammonium ILs displays increasingly pronounced VFT-like temperature dependence indicates that it may correspond to the collective motion of a sub-population of fast structural units.

One natural scenario emerges for the potential molecular origin of the fast relaxation from consideration of the spectral shapes and amplitudes in the ammonium based ionic liquids. Clearly, the nonexponentiality parameters of the fast relaxation process in all three ILs are equivalent, with $\beta_{KWW} = 0.3\pm0.02$. Secondly, it can be seen that the relative spectral weight of the fast process is correlated to the total number of carbons on the alkyl tails. The number of carbons on [N4441] ($n = 13$) and [N2228] ($n = 14$) are nearly identical, and it is seen that the fast processes of both ILs have nearly identical relative spectral weight ($f = 0.20$). The number of carbons on [N8881] is nearly doubled when compared to these ILs with $n = 25$, and intriguingly

we see that the fast process now accounts for approximately 40 percent of the spectral weight (double the fraction of the shorter chained ammonium ILs). These experimental observations indicate that the fast relaxation process observed in the DDLS spectrum of these three ammonium ionic liquids may be attributed to the fluctuations of the alkyl groups of the cation. It is expected that the alkyl side groups would be more mobile than the other parts of the IL at any given temperature due to the relative flexibility of these molecular moieties.

Since each ammonium IL exhibits two clear relaxations in the DDLS spectrum, where one component may be potentially related to the reorientational fluctuations of the alkyl side chains, the next important step is to determine which dynamical process corresponds to the calorimetric glass transition and the vitrification mechanism of the supercooled liquid. When plotted on the T_g/T scale, where T_g has been determined using differential scanning calorimetry, it can be seen in Fig. 5.5 that the slow relaxation process of the [N4441] and [N2228] based ILs corresponds to the structural relaxation process. Generally speaking, the dynamic glass transition temperature is defined as the temperature at which the relaxation time $\tau = 100$ s.[4] It can be seen in Fig. 5.5 that the calorimetric glass transition temperature lies very close (within a few kelvin) to the so-defined dynamic glass transition temperature in these ILs. We speculate that the slow relaxation process in these two ILs reflects the collective motion of the cation and anion charge centers.

The slow relaxation of [N8881][NTF_2] does not, however, correspond to the structural relaxation process, and instead the fast relaxation process is connected to glass transition and vitrification of the structure. This result is quite interesting in that it indicates that vitrification, viscosity, and ion motion in this IL may actually be controlled by the motion of the alkyl side chains of the cation, and not by the ion charge centers. From simple estimates of molecular

volume using the Van der Waals radii of the constituent atoms, we estimate that the volume fraction of neutral moieties (uncharged alkyl groups) is φ = 0.65 in [N8881][NTF_2]. Since nearly 2/3 of the liquid volume is occupied by the alkyl chains, it is certainly not surprising that the structural relaxation process, and thus viscous flow, might be related to the motion of alkyl moeities in this IL.

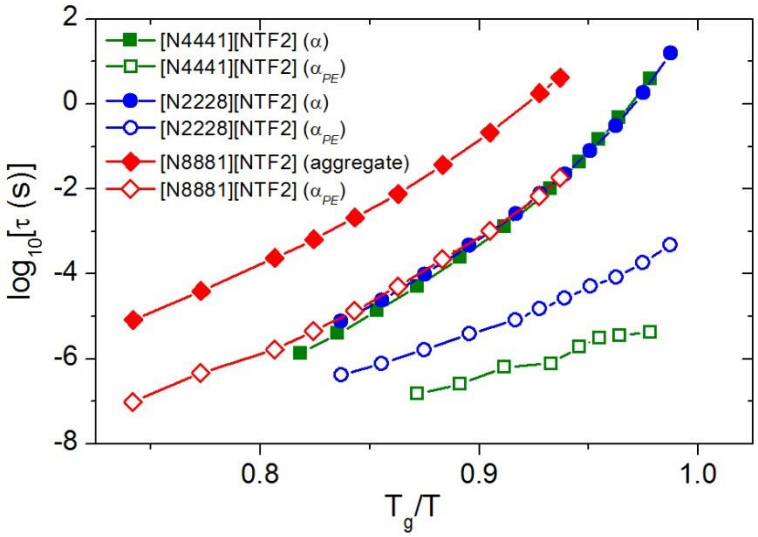

Figure 5.5. Primary and secondary relaxation times of the alkylammonium ILs measured via DDLS are shown as a function of inversed temperature scaled by the corresponding calorimetric glass transition temperature.

In order to further verify that the fast relaxation process is connected to viscous flow in [N8881][NTF_2], we have measured the shear mechanical spectrum near T_g via mechanical spectroscopy and the zero shear viscosity via creep compliance over a broad temperature range. According to Maxwell's relation, the mechanical relaxation time is equal to the ratio of the glassy shear modulus G_∞ and the zero-shear viscosity η such that $\tau_m = \frac{\eta}{G_\infty}$.[7] The infinite frequency (glassy) shear modulus was determined to be G_∞ = 0.4 GPa as seen in Fig. 5.6(a) at temperatures close to T_g. Since it is known that G_∞ changes only weakly with temperature,[7] we

assumed that this quantity was temperature independent over the range of temperatures in which the zero shear viscosity was measured and calculated the mechanical relaxation time of [N8881][NTF_2]. As can be seen in Fig. 5.6(b), the mechanical relaxation times are nearly identical to the fast relaxation times measured via DDLS. This result provides a strong indication that the fast relaxation process in the DDLS spectrum of this IL is connected to structural relaxation and glass transition.

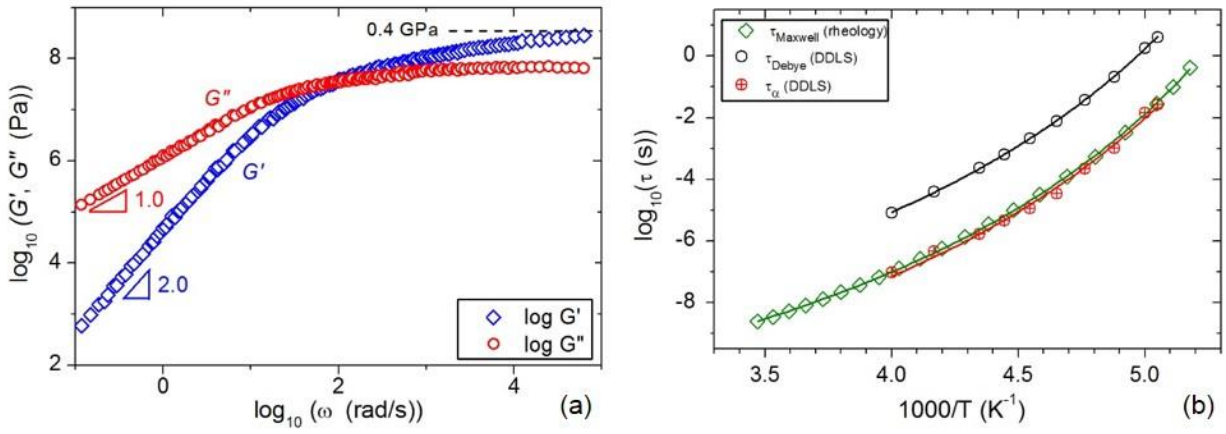

Figure 5.6. (a) Real and imaginary parts of the complex mechanical spectrum of [N8881][NTF_2] are shown for a temperature close to T_g.[176] The infinite frequency shear modulus was determined as shown to be G_∞ = 0.4 GPa. (b) Reorientational relaxation times determined by DDLS and mechanical relaxation times determined by rheology in [N8881][NTF_2] are shown plotted against inverse temperature. Solid lines are VFT fits to the data. The agreement between the fast DDLS relaxation times and the mechanical relaxation times indicate that the fast DDLS relaxation is connected to the calorimetric glass transition and structural vitrification.

The change in structural relaxation mechanism from the [N4441] and [N2228] ILs to the [N8881] IL is also paralleled by the change of the stretching parameter of the slow relaxation process. The stretching parameter of the slow process in the [N4441] and [N2228] ILs was found to be $\beta_{KWW} \approx 0.42$—a large degree of nonexponentiality, but not exactly unusual for ionic

liquids. Such levels of nonexponentiality have been observed in the ionic melt CKN referenced previously in Ch. 4.[169] What really stands out in the comparison between these three ILs is that the slow process of [N8881][NTF_2] has been found to be nearly Debye-like (defined as β_{KWW} = 1) at all measured temperatures. Such types of relaxation in neat molecular liquids cannot be attributed to molecular reorientation in the deep supercooled liquid state. Instead, this type of slow, Debye-like relaxation has been assigned to the rotational diffusion of mesoscale supramolecular structures in molecular liquids.[178] For example, many hydrogen bonded liquids, such as the family of monohydroxy alcohols, show a slow Debye-like relaxation in addition to the structural relaxation which has been attributed to the rotational motion of long-lived hydrogen bonded chains or clusters.[179-181] From this comparison, it is logical to assign the slow, Debye relaxation in [N8881][NTF_2] to the motion of supramolecular structures—potentially ionic aggregates or hydrophobically aggregated alkyl nanodomains.

Using the Debye-Stokes-Einstein relation, we can estimate the hydrodynamic radius of the mesoscopic moieties responsible for the slow relaxation process in the DDLS spectrum of [N8881][NTF_2]. According to the DSE relation, the rotational diffusion rate τ^{-1} of a spherical particle in a dilute solution of solvent molecules is inversely proportional to the viscosity η of the solvent such that $\tau^{-1} = \frac{l(l+1)k_BT}{8\pi\eta R^3}$, where l is the rank of the spherical harmonic correlation function associated with the rotational relaxation time τ, R is the hydrodynamic radius of the spherical particle, and k_B is Boltzmann's constant.[55, 56] We have found that the hydrodynamic size of the molecular moiety associated with the slow relaxation process is approximately D_H = 2R = 1.2 nm at all measured temperatures. This length scale is very similar to the distance between cation charge centers in [N8881][NTF_2], as seen in Fig. 5.7. The molecular model presented in Fig. 5.7(a) is a classical energy minimized simulation of four ion pairs performed

using *AVOGADRO*. Alternatively, the length scale D_H is also very close to the size of the aggregated cation heads and anions, also seen in Fig. 5.7. While this result does not allow for the conclusive determination of the precise molecular origin of the slow relaxation process, it certainly indicates that there are nanometer sized aggregates in the ionic liquid [N8881][NTF_2].

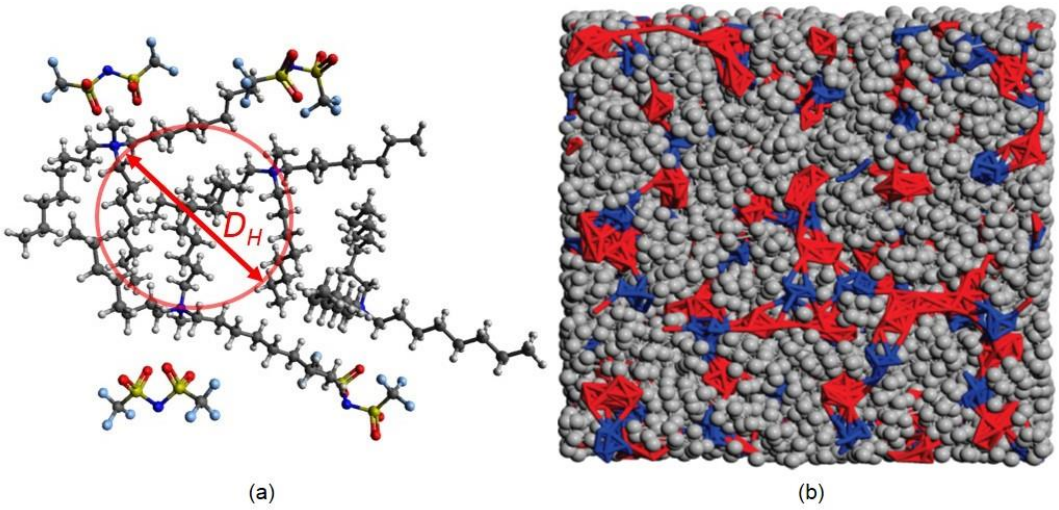

Figure 5.7. (a) A classical, energy-minimized chemical model of four ion pairs of [N8881][NTF_2] is shown with the corresponding hydrodynamic diameter calculated using the Debye-Stokes-Einstein relation. (b) Classical, atomistic MD simulation snapshots of 150 ions of [N8881][NTF_2]. The segregation of alkyl domains (grey spheres) from the charge rich domains (red (-) and blue (+)) is clearly observed.[110]

The complex dynamical picture that we have observed in these ammonium based ILs is quite reminiscent of what has been found in the large class of polymers with polar backbones and neutral polyethylene side chains. In 2003 Beiner and Huth studied a series of poly(n-alkyl acrylates) and poly(n-alkyl methacrylates) with systematically increasing alkyl side chains via broadband dielectric spectroscopy and x-ray diffraction.[182-184] Measurements via dielectric spectroscopy (Fig. 5.8(a)) revealed a bimodal permittivity spectrum in all polymer melts with alkyl side chains longer than $n = 4$. As the length of the side chain increased, the faster process in

the spectrum occupied increasingly more spectral weight, and it shifted to lower frequencies and correspondingly longer timescales relative to the slower polymer segmental relaxation process. Additionally, the authors found that the fast relaxation process showed increasingly more pronounced VFT temperature dependence as the length of the alkyl side chain increased (Fig. 5.8(b)). These factors led the authors to conclude that the fast relaxation process was associated with the segmental motion of polyethylene (PE) within nanoscale PE domains.

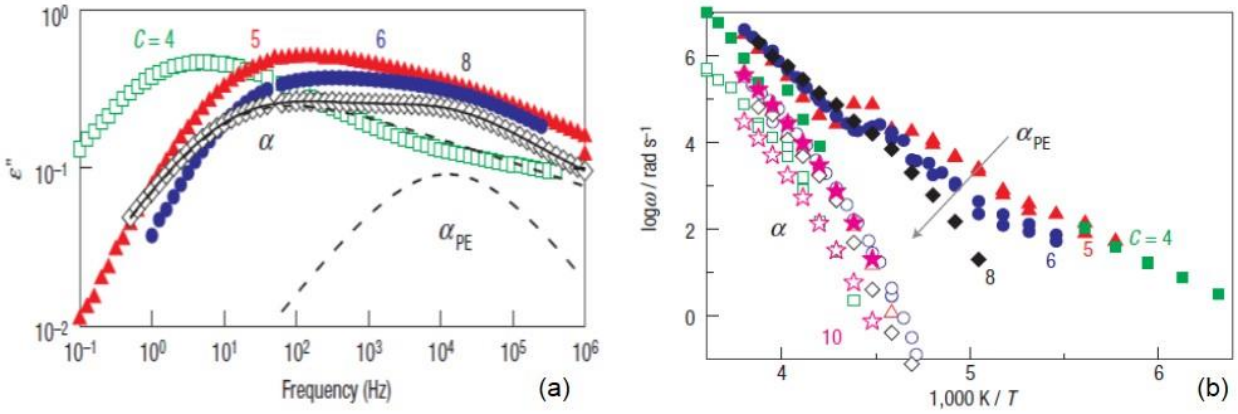

Figure 5.8. (a) Dielectric loss spectra of a series of poly(n-alkyl acrylates) at T = -40°C, where c is equal to the number of carbons on the alkyl side chain. (b) Relaxation times of the same series of poly(n-alkyl acrylates) determined from dielectric permittivity spectra are shown as a function of inverse temperature.[182]

In conjunction with these dynamical measurements, the authors also characterized the static structure of these polyethylene side chain polymers via XRD. It was found that for polymers with side chains longer than $n = 4$, a prepeak in the static structure factor emerged between 0.3–0.6 $Å^{-1}$.[14] The prepeak, corresponding to length scales of 1–2 nm, systematically shifted toward smaller wave vectors, becoming sharper and more intense as the alkyl side chains increased in length. These static structure measurements were interpreted as evidence for the

existence of nanophase segregation of the hydrophobic, nonpolar alkyl chains from the hydrophilic, polar polymer backbone. Interestingly, the ammonium ionic liquids studied in this chapter also show a pronounced prepeak in the static structure factor. In the works of Pott et al.[109] and Triolo et al.,[185] it was found that the prepeak in the static structure factor of alkyl-ammonium ILs shifted toward lower wave vectors, becoming sharper and more intense as the number of alkyl carbons on the cation increased. This unique dependence of the structural properties on the number of alkyl carbons in the ammonium ILs was interpreted, in an identical manner as the polyethylene side chain polymers, as arising from the nanophase segregation of hydrophobic alkyl tails from the ionic parts of the cation and anions.

We may deduce from this comparison that the complex dynamics that exist in the alkyl-ammonium ionic liquids are the direct result of the nanophase segregation of charged and neutral moieties. Because these liquids are not chemically homogeneous, they consist of two distinct phases where molecular motion in the charge-rich phase occurs much differently from the molecular motion in the polyethylene phase. Due to this well-defined phase separation between the ionic and neutral domains, these ionic liquids exhibit strong dynamical heterogeneity to the point where they show the two separate relaxation processes. This picture is corroborated by the complimentary structural information provided by the MD simulations and XRD data. Furthermore, the comparison to the studies of dynamics and structure of the polyethylene side chain polymers indicates that nanophase segregation is not a specific property of ILs, and it can be found in many complex liquids exhibiting pronounced amphiphilicity.

As discussed above, the nanophase segregation of the charge centers of the cation/anion from the neutral, aliphatic alkyl tails is the primary cause of the complex dynamics in these liquids. All three ILs were found to show a two-step decay of the reorientational correlation

function, indicating that nanophase segregation is present to some degree in these ILs. It was also observed, however, that the timescales, and temperature dependences thereof, associated with the alkyl dynamics varied greatly with alkyl chain length and volume fraction (Fig. 5.4). While the exact reason for these differences is not understood for these ionic liquids, some insight may once again be obtained by considering the physical picture that was developed for the polyethylene side chain polymers.

As the alkyl chain length and volume fraction increase in these ammonium ILs, the fast relaxation process can be seen to become slower and apparently more VFT-like (Fig. 5.4). This is similar to what was observed by Beiner and Huth, where the temperature dependence of the polyethylene relaxation time was found to vary in an identical and systematic fashion with increasing alkyl side chain length.[182] These authors suggested that nano-confinement of the alkyl domains is the underlying cause of this strong variation in the alkyl dynamics. For short side-chain polymers, the alkyl domains are small, resulting in correspondingly strong confinement. This high degree of confinement consequently disrupts the cooperativity of the motion of alkyl segments, dramatically decreasing the effective dynamic glass transition temperature and dynamic fragility *m* within the polyethylene domains.[186] As the length scale of confinement increases with increasing alkyl side chain length, the cooperativity of polyethylene segmental motion becomes less hindered, resulting in higher polyethylene glass transition temperatures and dynamic fragilities. Eventually, the chains become so long that bulk-like PE dynamics are recovered.

This physical picture applies quite well to the case of the three ammonium based ILs studied in this chapter. We observe in these liquids a systematic reduction of mobility and increase in apparent dynamic fragility *m* with increasing alkyl chain length/volume fraction. For

the case of [N8881][NTF_2], bulk-like PE dynamics are recovered and it is seen that this sub-population of molecular moieties is responsible for the calorimetric glass transition. In order to determine the effective PE dynamic glass transition for the [N4441] and [N2228] ILs, we have plotted the relaxation times for all three ILs on a plot similar to Fig. 5.5, but now instead the T_g is that of the fast, polyethylene domains (the calorimetric glass transition of the [N8881] IL was found to be the glass transition temperature of the PE nanodomains).

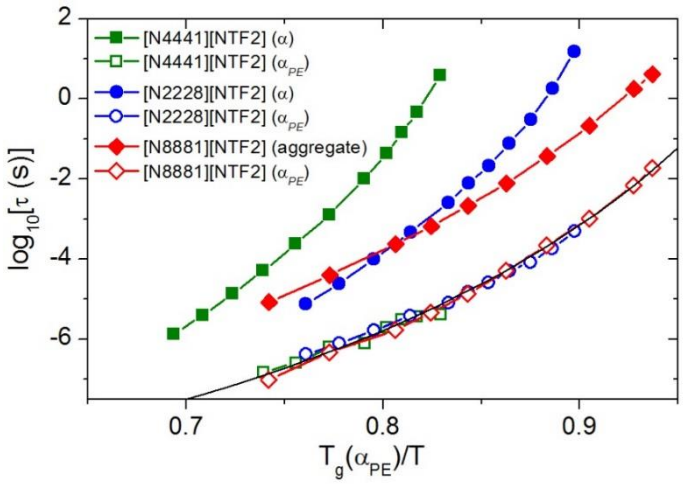

Figure 5.9. Primary and secondary relaxation times of the alkylammonium ILs measured via DDLS are shown as a function of inversed temperature scaled by the corresponding effective "polyethylene" glass transition temperature.

As is seen in Fig. 5.9, all of the fast, PE relaxation processes observed in DDLS can be collapsed onto a single master curve. The $T_{g(PE)}$ values determined from this scaling were $T_{g(PE)}$ = 186 K for [N8881][NTF_2], $T_{g(PE)}$ = 175 K for [N2228][NTF_2], and $T_{g(PE)}$ = 170 K for [N4441][NTF_2]. Thus we see that the dynamic glass transition is strongly suppressed in the PE nanodomains with decreasing alkyl chain length/volume fraction. It is also clear, however, that the actual dynamic fragility *m* does not change across these three ILs since the data collapse well onto a single

master curve. This interesting scaling analysis provides a final, strong indication that the dynamics of these ILs are highly complex and are a direct consequence of nanophase segregation of charged and alkyl moieties in the ammonium based ionic liquids.

5.3.2. Effects of nanophase segregation on charge transport

In the previous section, the influence of nanophase segregation on the reorientational structural dynamics of ammonium ionic liquids was explored. It was found that these liquids exhibited surprisingly pronounced dynamical heterogeneity, to the point where the rate of average molecular motion in the alkyl rich domains could be distinctly separated from the rate of motion in the charge rich domains. It is quite surprising that such dramatic changes in the dynamical profile of these liquids could be induced with only subtle modifications of the alkyl side chains of the ammonium cation. Having explored the influence of nanophase segregation on the structural dynamics, we will now explore how this feature of ammonium ionic liquids influences the charge transport properties.

As was the case in Ch. 4, the complex permittivity spectrum for one ammonium ionic liquid will be presented and analyzed in detail. Figure 5.10 presents the complex permittivity spectrum of [N8881][NTF_2] measured via dielectric spectroscopy at selected temperatures. The features observed in these spectra are very similar to those found for the [BMIM] based ILs presented in the previous chapter, and only subtle differences are present when comparing these spectra and those of the other two ammonium based ionic liquids. Given that the quasielastic light scattering spectra were so dramatically different in the ammonium ILs when compared to the [BMIM] ILs, it is somewhat surprising that the dielectric spectra do not show any correspondingly dramatic differences. We once again observe the three major regions of permittivity spectrum, with electrode polarization occurring at low frequencies, frequency

independent (dc) conductivity at intermediate frequencies, and the onset of ac conductivity at higher frequencies.

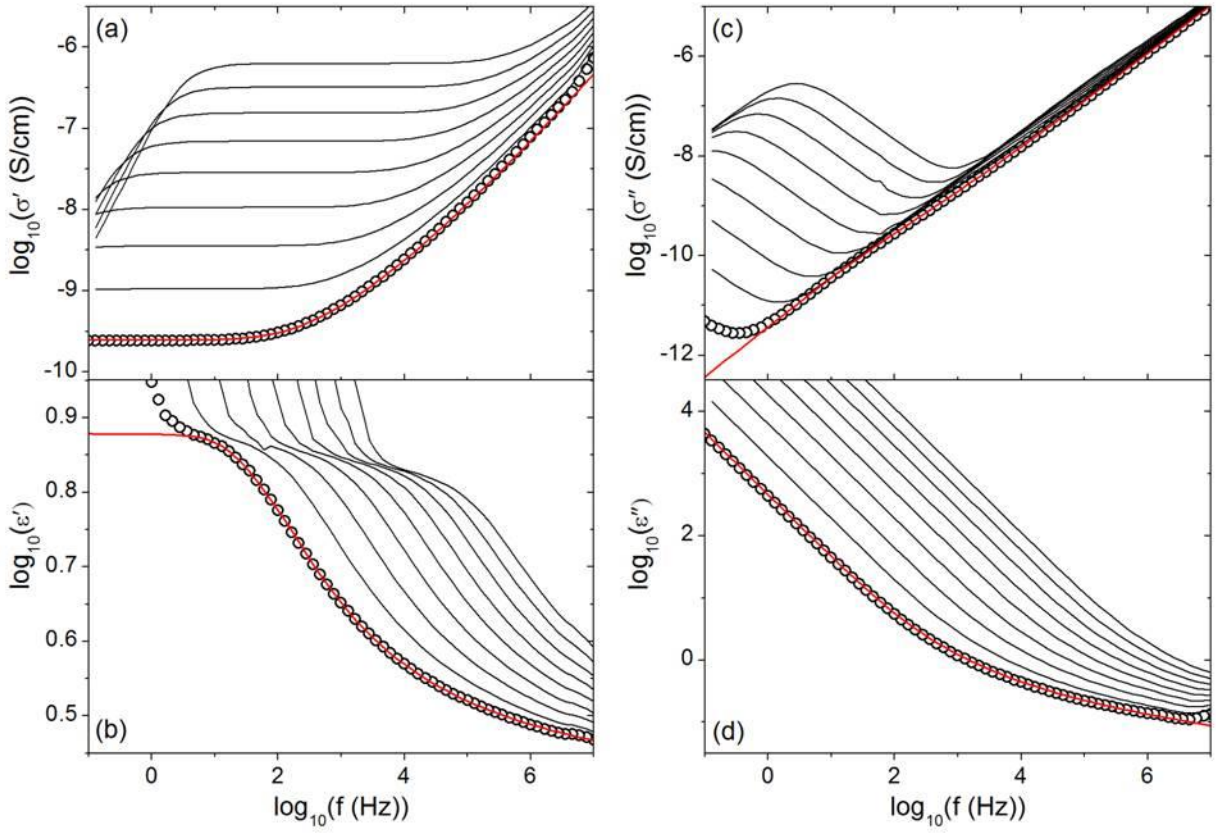

Figure 5.10. Real (a,b) and imaginary (c,d) parts of the complex conductivity σ and permittivity ε* spectrum of [N8881][NTF$_2$] are shown at several temperatures in the supercooled liquids regime. The red line is a fit to the data using the combined Random Barrier Model and Havriliak Negami function (Eq. 4.6).*[176]

Since the dielectric measurement is sensitive to the fluctuations of ions and permanent dipole moments, it is clear, however, why we observe only the ionic relaxation response typical of the ionic liquids studied in Ch. 4. The polyethylene side chains of the ammonium ILs have essentially no permanent dipole moment and instead have a significant optical polarizability.[118] Thus, fluctuations of the PE side chains should strongly contribute to the light scattering

spectrum, while there should be no clear signature of this process in the dielectric spectrum. Accordingly, the PE process in the polyethylene side chain polymers can be seen in Fig. 5.8 to exhibit low dielectric loss. In the ionic liquids, on the other hand, the dielectric loss due to ion motion is extremely large and likely obscures any measureable contribution from the PE process.

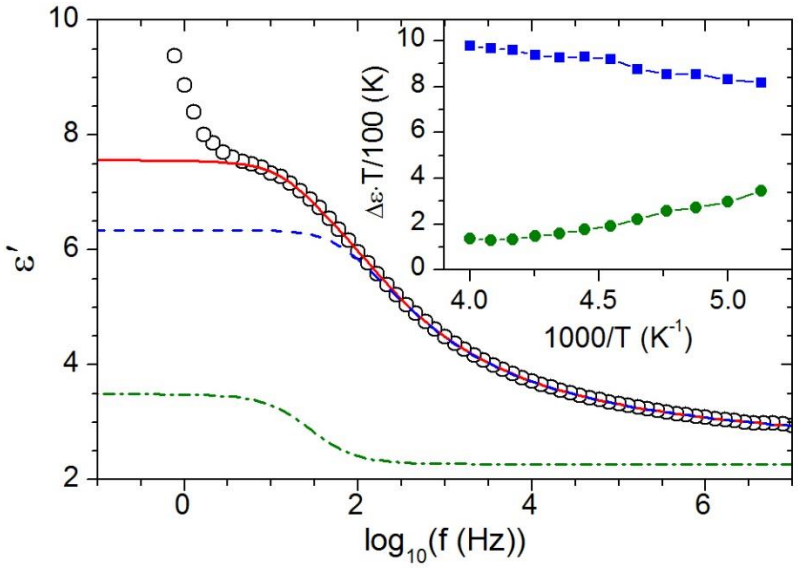

Figure 5.11. The detailed fitting of the real permittivity of [N8881][NTF₂] using eq. 4.6 is shown at one temperature. The dashed blue line is the contribution from the Random Barrier Model, the green dashed-dotted line is the contribution from the Cole-Cole relaxation, and the red line is the cumulative fit. The inset presents the temperature scaled dielectric strength of the RBM and CC process as a function of inverse temperature.[176]

The complex dielectric permittivity was analyzed using the superposition model combining the Random Barrier Model (RBM) and Havriliak-Negami (HN) function (eq. 4.6) in order to extract the mean ion hopping rate τ_e^{-1} and dc conductivity σ_0. It can be seen in Fig. 5.10 that the model describes the dielectric spectrum of [N8881][NTF_2] well with negligible deviations, and it was also found to describe equally well the spectra of the [N4441] and [N2228] based ILs. As was the case for the [BMIM] ILs, however, we once again found that the RBM

could not completely describe the spectrum of these ammonium ILs. As seen in Fig. 5.11, the RBM fits the high frequency side of the permittivity spectrum, but there is a small fraction of spectral weight that requires the additional HN function to be added to the model. While this additional process was once again found to have a Cole-Cole (symmetric) spectral shape, it was found to account for a much smaller fraction of the spectrum (Fig. 5.11 inset) and had a much more narrow dispersion ($\alpha_{cc} \approx 0.9$) in contrast to the [BMIM] ILs. The mean ion hopping times τ_e and the CC relaxation times (referred to as τ_{cc} in the figure) determined from the fitting of the dielectric spectra of [N8881][NTF_2] are shown in Fig. 5.12 along with the relaxation times determined via DDLS and rheology in the previous section.

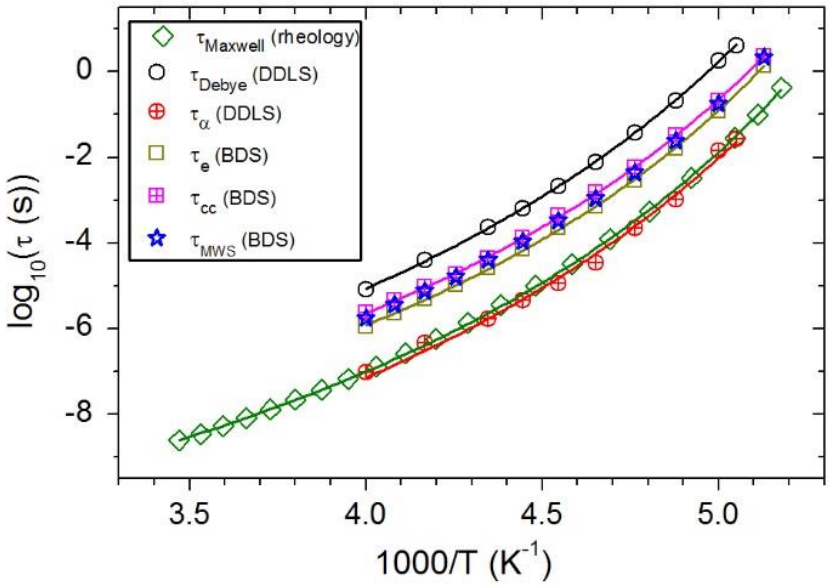

Figure 5.12. Relaxation times of [N8881][NTF_2] measured via rheology, DDLS, and BDS as a function of inverse temperature.[176]

The origin of this Cole-Cole relaxation process is not precisely clear, as was mentioned previously in Ch. 4. While the spectral shape and amplitude of this process was found to not be

significantly influenced by the chemical structure of the anion in the three [BMIM] ILs, it is quite evident when comparing the [BMIM] ILs to the ammonium ILs that the chemical structure of the cation has a significant effect on this spectral feature. The two most probable microscopic origins of this relaxation are either that it is the signature of dipolar reorientational motions of the cations in the liquid matrix, or it is the result of the interfacial polarization of the boundary resulting from the nanophase segregation of insulating alkyl tails from the cation and anion charge centers—the so-called Maxwell-Wagner-Sillars (MWS) effect.[119]

The chemical structure of the ammonium ionic liquids are comprised of a large fraction of neutral alkyl moieties, and we have seen in the previous section that the amphiphilicity of the ammonium cation results in nanophase segregation of the charged and neutral parts of the IL. Thus, it is natural to hypothesize that these nanoscale inhomogeneities give rise to the MWS interfacial polarization effect. We have estimated using the atomic Van der Waals volumes that the charged regions of the molecule (cation and anion) account for approximately 35% of the total volume while the remaining alkyl chains comprise the remaining 65%. Assuming the alkyl chains have a temperature independent dielectric constant (ε_s = 2.3) and dc conductivity (σ_{PE} = 10^{-17} S/cm) identical to polyethylene,[187] and the ionic components are identical and spherical, it is possible to calculate the relaxation time of this hypothetical interfacial polarization process as a function of temperature, such that

$$\tau_{MWS} = \varepsilon_0 \frac{(1-n)\varepsilon_{PE}+n\varepsilon_{ion}+n(\varepsilon_{PE}-\varepsilon_{ion})\varphi_{ion}}{(1-n)\sigma_{PE}+n\sigma_{ion}+n(\sigma_{PE}-\sigma_{ion})\varphi_{ion}} \quad (5.1)$$

where n = 0.33 for spherical particles, φ_{ion} is the volume fraction of the ionic component estimated above, ε_{PE} and ε_{ion} are the static dielectric constants of polyethylene and the measured conductivity relaxation process of the bulk liquid, respectively, and σ_{PE} and σ_{ion} are the conductivity of polyethylene and the measured dc conductivity of the bulk liquid, respectively.[119]

The MWS relaxation times calculated via eq. 5.1 are plotted as a function of temperature in Fig. 5.12. Surprisingly, the calculated MWS relaxation times agree quantitatively with the Cole-Cole relaxation times at all measured temperatures. This quantitative agreement suggests that the CC relaxation process may arise from the MWS interfacial polarization process in these ammonium based ionic liquids. While the above calculation provides strong evidence for the MWS process in the ammonium based ILs, it is also probable that both the MWS process as well as cationic dipolar reorientational motions contribute to this additional spectral feature in the [BMIM] based ILs. The ammonium cations studied in this chapter have very weak permanent dipole moments due to the symmetry and lack of electronegative atoms, while the [BMIM] cations have a higher degree of asymmetry, in addition to the pair of electronegative nitrogen atoms on the imidazolium ring. The chemical structure differences between these two types of cations may be the underlying reason why the dielectric strength of the additional CC process is stronger and broader for the [BMIM] based ILs when compared to the ammonium based ILs.

While the dielectric spectra do not exhibit any significant differences with varying chemical structure, the dc conductivities can be seen in Fig. 5.13(a) to show strong variations across the set of ammonium ILs. Furthermore it is seen that relative to [BMIM][NTF_2] (all four ionic liquids have the same anion), the dc conductivities are significantly lower at all measured temperatures. In contrast to the case of the [BMIM] based ILs, there are even strong changes in the temperature dependences of the dc conductivities, where we can see, for example, that the dc conductivity of [N8881][NTF_2] has such different temperature dependence that it crosses “paths” with the [N4441] and [N2228] IL datasets.

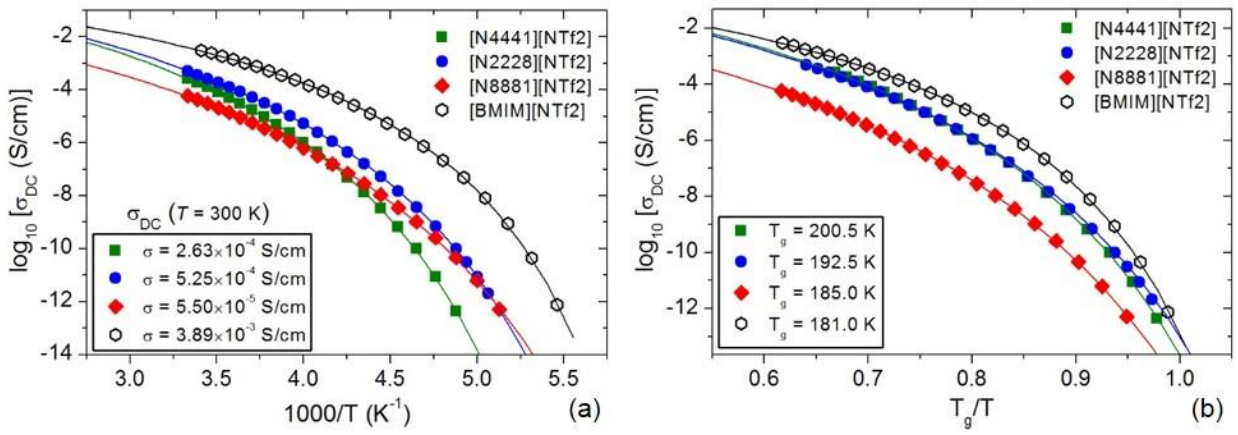

Figure 5.13. DC conductivity of the ammonium ILs and [BMIM][NTF$_2$] plotted as a function of inverse temperature (a) and T_g/T (b). The solid lines are Vogel-Fulcher-Tammann fits to the data.

This difference in temperature dependence is more apparent on the T_g/T scaled plot shown in Fig. 5.13(b). The dc conductivities of the [N4441] and [N2228] based ILs show very similar temperature dependences relative to T_g, and this indicates, similar to the case of the [BMIM] ILs, that the primary factor controlling the transport of charge in these ILs is the variation of the glass transition temperature and ionic mobility with varying chemical structure. The dc conductivity of [N8881][NTF$_2$] does not fall onto the data from the other two ammonium ILs at any relative temperature. It is also seen in Fig. 5.13(b) that the dc conductivity of all three ammonium ILs are lower than [BMIM][NTF$_2$] at all temperatures relative to their respective glass transition temperatures.

So what is the primary cause of the significant reduction of ionic conductivity in these ammonium ILs when compared to the [BMIM] based ILs? Do the ions move slower (relative to T_g), are there less available free ions for conduction, or is it perhaps a combination of both of these factors? In order to answer these questions, we will apply the technique laid out in Ch. 4

that allowed for the determination of the free ion diffusion coefficients and the free ion concentration from the analysis of dielectric spectra.

According to the calculation method presented in Ch. 4, the ion self-diffusion coefficients are related to the mean ion hopping rate τ_e^{-1} and the mean ion hopping length λ such that $D = \frac{\lambda^2}{2\tau_e}$.[80] Combining this equation and the Einstein relation (eq. 4.7), we arrive at the expression relating dc conductivity to the ion diffusion coefficient (ion hopping rate) and the free ion concentration (eq. 4.8). The ion hopping rate is determined from the RBM fitting, while the ion hopping length is a parameter which can be determined by comparing diffusion coefficients measured via dielectric spectroscopy to those measured via PFG NMR. For [N8881][NTF_2], self-diffusion coefficients were measured via PFG NMR, and these data are shown plotted vs. T_g/T in Fig. 5.14. Following the method presented in Ch. 4, the temperature dependent self-diffusion coefficient (Fig. 5.14), temperature dependent free ion concentration (Fig. 5.15), and the mean ion hopping length λ = 2.1 Å were determined for [N8881][NTF_2].

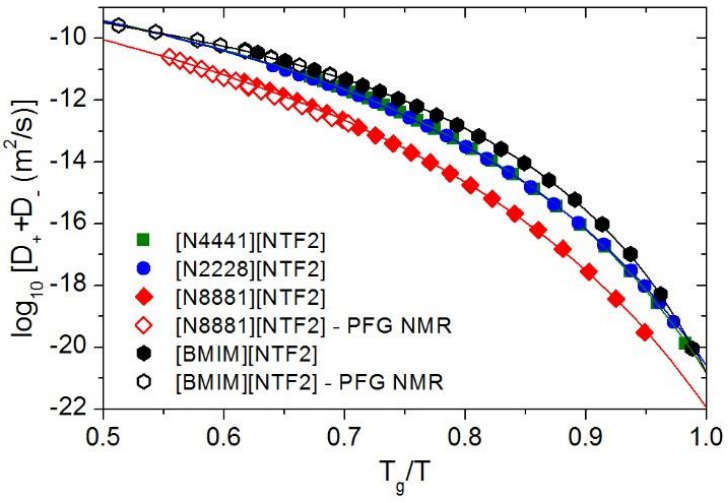

Figure 5.14. Self diffusion coefficients of the ammonium ILs and [BMIM][NTF_2] plotted as a function of T_g/T. The solid lines are Vogel-Fulcher-Tammann fits to the data.

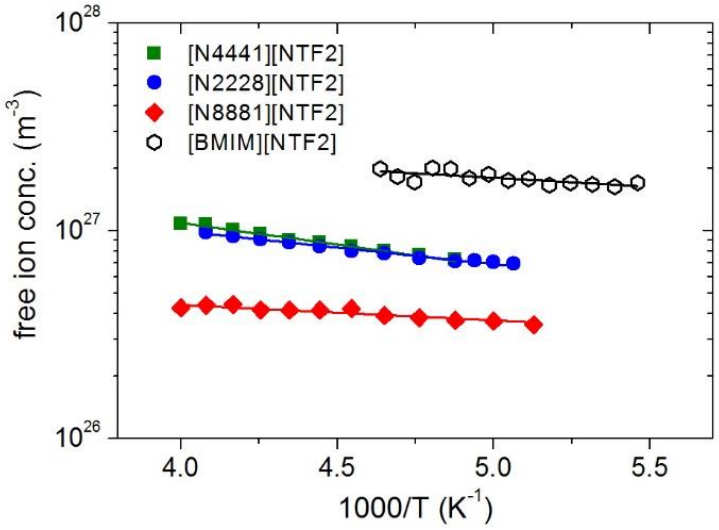

Figure 5.15. Free ion concentration of the ammonium ILs and [BMIM][NTF$_2$] plotted as a function of inverse temperature. The solid lines are Arrhenius fits to the data.

Unfortunately, PFG NMR diffusion measurements were not performed and are not available in the literature for [N4441][NTF$_2$] and [N2228][NTF$_2$]. Because of this, it is necessary to estimate the mean ion hopping lengths for these materials in order to quantify the ion diffusion coefficients and free ion concentrations. It has been shown that the mean ion jump length determined from the PFG NMR and BDS diffusivity measurements is correlated to the molecular weight of the ionic liquid.[158] We have also found a correlation between molecular weight and ion jump length for the four ionic liquids presented in this dissertation in which PFG NMR measurements were available. As seen in Fig. 5.16, a rough linear relationship between molecular weight M_W and ion hopping length λ can be found from our data where

$$\lambda\,(\text{Å}) \approx (-0.20 + 0.0035 \times M_W)\ (\text{Å}) \tag{5.2}$$

Using this relation we have calculated that the ion hopping lengths for [N4441][NTF$_2$] and [N8881][NTF$_2$] are nearly identical, where $\lambda \approx 1.5$ Å (the molecular weights of these ionic liquids were found to be very similar). Of course, this hopping length is based off of the

assumption that the correlation (eq. 5.2) holds for these ionic liquids, and our estimation would require experimental verification via PFG NMR diffusion measurements. The ion diffusion coefficients and free ion concentrations of [N4441][NTF_2] and [N8881][NTF_2] calculated using the above hopping length are shown in Fig. 5.14 and Fig. 5.15, respectively.

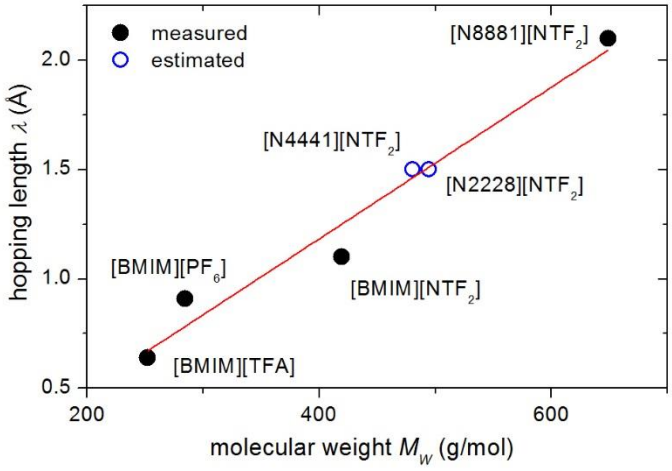

Figure 5.16. Molecular weight dependence of the mean ion hopping length in the studied room temperature ionic liquids. The red line is a linear fit to the ion hopping length data measured via BDS and PFG NMR. The open blue circles present the hopping lengths estimated from this correlation for the short chained ammonium ILs.

As seen in Fig. 5.14, the ion diffusion coefficients of the three ammonium based ILs show similar trends as their corresponding dc conductivities when plotted on the T_g/T scale. This indicates that the changes in the dc conductivity with variation of the cation chemical structure is primarily the result of the change in the ion diffusion coefficients. Interestingly, the ion diffusion coefficients of the [N4441] and [N2228] ILs are only slightly reduced relative to [BMIM][NTF_2], while the ion diffusion coefficients of [N8881][NTF_2] are nearly two orders of magnitude lower than those of [BMIM][NTF_2] at all T_g-scaled temperatures. This trend in chemical structure dependent diffusion coefficients parallels the trends in the structural dynamics

measured via DDLS, in which the signature of nanophase segregation was found to be only weakly pronounced in the [N4441] and [N2228] ILs, whereas it was strongly pronounced in [N8881][NTF_2].

In addition to the reduction in ion diffusivity, we also have observed a significant reduction in the free ion concentration upon increasing the volume fraction of alkyl side chains. The free ion concentration of [N4441][NTF_2] and [N2228][NTF_2] were found to be very similar and approximately half the level of [BMIM][NTF_2]. The free ion concentration of [N8881][NTF_2] was significantly lower for these three ILs, and was found to be approximately five times lower than in [BMIM][NTF_2]. Once again, some of this reduction in free ion concentration is likely due to the reduced total number of ions in the liquid as a result of lower mass densities and higher molecular weights of the ammonium ILs. In order to separate this factor from the intrinsic ion association effect, we have calculated the mole fraction of free ions at one temperature (T = 295 K), such that $f_{free\ ions} = \frac{n_{free}}{n_{tot}}$ and $n_{tot} = 2\rho_m M_W N_A$, where ρ_m is the mass density, M_W is the molecular weight, and N_A is Avogadro's number. The free ion concentration was determined by extrapolating the Arrhenius fits of the data to T = 295 K, and the mass density at T = 295 K was taken from the literature. Whereas the mole fraction of free ions in [BMIM][NTF_2] was found to be f_{free} = 0.57±0.05, the mole fraction of free ions in the ammonium ILs were significantly lower with f_{free} = 0.46±0.05 for [N4441][NTF_2], f_{free} = 0.41±0.05 for [N2228][NTF_2], and f_{free} = 0.28±0.05 for [N8881][NTF_2]. We once again observe the familiar trend where the fraction of free ions in the ammonium ILs decreases significantly as nanophase segregation becomes increasingly prominent in the liquid matrix.

The reduction of the ion diffusion coefficients and free ion concentrations in the ammonium ILs is clearly connected to the presence of nanophase segregation of the anion and

cation charge centers from the alkyl side chain moieties. As the alkyl chains increase in length and occupy a larger fraction of the liquid volume, the anion and cation charge centers become separated by increasingly larger islands of hydrophobically aggregated alkyl nanodomains.[110] Due to this complex heterogeneous solvation structure, a collective reorganization of the hydrophobic network must occur as a cation/anion charge center hops through the liquid matrix. This not only forces the ions to hop over increasingly longer distances, but it also causes the ion hopping process to occur less frequently, resulting in lower ion diffusion coefficients. Furthermore, the longer residence times of associated ions will result in increasingly lower free ion concentrations, as is observed in Fig. 5.15. Thus, the impact of nanophase segregation on the charge transport properties is twofold—not only does it hinder free ion motion due to the strongly heterogeneous solvation environment, but this hindered ion motion consequently causes lower free ion concentrations and longer-lived ion association clusters.

5.4. Conclusions

We have shown in this chapter that the dynamics and charge transport properties of ammonium based ionic liquids are highly complex due to the strong amphiphilicity of the ammonium cation. The glass transition temperatures, dc conductivities, and structural dynamics were found to change dramatically with changes to the lengths and symmetry of the cation side chains, indicating the importance of the alkyl moieties in controlling the physicochemical properties of these materials. The hydrophobic alkyl side chains of the cation have been shown to phase segregate from the hydrophilic charge centers of the cation and anion to form nanometer sized "polyethylene" domains. This nanophase segregation has a great impact on the dynamics of these ionic liquids, and the molecular mobility in the charge rich domains has been found to be significantly different from the mobility in the neutral PE nanodomains. In fact, the dynamical

heterogeneity is so strongly pronounced that two distinct structural relaxation modes can be clearly observed in the quasielastic light scattering spectrum of these liquids. As the length of the alkyl side chains increase and the polyethylene domains become larger, it was found that the structural relaxation process within the PE domain shows increasingly more pronounced Vogel-Fulcher-Tammann temperature dependence, indicating that the walls of the PE domains may exert a degree of self-imposed nanoscale confinement on the PE moieties. Interestingly, the characteristic bimodal relaxation spectrum of ammonium ILs has also been observed for the family of polar polymers with polyethylene side chains, indicating that nanophase segregation may be a general feature of amphiphilic molecular, polymeric, and ionic liquids.

Having characterized the influence of nanophase segregation on the structural dynamics in this set of ammonium ILs, the second part of this chapter was devoted to understanding how the charge transport properties are affected by the presence of nanophase segregation. We have found that relative to the imidazolium based ILs which show no signature of phase segregation, the dc conductivity is significantly lower in all three ammonium ILs, and this is only due in part to the slightly higher glass transition temperatures when compared to [BMIM][NTF_2]. Relative to their respective calorimetric glass transition temperatures, the conductivity is still lower in these ammonium ILs. As the length and volume fraction of the alkyl side chains of the ammonium cations increase and the nanophase segregation becomes increasingly pronounced, it was found that the dc conductivity, ion self-diffusion coefficients, and free ion concentrations systematically decrease. We hypothesize that as the alkyl domains occupy more of the liquid volume, the heterogeneous solvation environment causes the ion charge centers to reside for longer periods of time within a solvation site, resulting in slower ion mobility at any given temperature. The chemical heterogeneity not only slows down the ions, but it also causes them to

form more cohesive ion association clusters, causing a significant reduction in the mole fraction of free ions. Thus, we have shown that strong amphiphilicity is the underlying cause of the poor ionic conductivity in alkylammonium based ionic liquids.

6. Dynamics and Charge Transport in Carboxylic Acid-Based Protic ILs

6.1. Introduction

In the previous chapters, the influence of chemical structure on the molecular dynamics and charge transport properties was studied for two homologous series of aprotic ionic liquids. Whereas aprotic ionic liquids consist of permanently charge ions formed by covalently attaching molecular side groups to previously neutral molecules, another perhaps more diverse and versatile class of ionic liquids is formed through the ionization of neutral molecules due to the reversible proton transfer reaction between a Brønsted acid and a Brønsted base. These types of ionic liquids are known as protic ionic liquids (PILs).[68] Unlike the aprotic ILs, PILs may ionize completely or exist as a mixture of ionized and neutral molecules, and this equilibrium primarily depends on the level of free energy reduction due to the proton transfer reaction.[70]

It is very important to accurately determine the degree of ionization in PILs because many of the technological applications depend primarily on this property. As a result, several experimental studies based on analysis of the so-called Walden product have been performed to determine the degree of ionicity in PILs.[72, 74] According to Walden, the molar conductivity of an electrolyte or ionic liquid should be inversely proportional to the shear viscosity, such that the product $\Lambda \cdot \eta = Const$ is temperature invariant ($\Lambda = \sigma_0/n$ is the molar conductivity, n is the number density of free ions, and η is the shear viscosity).[94] If a protic ionic liquid has a low degree of ionization, the Walden product of this material will generally be reduced relative to a PIL with a higher degree of ionization. Angell and coworkers were the first to systematically assess the ionicity of PILs based on comparisons of Walden products, developing the concept of "good" and "poor" PILs.[72] MacFarlane and coworkers have taken a more holistic approach in their attempts to characterize the ionicity of PILs by analyzing Walden products in tandem with

acid indicator tests and infrared spectroscopy.[74, 96] These techniques can only qualitatively and relatively assess the degree of proton transfer in PILs, however. In order to quantify the degree of proton transfer in PILs, it is essential to characterize the microscopic transport properties, as was performed for the aprotic ionic liquids studied in the previous chapters.

Another important factor that distinguishes protic ILs from aprotic ILs is that the intrinsic charge carrier is no longer a permanently charged and bulky ion. Instead it is the transient protonic defect which results from proton transfer between an acid-base pair.[188] It is possible that due to the dramatic difference in the nature of the intrinsic charge carrier, the mechanism of charge transport could be significantly different in protic ILs when compared to aprotic ILs. It has been suggested that for some proton conducting liquids such as water[189] and phosphoric acid,[190] the migration of protons occurs via a "super-protonic" transport mechanism, wherein charge transport occurs much more rapidly than structural diffusion.

In this chapter, we will explore these interesting questions in a model protic ionic liquid formed by the neutralization reaction of a 1:2 mole ratio mixture of lidocaine (weak base) and decanoic acid (weak acid). We have found through analysis of dielectric and infrared spectroscopy data that the degree of ionicity in this PIL is moderately low, with only 25% of the decanoic acid existing in the ionized state at room temperature. Interestingly, the dielectric spectrum of this PIL can be effectively modeled using the Random Barrier Model, indicating that the charge transport mechanism of this PIL may be similar to the mechanism found for the aprotic ILs. Finally, we have found through the comparison of structural reorientation rates measured via quasielastic light scattering and the characteristic rates of charge transport measured via BDS that a super-protonic transport mechanism does not occur in this PIL. This indicates that anomalously fast charge transport is not a general phenomenon of all protic ionic

liquids. Our results demonstrate that despite the important distinctions which exist between the aprotic and protic ILs studied in this dissertation, the characteristic structural dynamics and charge transport mechanisms in these two families of ILs show many general similarities.

6.2. Experimental Details

Lidocaine (LID) powder (MW = 234.34 g/mol) and decanoic acid (DA) (MW = 172.26 g/mol) were purchased from Sigma Aldrich and used as received. The chemical structures of these compounds are shown in Fig. 6.1. The 1:2 mole ratio mixture of lidocaine to decanoic acid (heretofore known as LID-DA) was prepared by weighing out the proper amounts of the parent compounds into a cleaned, dried screw cap vial which was quickly sealed after loading.

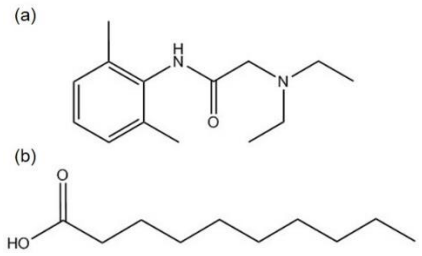

Figure 6.1. Chemical structure of (a) 2-diethylamino-N-(2,6-dimethylphenyl)acetamide (lidocaine) and (b) decanoic acid.

In order to thoroughly mix the sample, the LID-DA sealed sample was heated on a hot plate at 75°C and shaken until there was no visible phase separation remaining in the liquid mixture. The 1:2 mole ratio liquid was then cooled to room temperature and passed through a 220 nm PVDF filter into several cleaned, dried mL sized target vials for further characterization. This procedure was used to prepare mixtures of lidocaine and decanoic acid across the entire range of molar compositions. Some of the mixtures with high lidocaine content crystallized upon cooling and

were not filtered prior to further characterization. The mass density of the LID-DA sample was determined at room temperature (295 K) by weighing a measured volume of liquid sample five times and averaging the results. The density of LID-DA was measured to be ρ = 0.84 g/mL.

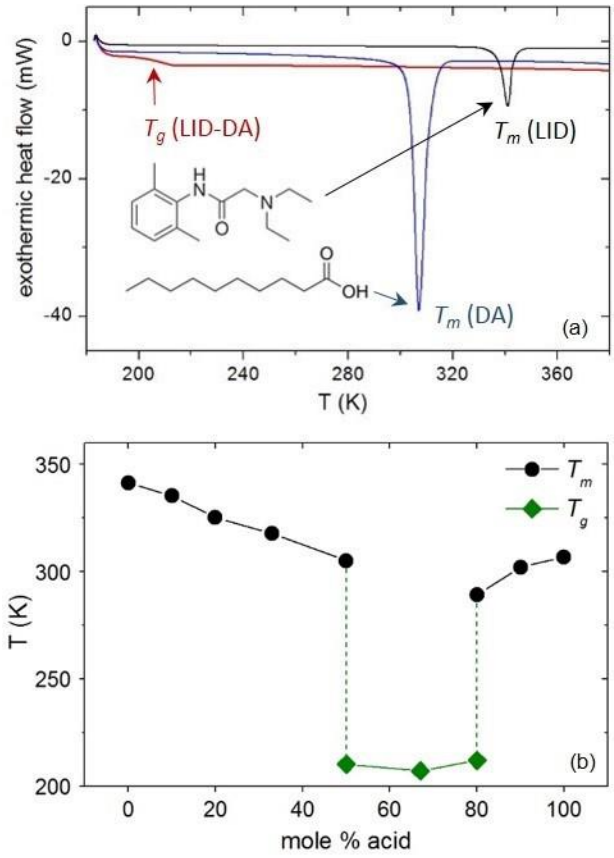

Figure 6.2. (a) DSC thermograms on heating at 10 K/min for the 1:2 mole ratio mixture of lidocaine and decanoic acid (LID-DA), neat lidocaine (LID), and neat decanoic acid (DA). (b) Thermal phase diagram of all measured molar compositions of lidocaine and decanoic acid.

Differential scanning calorimetry (DSC) measurements were performed using a Q2000 differential scanning calorimeter (TA instruments). The samples were measured on cooling and heating with a temperature ramp of 10 K/min. Figure 6.2(a) shows the DSC thermograms for the

LID-DA mixture and the parent compounds on heating after cooling from 400 K down to 185 K. Figure 6.2(b) shows the thermal phase diagram for the lidocaine:decanoic acid mixtures for all measured molar compositions. The melting transitions of lidocaine (Tm = 341 K) and decanoic acid (Tm = 307 K) were clearly visible in the DSC thermograms, but no crystallization or melting was apparent for the LID-DA sample. Instead, the glass transition was observed at Tg = 207 ± 2 K.

Broadband dielectric spectroscopy (BDS) measurements were performed on LID-DA at temperatures ranging from 330 K down to 200 K. The measurements were made using the Novocontrol Alpha-A dielectric analyzer in the frequency window 10-1 Hz to 10 MHz. The sample was measured in nitrogen atmosphere and the temperature was controlled using the Novocontrol Quatro system with temperature stability of ± 0.1 K.

Dynamic light scattering (DLS) measurements were performed to determine the structural reorientation rates of LID-DA over a temperature window from 270 K down to Tg. The measurements were performed in right angle geometry, laser wavelength = 647 nm and laser power = 125 mW. Vertically polarized laser light was focused on the sample in an Oxford Optistat cryostat (temperature stability of ± 0.1 K), and horizontally polarized scattered light was collected with a single mode optical fiber, split between two photodiode detectors, and cross-correlated using the ALV-7004/FAST multitau digital correlator.

6.3. Results and Discussion

6.3.1. Characterizing ionicity via FTIR and BDS

The FTIR spectra of the 1:2 mole ratio mixture, neat lidocaine, and neat decanoic acid were measured at room temperature in order to determine whether or not proton exchange had occurred between the acid and base parent compounds. Figure 6.3 presents the FTIR spectra of

these three materials in the carbonyl (C=O) stretching region (1400–1800 cm^{-1}).[191] It is evident from the comparison of the three spectra that a new vibrational mode is present in the LID-DA mixture centered near 1550 cm^{-1}. This vibrational mode corresponds to the stretching vibration of the carboxylate anion, which in this case is deprotonated decanoic acid.[191, 192] There is also a relatively large spectral signature of the neutral carbonyl stretching vibration near 1710 cm^{-1}, indicating that the LID-DA mixture consists of neutral and ionized decanoic acid moieties. Since the ΔpKa of the parent compounds is approximately 3,[193] it is expected that some degree of proton transfer should occur between decanoic acid and lidocaine.

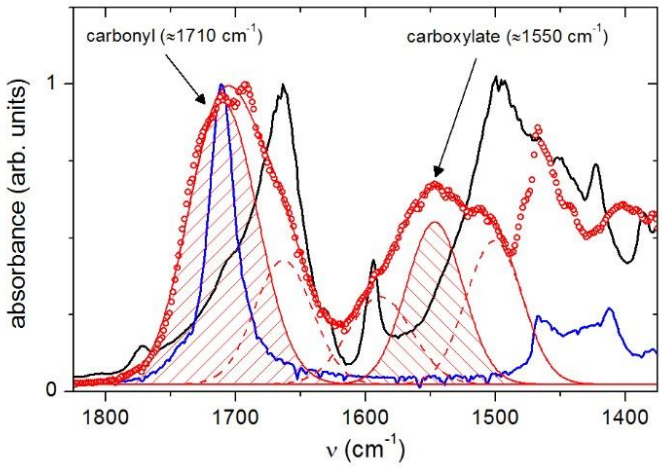

Figure 6.3. FTIR spectra of 1:2 lidocaine:decanoic acid mixture (red circles), lidocaine (black line), and decanoic acid (blue line) in the carbonyl stretching region. The LID-DA spectrum was fit using five Gaussian functions, with two components (filled) corresponding to decanoic acid vibrations and three components (unfilled) corresponding to lidocaine vibrations. The presence of the new carboxylate peak at 1550 cm^{-1} indicates that the LID-DA mixture is partially ionized.

In order to quantitatively estimate the degree of ionicity of LID-DA, we fit the two main bands of the vibrational spectrum with a superposition of five Gaussian functions in the carbonyl stretching region, as shown in Fig. 6.3, with two peaks accounting for the vibrations of ionized

and neutral decanoic acid molecules, while the remaining three peaks accounted for vibrations of lidocaine. The mole fraction of ionized decanoic acid was calculated such that

$$f_{COO^-} = \frac{A_{COO^-}}{A_{COO^-} + A_{COOH}} \quad (6.1)$$

where A_{COO^-} and A_{COOH} are the integrated absorbance of the carboxylate and carbonyl stretching vibrations, respectively. Using eq. 6.1, we have determined that approximately 30% of the decanoic acid in the LID-DA mixture is in the deprotonated state at room temperature. This degree of ionicity indicates that LID-DA might be considered a "poor" ionic liquid, similar to other mixtures of carboxylic acids and tertiary amines.[96] While it may have a relatively low degree of ionicity, the glass transition temperature of this mixture is much lower than that of most "good" protic ionic liquids, leading to a higher level of proton conductivity at room temperature.[194]

We proceeded to measure the complex dielectric spectrum of LID-DA via BDS in order to gain a better understanding of the microscopic dynamics and composition of this mixture. Figure 6.4 presents the complex conductivity $\sigma^*(f)$ and permittivity $\varepsilon^*(f)$ spectrum of LID-DA at several temperatures in the supercooled liquid regime. These spectra show many characteristics similar to those of the aprotic ionic liquids measured in the previous chapters, although there are some subtle differences which will be analyzed below.

The superposition model (eq. 4.6), which combines the Random Barrier Model (RBM) with the Havriliak Negami (HN) function, was used to analyze the dielectric spectrum of LID-DA. Using eq. 4.6, we have fit the dielectric data to extract the dc conductivity σ_0 and characteristic ion hopping rate $1/\tau_e$, as well as the dielectric strength $\Delta\varepsilon_{HN}$, characteristic relaxation rate τ_{HN}, and shape parameters α,β of the HN process at all measured temperatures. As was observed in Fig. 6.3, the composition of LID-DA is such that approximately 30% of the

molecules are ionized, while the remaining 70% exist in the neutral state. Due to the multicomponent nature of LID-DA, we interpret the HN contribution as arising primarily from the non-ionized, permanent dipole moieties of the LID-DA mixture. This type of bi-modal, ionic/nonionic dielectric spectrum has been observed before in moderately concentrated mixtures of glycerol and lithium chloride.[195]

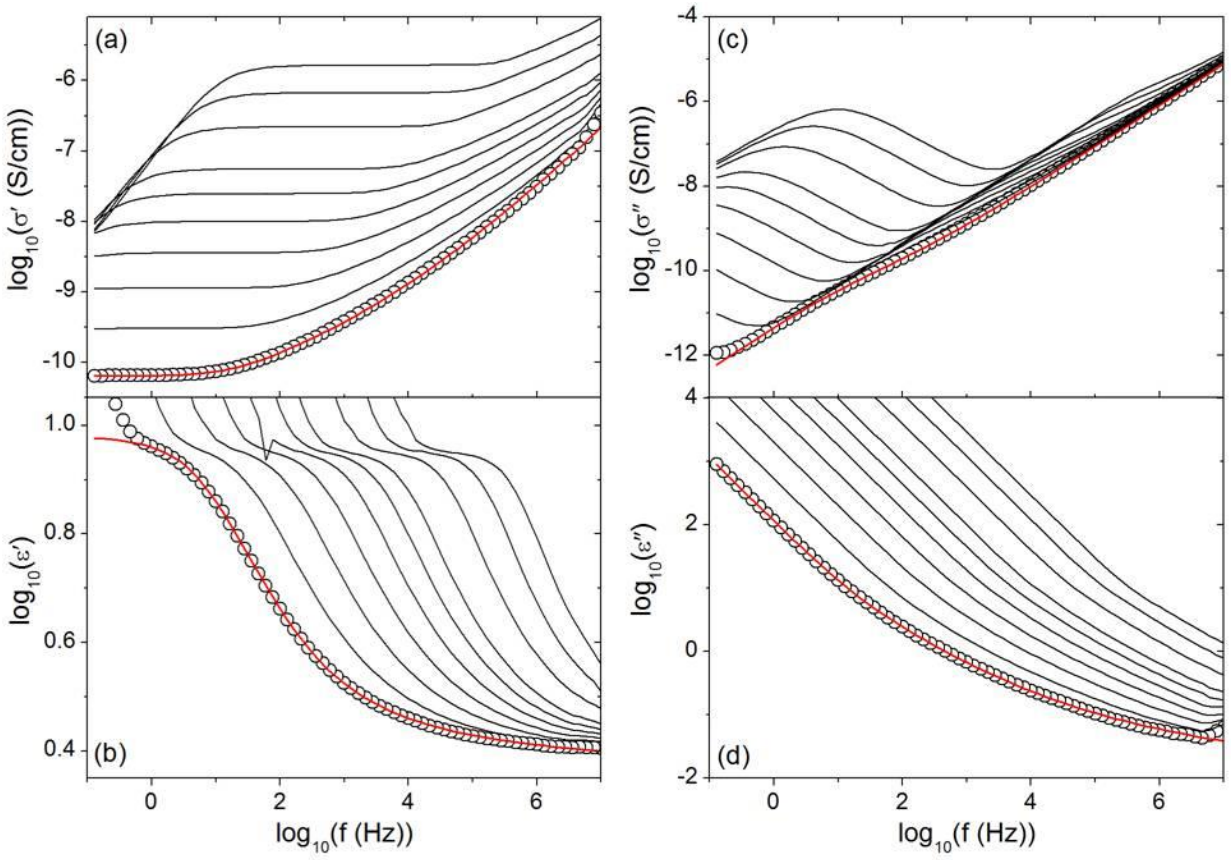

Figure 6.4. Real (a,c) and imaginary (b,d) parts of the complex conductivity and permittivity spectrum of 1:2 LID-DA measured at several temperatures in the supercooled liquid state. The red lines are fits of the spectra using the combined Random Barrier Model and Havriliak Negami function (eq. 4.6).

The detailed fitting of eq. 4.6 to the real part of the permittivity spectrum at ≈ T_g + 15 K is shown in Fig. 6.5(a), where it is seen that a majority of the spectral weight in the dielectric spectrum is contributed by the HN process, while a much smaller fraction is contributed by the RBM process. The Δε of the RBM contribution (ionic component of the permittivity spectrum) comprises approximately 25% of the cumulative dielectric strength at all measured temperatures, indicating that LID-DA is approximately 25% ionized at all measured temperatures.

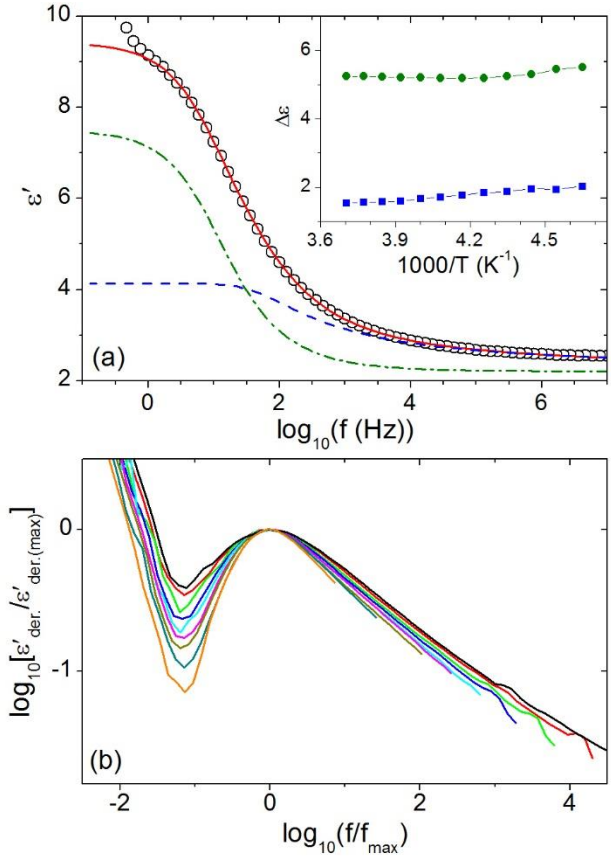

Figure 6.5. (a) Real permittivity of LID-DA measured at 225 K (open circles). The dashed blue line is the contribution from the Random Barrier Model (RBM), the green dashed-dotted line is the contribution from the Havriliak-Negami (HN) relaxation, and the red line is the cumulative fit. The inset presents the dielectric strength of the RBM and HN process as a function of inverse temperature. (b) The normalized real permittivity derivative spectra of LID-DA are shown at select temperatures.

One important distinction between the aprotic ILs studied in the previous chapter and the protic mixture LID-DA can be seen in the temperature dependence of the spectral shape of the complex permittivity (Fig. 6.4). It is observed that the ε′ spectrum of LID-DA (Fig. 6.4(b)) changes significantly as the temperature of the mixture decreases toward T_g. These changes in spectral shape are much more readily observed in the ε′ derivative ($\varepsilon'_{der.} = -\frac{\pi}{2} d\varepsilon'/d(\ln f)$) shown in Fig. 6.5(b), where the spectrum can be seen to broaden substantially with decreasing temperature. This is unlike the aprotic ILs studied in the previous chapters which roughly obey frequency-temperature superposition, and for which no strong changes in spectral shape occur with variation of temperature. Additionally, the slower, non-RBM relaxation process that was observed in the aprotic ionic liquids was found to have a Cole-Cole dispersion that did not change spectral shape or amplitude with temperature. For the LID-DA mixture, however, this slower relaxation process was found to have Havriliak-Negami dispersion at all measured temperatures, indicating that these spectral features likely have different microscopic origins.

The multicomponent nature of LID-DA may account for this strong, temperature dependent spectral broadening, similar to what has been observed for miscible polymer blends.[196] Spectral broadening on the high frequency side of the relaxation maximum is commonly observed for molecular and polymeric liquids.[197] While the reasons for high frequency spectral broadening are not well understood, this type of relaxation spectrum is generally explained by invoking the dynamical heterogeneity hypothesis. In polymer blends, on the other hand, composition fluctuations lead to strongly pronounced dynamical heterogeneity, where it is hypothesized that nanoscopic regions of the polymer melt have locally higher glass transition temperatures and consequently slower relaxation dynamics. Additionally, it is possible that as the temperature decreases, hydrophobic aggregation of the decanoic acid alkyl tails causes

the formation of nanoscale insulating moieties which lead to a Maxwell-Wagner-Sillars (MWS) interfacial polarization in the liquid matrix,[119] as was found for the case of the aprotic-ammonium ionic liquids discussed in the previous chapter. This process, would also contribute to the dielectric spectrum on the low frequency side of the charge transport process, leading to the observed spectral broadening.

The next step in the analysis of the dielectric data of LID-DA is to quantify the free ion concentration from the measurements of dc conductivity and the ion hopping rate. The charge carrying unit in the protic ionic liquids, however, is not a permanently charged ion as is the case of the aprotic ionic liquids, but instead it is the protonic defect which migrates through the acid-base matrix. In our hypothetical picture, protonic defects are transported through a transient chain of acid-base neutralization reactions. Under the assumption that this proton transport mechanism occurs via Brownian-like hopping, the Einstein relation and the RBM hopping time can be used to calculate the number density of protonic defects in LID-DA. In this case, the self diffusion coefficient of protonic defects can be calculated such that $D_{H^+} = \frac{\lambda^2}{2\tau_e}$, where λ is interpreted as the length a proton must hop in order to ionize an acid-base pair, and τ_e^{-1} is the ion hopping rate obtained from the analysis of the dielectric spectra using the RBM. Using the Einstein relation (eq. 4.7) and assuming that $D_{H^+} = D_+ = D_-$, $n_{H^+} = n_+ = n_-$, and $q_+ = q_- = e$ (the elementary charge), the concentration of protonic defects can be determined such that

$$n_{H^+} = \frac{\sigma_0 k_B T \tau_e}{\lambda^2 e^2} \tag{6.2}$$

Measurements of the self-diffusion coefficients of LID-DA were not performed and are not available in the literature. Consequently, it is necessary to estimate the hopping length λ in order to quantify the free ion concentration according to eq. 6.2. NMR chemical shift measurements of LID-DA indicate that the molecular moieties involved in proton exchange are

the carboxyl hydrogen of decanoic acid (donor) and the tertiary amine nitrogen of lidocaine (acceptor).[193] In order for ionization to occur, the covalent O–H bond must be cleaved and the new, ionized H–N^+ bond must be formed. The mean hydrogen bond length (H···N distance) for the O–H···N complex for similar mixtures is approximately 2 Å, and the H atom must jump a distance $d_{(H\cdots N)} - d_{(H-N^+)} \approx 1$ Å when ionization occurs.[198]

The temperature dependent number density of protonic defects in LID-DA was calculated using the above determined jump length in eq. 6.2. Using the measured mass density at 295 K and assuming that ionized protons can only be contributed by the decanoic acid carboxyl group, we have calculated the concentration of total ionizable protons in LID-DA to be $n_H = 1.75\times10^{27}$ m^{-3}. Combining this result with the calculated concentration of protonic defects (eq. 6.2), we have found that the mole fraction of protonic defects in LID-DA is $f = \frac{n_{H^+}}{n_H} = 0.23 \pm 0.05$ at room temperature. Surprisingly there is quantitative agreement between estimates of ionicity in LID-DA via FTIR, comparisons of the dielectric amplitudes of the RBM and HN processes, and also the calculation outlined above. This adds a strong support for our assignment of the proton hopping length to the hydrogen bond–covalent bond length difference, and it also adds validity to the proposed dielectric model (eq. 4.6) used to analyze the data.

It is interesting that the number density of protonic defects in LID-DA is temperature independent over the measured temperature range, as seen in the inset of Fig. 6.7. In proton conducting liquids such as LID-DA, charge transport occurs at the elementary level of the acid-base reaction and the proton hopping process.[188] Since the exchange of protons between hydrogen-bonded acid-base pairs occurs rapidly, equilibrium can be achieved during all but the most rapid structural rearrangement events (which may only occur at temperatures much higher than those probed in the experiment). The state of this equilibrium largely depends on the local

electronic properties of the lidocaine and decanoic acid molecules, which are relatively insensitive to temperature changes in the measured temperature range.[199] It thus follows that the number density (at the measured temperatures) of protonic defects in LID-DA should also be insensitive to temperature—as has been found from analysis of the dielectric spectrum. This observed behavior of the protic IL mixture LID-DA is very different from what was found for the aprotic ionic liquids studied in the previous chapters, in which the number density of free ions decreases with decreasing temperature with an Arrhenius type of thermal activation as a result of the long range electrostatic interaction.

6.3.2. Structural dynamics and the question of "superionic" transport

Having assessed the ionicity and characteristic charge transport properties of the LID-DA mixture in the previous section, the next question to address is how the rate of charge transport relates to structural reorientation in LID-DA. In order to explore this question in more detail, we have measured the characteristic molecular reorientation times using dynamic light scattering (DLS). The normalized intensity correlation functions (ICF) measured via DLS at selected temperatures are shown in Fig 6.6(a). While it is not immediately evident by visual inspection of the data, these ICFs are comprised of two superposed decays at all measured temperatures, as is demonstrated in the fitting of the field correlation representation in Fig. 6.6(b). The characteristic reorientational relaxation times were deduced by fitting the ICFs with a superposition of two KWW stretched exponential functions (eq. 4.3). Fig. 6.6 depicts the fitting of the ICF, as well as the field correlation function $g^1(t)$, using eq. 4.3, and the contributions of the fast and slow relaxation processes to the FCF are illustrated in Fig. 6.6(b). The reorientational relaxation times determined from these fits are plotted in Fig. 6.7, and the stretching parameters of the two

relaxation processes were found to be temperature independent at all measured temperatures, with $\beta_{fast} \approx 0.30$ and $\beta_{slow} \approx 0.60$.

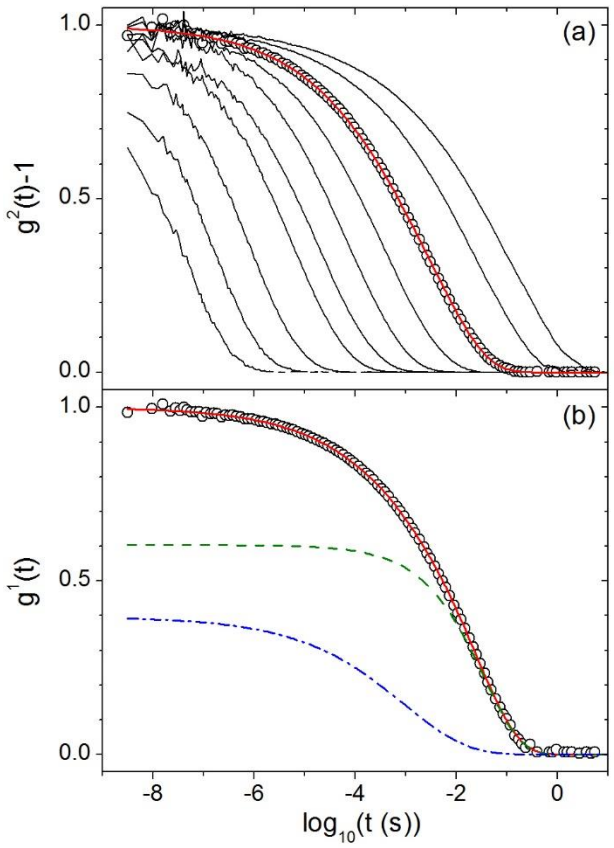

Figure 6.6. (a) Normalized intensity correlation functions measured in LID-DA at selected temperatures. The red line represents the fit of the data at one temperature using a superposition of 2 KWW functions (eq. 4.3). (b) The normalized field correlation function measured at one temperature is shown fit to eq 4.3 (red line). The dashed green line and dash-dotted blue line represent the single KWW relaxation functions contributing to the total fit.

The relaxation times measured via DLS were fit with the Vogel-Fulcher-Tammann (VFT) function $\tau = \tau_0 \exp(\frac{A}{T-T_0})$,[18, 19] where τ_0, A, and T_0 are fit parameters, in order to determine which relaxation process is associated with the calorimetric glass transition. The

dynamic glass transition temperature (at τ = 100 s) was calculated for both the fast ($T_{g\text{-}fast}$ = 199 K) and slow process ($T_{g\text{-}slow}$ = 205 K). Since the dynamic glass transition temperature associated with the slow process is nearly identical to the calorimetric glass transition temperature (T_g = 207 K), we assign this feature to the structural relaxation process of the LID-DA mixture. The dynamic fragility of the structural relaxation process was also calculated to be m = 70, indicating that LID-DA is a moderately fragile glass-forming liquid.

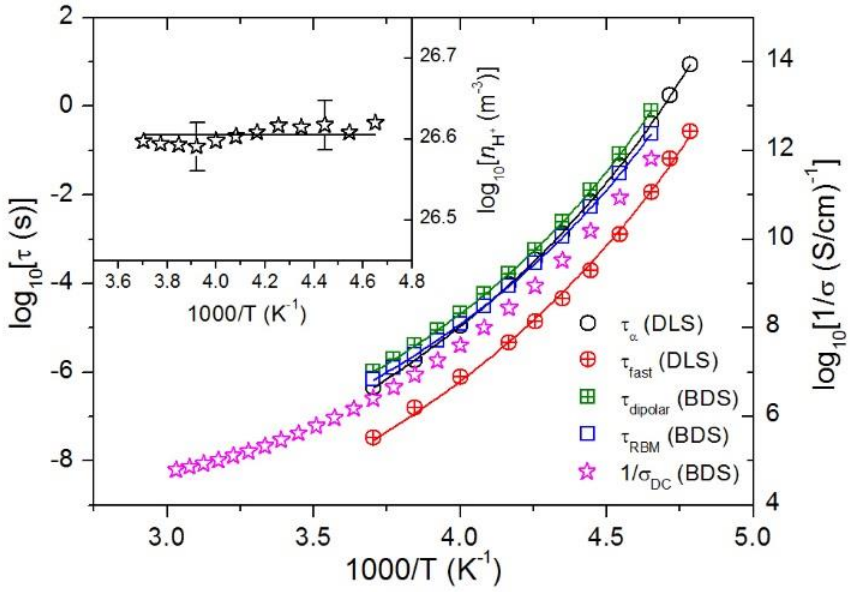

Figure 6.7. The characteristic relaxation times measured via BDS and DLS, as well as the dc conductivity are shown plotted against inverse temperature. The solid lines are Vogel-Fulcher-Tammann fits to the corresponding data. The inset presents the temperature dependent number density of protonic defects calculated via eq. 6.2.

It is very interesting that we once again see two structural relaxation modes in the DLS spectrum of LID-DA, similar to the case of the alkylammonium ILs. This indicates that the nanoscale chemical structure of LID-DA may be highly heterogeneous. The heterogeneity scenario is corroborated by our dielectric measurements, in which strong spectral broadening

was observed that may be contributed to local composition fluctuations.[197] We speculate that the fast relaxation process in the ICF may be connected to fluctuations of the alkyl tails of the decanoic acid, while the slow process may be connected to fluctuations of the phenyl rings of the lidocaine molecule. Interestingly, the stretching parameter of the fast DLS process was found to be $\beta_{KWW} \approx 0.30$, which is identical to the stretching parameter associated with the fluctuations of the alkyl tails of the aprotic-ammonium ILs studied in the previous chapter. It is likely that the flexibility of the alkyl chains allows for faster motions relative to the rotation of phenyl rings, which are rigid and require a concerted motion of the entire lidocaine molecule.

The DLS spectrum of LID-DA differs considerably when compared to the spectrum of the hydrogen bonded liquid 2-ethyl-4-methylimidazole (2E4MIm), a neat molecular liquid proton conductor.[178] A two-step DLS spectrum was also observed for 2E4MIm, although the fast process was found to be related to structural relaxation, while the slow process (which was Debye-like) was demonstrated to be connected to the coherent motion of supramolecular chains comprised of 3-4 molecules. In LID-DA, we find no evidence of a Debye-like process associated with supramolecular aggregates or clusters, which are postulated to be connected to a potential ultra-fast transport mechanism in proton conducting liquids.[200]

It is hypothesized that a "super-protonic" transport mechanism may exist in some kinds of protic ionic liquids, in which protonic defects are able to migrate much more rapidly than the host molecules can execute molecular reorientations. This hypothetical process is similar to the Grotthuss mechanism in water,[189] and it was recently suggested that fast proton transport occurs in phosphoric acid,[190] as well as in some pharmaceutical based protic ionic liquids.[201] As is seen in Fig. 6.7, the charge transport rate in LID-DA is nearly identical to the rate of structural reorientation measured via DLS. The type of conduction mechanism observed for LID-DA is

reminiscent of the "vehicle mechanism", in which protonic defects migrate as passengers on the parent molecules.[202] Our results indicate that the charge transport properties of protic ionic liquids may vary dramatically depending on the chemical properties of the liquid molecules, and clearly, the mechanism of proton transport found in LID-DA is much different than in water and phosphoric acid, which exhibit a Grotthuss-like transport mechanism.

6.4. Conclusions

In this chapter, we have studied the structural dynamics and charge transport properties of a 1:2 mole ratio mixture of lidocaine and decanoic acid. Corroborating earlier studies, we have found that this mixture can be characterized as a "deep eutectic mixture", in which there is no measureable melting transition, and only a glass transition can be detected.[193] Additionally, this mixture exhibits a modest level of intrinsic proton conductivity, leading us to classify it as a weakly ionized, "poor" protic ionic liquid. From the analysis of FTIR and BDS measurements, we have determined that the fraction of ionized moieties in this mixture is relatively low, with approximately 25% of the decanoic acid existing in the ionized state at ambient temperature. Even though the charge carrier (the protonic defect) in this protic ionic liquid mixture is quite different from the case of the aprotic ionic liquids, in which charge is transported via permanently charged counterions, we have demonstrated that the Random Barrier Model (RBM) can adequately describe the permittivity spectrum of LID-DA. This may indicate that the Brownian-like hopping mechanism which is at the core of the RBM occurs in a wide variety of conducting liquids, regardless of the nature of the charge carrier.

The structural dynamics as measured via dynamic light scattering were also found to be quite complex in this protic ionic liquid, where a bi-modal relaxation function was observed at all measurement temperatures. Similar to the case of the alkylammonium ionic liquids studied in

the previous chapter, we hypothesize that pronounced compositional heterogeneity causes a degree of nanophase segregation to occur in this mixture. We speculate that fluctuations of the alkyl tails of decanoic acid are connected to the faster relaxation process, while the fluctuations of the phenyl rings of lidocaine are connected to the slow relaxation process and the calorimetric glass transition.

One of the major questions about conductivity in protic ionic liquids is whether or not a "super-protonic" transport mechanism may occur in the liquid state of these materials. While the ionic liquid mixture LID-DA is indeed an intrinsic proton conductor, we have demonstrated that the characteristic rate of charge transport is practically identical to the characteristic rate of structural relaxation at all measured temperatures. Thus, proton transport is directly coupled to and rate-limited by structural motions in LID-DA. This result stands in contrast to the generally accepted proton transport mechanism of water and phosphoric acid, in which protonic defects are known to migrate faster than structural relaxation can occur. Our results, in conjunction with studies of other proton conducting liquids, suggest that the details of the chemical structure of the proton donor and acceptor molecules can strongly alter the conduction mechanism in protic ionic liquids.

7. Concluding Remarks

Room temperature ionic liquids are an important class of materials which have the potential to be used to solve many of the pressing chemical and electrochemical challenges facing society both today and in the future. Whether as recyclable, "green" reaction media in modern chemical synthesis, or as non-volatile and non-hazardous electrolytes in batteries and fuel cells, ionic liquids are currently being explored for a multitude of technological applications. In order to properly utilize these materials, however, it is essential to develop a predictive understanding of the fundamental relationships between chemical structure and physicochemical properties of ionic liquids. To this end, this dissertation presented experimental studies of three subsets of ionic liquids which were performed to characterize how the molecular level transport properties are connected to and influenced by the chemical structure of the constituent ions. In addition, these studies have also elucidated the interrelationship between the reorientational molecular (structural) dynamics and the translational charge transport process in ionic liquids.

In the first part of this dissertation, the reorientational structural dynamics and charge transport properties were characterized in a homologous series of 1-butyl-3-methylimidazolium based ionic liquids, in which the anion size and chemical structure were systematically varied. It was found that the glass transition temperatures of these ionic liquids decrease as the anion becomes larger and the degree of asymmetry increases. As a result, the ionic mobility strongly increases for those materials with lower glass transition temperatures, and the ionic conductivity also increases significantly. Interestingly, the anion chemical structure was found to have no measurable impact on the mole fraction of simultaneously conducting (free) ions. These results suggest that whereas ion association is likely controlled by the coarse-grained nature of the

electrostatic interaction, the ion transport process is instead strongly influenced by the local, molecular level friction mechanism.

The studied ionic liquids were also found to exhibit dynamical properties which are quite different from those of most molecular glass forming liquids. Remarkably, none of the ionic liquids exhibited the so-called dynamic crossover, which is nearly ubiquitously observed in molecular liquids. Furthermore, the spectral shape of the reorientational structural relaxation process was found to be temperature independent from above the melting temperature down to the glass transition temperature—another unusual finding. Finally, the decoupling of translational from rotational motions in these ionic liquids, while certainly present, was found to be only weakly pronounced when compared to other supercooled liquids with similar glass transition temperatures and dynamic fragilities. These unique dynamical characteristics differentiate ionic liquids from many other glass forming liquids, and it is hypothesized that these differences are connected to the distinctive interionic interaction mechanisms of ionic liquids.

Having characterized the influence of the anion chemical structure, the next part of the dissertation presented studies of the structural dynamics and charge transport properties of a series of three tetraalkylammonium bis(trifluoromethylsulfonyl)imide ionic liquids in which the alkyl side chains were systematically varied. Upon changing the alkyl side chain length and volume fraction, strong changes in the ionic conductivities, glass transition temperatures, and structural dynamics were found to occur. It was shown, remarkably so, that the nanophase segregation of apolar alkyl side chains from the charge-rich ion centers—which is known to occur in these liquids—has a surprisingly pronounced effect on the structural dynamics. This nanophase segregation induces strong dynamical heterogeneity in the ammonium based ionic

liquids. It is so strongly pronounced that two distinct structural relaxation modes—corresponding to relaxation in the alkyl-rich and the charge-rich domains—were observed in the relaxation spectra of all three studied materials at all measured temperatures.

Not only did the cation chemical composition significantly impact the structural dynamics in these liquids, but it also had a strong impact on the charge transport properties. As the length and volume fraction of the alkyl side chain moieties increased, it was found that the ionic mobility, as well as the mole fraction of free ions, strongly decreased. It was hypothesized that as the alkyl domains occupy more of the liquid volume, the ion charge centers are forced to form long-lived aggregates which reduce the mole fraction of free ions and considerably hinder charge mobility. Thus, strong amphiphilicity of the cation significantly limits charge transport in ionic liquids.

Whereas the first two parts of this dissertation were concerned with aprotic ionic liquids, the final part presented studies of the structural dynamics and charge transport properties of a carboxylic acid-tertiary amine based protic ionic liquid. One of the key properties of the protic ionic liquids, which are formed upon reaction of a Brønsted acid and Brønsted base, is that they generally do not completely ionize and instead consist of a mixture of ionized and neutral moieties. This dissertation demonstrated a potential way to quantify the degree of ionicity in protic ionic liquids using a combination of infrared and dielectric spectroscopy. While the charge carrier in protic ionic liquids (the protonic defect) is intrinsically different from that of aprotic ionic liquids, the mechanism of charge transport was found to be nonetheless very similar to the aprotic ionic liquids, in which ion transport occurs via a Brownian-like hopping mechanism according to the Random Barrier Model. Finally, it was shown that the rate of proton transport

in the carboxylic acid-based protic ionic liquid is nearly identical to the rate of structural relaxation, indicating that a "super-protonic" transport mechanism is not present in this liquid.

Through these studies, the interrelationship between chemical structure and molecular transport properties of ionic liquids was explored. Certainly there is a great deal of work left to be done in order to fully understand the properties of these important materials. There remains much to understand about the influence of nanophase segregation on the microscopic structural dynamics and charge transport properties of ionic liquids, and consequentially this is a very active area of current ionic liquid research. Research along the lines presented in this dissertation could have a significant impact on the field. Furthermore, studies of the molecular transport properties of protic ionic liquids have only scratched the surface of this very large and technologically significant field of research. There are many important discoveries to be made here, and studies similar to those presented in this dissertation will certainly help to uncover the interesting nature of the protic ionic liquids as well.

References

1. R. D. Rogers and K. R. Seddon, *Science*, 2003, **302**, 792.
2. M. Armand, F. Endres, D. R. MacFarlane, H. Ohno and B. Scrosati, *Nat. Mater.*, 2009, **8**, 621.
3. N. V. Plechkova and K. R. Seddon, *Chem. Soc. Rev.*, 2008, **37**, 123.
4. C. A. Angell, K. L. Ngai, G. B. McKenna, P. F. McMillan and S. W. Martin, *J. Appl. Phys.*, 2000, **88**, 3113.
5. P. G. Debenedetti and F. H. Stillinger, *Nature*, 2001, **410**, 259.
6. M. Ediger, C. Angell and S. R. Nagel, *J. Phys. Chem.*, 1996, **100**, 13200.
7. J. C. Dyre, *Rev. Mod. Phys.*, 2006, **78**, 953.
8. M. Ediger and P. Harrowell, *J. Chem. Phys.*, 2012, **137**, 080901.
9. H. Tanaka, *J. Non-Cryst. Solids*, 2005, **351**, 678.
10. H. Tanaka, *J. Chem. Phys.*, 1999, **111**, 3163.
11. H. Tanaka, *J. Chem. Phys.*, 1999, **111**, 3175.
12. D. Kivelson, S. A. Kivelson, X. Zhao, Z. Nussinov and G. Tarjus, *Physica A*, 1995, **219**, 27.
13. D. Kivelson and G. Tarjus, *J. Non-Cryst. Solids*, 1998, **235**, 86.
14. E. W. Castner Jr and J. F. Wishart, *J. Chem. Phys.*, 2010, **132**, 120901.
15. C. A. Angell, *Science*, 1995, **267**, 1924.
16. S. Arrhenius, *Z. Phys. Chem.*, 1889, **4**, 226.
17. L.-M. Martinez and C. Angell, *Nature*, 2001, **410**, 663.
18. H. Vogel, *Phys. Z.*, 1921, **22**, 645.
19. G. S. Fulcher, *J. Am. Ceram. Soc.*, 1925, **8**, 339.
20. W. Kauzmann, *Chem. Rev.*, 1948, **43**, 219.
21. J. H. Gibbs and E. A. DiMarzio, *J. Chem. Phys.*, 1958, **28**, 373.
22. H. Tanaka, *Phys. Rev. E*, 2003, **68**, 011505.
23. F. H. Stillinger, *J. Chem. Phys.*, 1988, **88**, 7818.
24. J. C. Mauro, R. J. Loucks and S. Sen, *J. Chem. Phys.*, 2010, **133**, 164503.
25. R. Böhmer and C. A. Angell, *Phys. Rev. B*, 1992, **45**, 10091.
26. Q. Qin and G. B. McKenna, *J. Non-Cryst. Solids*, 2006, **352**, 2977.
27. G. Adam and J. H. Gibbs, *J. Chem. Phys.*, 1965, **43**, 139.
28. O. Yamamuro, I. Tsukushi, A. Lindqvist, S. Takahara, M. Ishikawa and T. Matsuo, *J. Phys. Chem. B*, 1998, **102**, 1605.
29. S. Takahara, O. Yamamuro and T. Matsuo, *J. Phys. Chem.*, 1995, **99**, 9589.
30. F. Stickel, Ph.D. Thesis, Johannes Gutenberg-Universitat Mainz, 1995.
31. F. Stickel, E. Fischer and R. Richert, *J. Chem. Phys.*, 1995, **102**, 6251.
32. F. Stickel, E. W. Fischer and R. Richert, *J Chem Phys*, 1996, **104**, 2043.
33. M. Goldstein, *J. Chem. Phys.*, 1969, **51**, 3728.

34. W. Götze, *Condens. Matter Phys.*, 1998, **4**, 873.
35. D. R. Reichman and P. Charbonneau, *J. Stat. Mech.*, 2005, **05**, P05013.
36. V. Novikov and A. Sokolov, *Phys. Rev. E*, 2003, **67**, 031507.
37. S. Chong, S. Chen and F. Mallamace, *J. Phys.-Condens. Mat.*, 2009, **21**, 504101.
38. M. D. Ediger, *Ann. Rev. Phys. Chem.*, 2000, **51**, 99.
39. L. Berthier and G. Biroli, *Rev. Mod. Phys.*, 2011, **83**, 587.
40. J. Phillips, *Rep. Prog. Phys.*, 1996, **59**, 1133.
41. G. Williams and D. C. Watts, *T. Faraday Soc.*, 1970, **66**, 80.
42. B. J. Berne and R. Pecora, *Dynamic Light Scattering: with Applications to Chemistry, Biology, and Physics*, Dover, New York, 2000.
43. R. Böhmer, R. Chamberlin, G. Diezemann, B. Geil, A. Heuer, G. Hinze, S. Kuebler, R. Richert, B. Schiener and H. Sillescu, *J. Non-Cryst. Solids*, 1998, **235**, 1.
44. R. Richert, *J. Phys.-Condens. Mat.*, 2002, **14**, R703.
45. R. G. Palmer, D. L. Stein, E. Abrahams and P. W. Anderson, *Phys. Rev. Lett.*, 1984, **53**, 958.
46. A. S. Keys, L. O. Hedges, J. P. Garrahan, S. C. Glotzer and D. Chandler, *Phys. Rev. X*, 2011, **1**, 021013.
47. F. Demmel and C. Morkel, *Phys. Rev. E*, 2012, **85**, 051204.
48. A. Faraone, K. Hong, L. R. Kneller, M. Ohl and J. R. Copley, *J. Chem. Phys.*, 2012, **136**, 104502.
49. S. Reinsberg, X. Qiu, M. Wilhelm, H. Spiess and M. Ediger, *J. Chem. Phys.*, 2001, **114**, 7299.
50. K. Schmidt-Rohr and H. Spiess, *Phys. Rev. Lett.*, 1991, **66**, 3020.
51. B. Schiener, R. Böhmer, A. Loidl and R. Chamberlin, *Science*, 1996, **274**, 752.
52. C.-Y. Wang and M. Ediger, *J. Phys. Chem. B*, 1999, **103**, 4177.
53. C.-Y. Wang and M. Ediger, *J. Chem. Phys.*, 2000, **112**, 6933.
54. S. F. Swallen, K. Traynor, R. J. McMahon, M. Ediger and T. E. Mates, *J. Phys. Chem. B*, 2009, **113**, 4600.
55. A. Einstein, *Investigations on the Theory of Brownian Motion*, Dover, New York, 1956.
56. P. Debye, *Polar Molecules*, Dover, New York, 1929.
57. M. K. Mapes, S. F. Swallen and M. Ediger, *J. Phys. Chem. B*, 2006, **110**, 507.
58. K. S. Schweizer and E. J. Saltzman, *J. Phys. Chem. B*, 2004, **108**, 19729.
59. J. C. Dyre, *Phys. Rev. Lett.*, 2013, **110**, 245901.
60. D. B. Sirdeshmukh, L. Sirdeshmukh and K. Subhadra, *Alkali Halides*, Springer, Berlin, 2001.
61. D. MacFarlane, P. Meakin, N. Amini and M. Forsyth, *J. Phys.-Condens. Mat.*, 2001, **13**, 8257.
62. C. A. Angell, N. Byrne and J.-P. Belieres, *Accounts Chem. Res.*, 2007, **40**, 1228.
63. H. Ohno, *Electrochemical aspects of ionic liquids*, John Wiley & Sons, New Jersey, 2011.
64. D. R. MacFarlane, N. Tachikawa, M. Forsyth, J. M. Pringle, P. C. Howlett, G. D. Elliott, J. H. Davis, M. Watanabe, P. Simon and C. A. Angell, *Energ. Environ. Sci.*, 2014, **7**, 232.

65. M. Smiglak, J. Pringle, X. Lu, L. Han, S. Zhang, H. Gao, D. MacFarlane and R. Rogers, *Chem. Comm.*, 2014. DOI: 10.1039/C4CC02021A

66. D. R. MacFarlane, M. Forsyth, P. C. Howlett, J. M. Pringle, J. Sun, G. Annat, W. Neil and E. I. Izgorodina, *Accounts Chem. Res.*, 2007, **40**, 1165.

67. J. Sun, D. MacFarlane and M. Forsyth, *Ionics*, 1997, **3**, 356.

68. T. L. Greaves and C. J. Drummond, *Chem. Rev.*, 2008, **108**, 206.

69. M. A. Susan, A. Noda, S. Mitsushima and M. Watanabe, *Chem. Comm.*, 2003, 938.

70. J.-P. Belieres and C. A. Angell, *J. Phys. Chem. B*, 2007, **111**, 4926.

71. P. Walden, *Bull. Acad. Imper. Sci.(St. Petersburg)*, 1914, **8**, 405.

72. M. Yoshizawa, W. Xu and C. A. Angell, *J. Am. Chem. Soc.*, 2003, **125**, 15411.

73. J. Stoimenovski and D. R. MacFarlane, *Chem. Comm.*, 2011, **47**, 11429.

74. J. Stoimenovski, P. M. Dean, E. I. Izgorodina and D. R. MacFarlane, *Faraday Discuss.*, 2012, **154**, 335.

75. H. Nakamoto and M. Watanabe, *Chem. Comm.*, 2007, 2539.

76. K. Kreuer, *Solid State Ionics*, 1997, **97**, 1.

77. W. Xu and C. A. Angell, *Science*, 2003, **302**, 422.

78. D. McFarlane, J. Sun, J. Golding, P. Meakin and M. Forsyth, *Electrochim. Acta*, 2000, **45**, 1271.

79. W. Xu, E. I. Cooper and C. A. Angell, *J. Phys. Chem. B*, 2003, **107**, 6170.

80. J. Sangoro, A. Serghei, S. Naumov, P. Galvosas, J. Kärger, C. Wespe, F. Bordusa and F. Kremer, *Phys. Rev. E*, 2008, **77**, 051202.

81. J. R. Sangoro and F. Kremer, *Accounts Chem. Res.*, 2011, **45**, 525.

82. P. Atkins and J. de Paula, *Atkins' Physical Chemistry*, W. H. Freeman and Company, New York, 2006.

83. H. Tokuda, K. Hayamizu, K. Ishii, M. A. B. H. Susan and M. Watanabe, *J. Phys. Chem. B*, 2004, **108**, 16593.

84. H. Tokuda, K. Hayamizu, K. Ishii, M. A. B. H. Susan and M. Watanabe, *J. Phys. Chem. B*, 2005, **109**, 6103.

85. H. Tokuda, K. Ishii, M. A. B. H. Susan, S. Tsuzuki, K. Hayamizu and M. Watanabe, *J. Phys. Chem. B*, 2006, **110**, 2833.

86. H. Tokuda, S. Tsuzuki, M. A. B. H. Susan, K. Hayamizu and M. Watanabe, *J. Phys. Chem. B*, 2006, **110**, 19593.

87. D. A. Turton, J. Hunger, A. Stoppa, G. Hefter, A. Thoman, M. Walther, R. Buchner and K. Wynne, *J. Am. Chem. Soc.*, 2009, **131**, 11140.

88. C. Hardacre, J. D. Holbrey, M. Nieuwenhuyzen and T. G. Youngs, *Accounts Chem. Res.*, 2007, **40**, 1146.

89. J. N. Canongia Lopes and A. A. Pádua, *J. Phys. Chem. B*, 2006, **110**, 3330.

90. J. Sangoro, C. Iacob, A. Serghei, S. Naumov, P. Galvosas, J. Kärger, C. Wespe, F. Bordusa, A. Stoppa and J. Hunger, *J. Chem. Phys.*, 2008, **128**, 214509.

91. C. Krause, J. Sangoro, C. Iacob and F. Kremer, *J. Phys. Chem. B*, 2009, **114**, 382.

92. J. Sangoro, C. Iacob, A. Serghei, C. Friedrich and F. Kremer, *Phys. Chem. Chem. Phys.*, 2009, **11**, 913.

93. P. Griffin, A. L. Agapov, A. Kisliuk, X.-G. Sun, S. Dai, V. N. Novikov and A. P. Sokolov, *J. Chem. Phys.*, 2011, **135**, 114509.

94. P. Walden, *Z. Phys. Chem.*, 1906, **55**, 207.

95. D. R. MacFarlane, M. Forsyth, E. I. Izgorodina, A. P. Abbott, G. Annat and K. Fraser, *Phys. Chem. Chem. Phys.*, 2009, **11**, 4962.

96. J. Stoimenovski, E. I. Izgorodina and D. R. MacFarlane, *Phys. Chem. Chem. Phys.*, 2010, **12**, 10341.

97. Y. Nishiyama, M. Fukuda, M. Terazima and Y. Kimura, *J. Chem. Phys.*, 2008, **128**, 164514.

98. A. Kaintz, G. Baker, A. Benesi and M. Maroncelli, *J. Phys. Chem. B*, 2013, **117**, 11697.

99. C. Schreiner, S. Zugmann, R. Hartl and H. J. Gores, *J. Chem. Eng. Data*, 2009, **55**, 1784.

100. A. Rivera, A. Brodin, A. Pugachev and E. Rössler, *J. Chem. Phys.*, 2007, **126**, 114503.

101. N. Ito and R. Richert, *J. Phys. Chem. B*, 2007, **111**, 5016.

102. A. Triolo, O. Russina, H.-J. Bleif and E. Di Cola, *J. Phys. Chem. B*, 2007, **111**, 4641.

103. C. Schröder, T. Rudas, G. Neumayr, W. Gansterer and O. Steinhauser, *J. Chem. Phys.*, 2007, **127**, 044505.

104. Y. Wang and G. A. Voth, *J. Am. Chem. Soc.*, 2005, **127**, 12192.

105. O. Russina, A. Triolo, L. Gontrani and R. Caminiti, *J. Phys. Chem. Lett.*, 2011, **3**, 27.

106. J. J. Hettige, H. K. Kashyap, H. V. Annapureddy and C. J. Margulis, *J. Phys. Chem. Lett.*, 2012, **4**, 105.

107. H. V. Annapureddy, H. K. Kashyap, P. M. De Biase and C. J. Margulis, *J. Phys. Chem. B*, 2010, **114**, 16838.

108. Y. Wang and G. A. Voth, *J. Phys. Chem. B*, 2006, **110**, 18601.

109. T. Pott and P. Méléard, *Phys. Chem. Chem. Phys.*, 2009, **11**, 5469.

110. K. Shimizu, A. l. A. Pádua and J. N. Canongia Lopes, *J. Phys. Chem. B*, 2010, **114**, 15635.

111. H. K. Kashyap, C. S. Santos, H. V. Annapureddy, N. S. Murthy, C. J. Margulis and E. W. Castner Jr, *Faraday Discuss.*, 2012, **154**, 133.

112. J. O'M. Bockris and A. K. N. Reddy, *Modern Electrochemsitry 1:Ionics*, Plenum Press, New York, 1998.

113. H. Namikawa, *J. Non-Cryst. Solids*, 1975, **18**, 173.

114. J. C. Dyre, *J. Appl. Phys.*, 1988, **64**, 2456.

115. J. C. Dyre, *J. Non-Cryst. Solids*, 1991, **135**, 219.

116. J. C. Dyre, *J. Non-Cryst. Solids*, 1986, **88**, 271.

117. J. C. Dyre, P. Maass, B. Roling and D. L. Sidebottom, *Rep. Prog. Phys.*, 2009, **72**, 046501.

118. L. Pauling, *The Nature of the Chemical Bond*, Cornell University Press, New York, 1960.

119. F. Kremer and A. Schönhals, *Broadband Dielectric Spectroscopy*, Springer, Berlin, 2003.
120. J. D. Jackson, *Classical Electrodynamics*, Wiley, New York, 1999.
121. K. C. Kao, *Dielectric Phenomena in Solids*, Elsevier, San Diego, 2004.
122. H. B. Callen and T. A. Welton, *Phys. Rev.*, 1951, **83**, 34.
123. C. Lindsey and G. Patterson, *J. Chem. Phys.*, 1980, **73**, 3348.
124. H. Fröhlich, *Theory of Dielectrics*, Oxford University Press, London, 1949.
125. R. Böhmer, K. Ngai, C. Angell and D. Plazek, *J. Chem. Phys.*, 1993, **99**, 4201.
126. K. S. Cole and R. H. Cole, *J. Chem. Phys.*, 1941, **9**, 341.
127. D. Davidson and R. Cole, *J. Chem. Phys.*, 1950, **18**, 1417.
128. S. Havriliak and S. Negami, *Polymer*, 1967, **8**, 161.
129. H. C. Van De Hulst, *Light Scattering by Small Particles*, Wiley, New York, 1957.
130. B. Chu, *Laser Light Scattering*, Academic Press, Inc., San Diego, 1974.
131. H. Cummins, G. Li, W. Du, R. M. Pick and C. Dreyfus, *Phys. Rev. E*, 1996, **53**, 896.
132. R. K. Pathria, *Statistical Mechanics*, Butterworth-Heinemann, Oxford, 1996.
133. G. Williams, *Chem. Soc. Rev.*, 1978, **7**, 89.
134. A. Agapov, Ph.D. Thesis, University of Akron, 2011.
135. J. Sandercock, *Tandem Fabry Perot Interferometer Operator Manual*, 2001.
136. J. D. Ferry, *Viscoelastic properties of polymers*, John Wiley & Sons, New York, 1980.
137. K. Ngai, *Relaxation and Diffusion in Complex Systems*, Springer, New York, 2011.
138. J. Sestak, J. Mares and P. Hubik, *Thermal Analysis of Micro, Nano- and Non-Crystalline Materials*, Springer, New York, 2011.
139. B. Kirchner and B. Clare, *Ionic Liquids*, Springer, Berlin, 2009.
140. H. Weingärtner, *Angew. Chem. Int. Ed.*, 2008, **47**, 654.
141. G. Giraud, C. M. Gordon, I. R. Dunkin and K. Wynne, *J. Chem. Phys.*, 2003, **119**, 464.
142. E. W. Castner Jr, J. F. Wishart and H. Shirota, *Accounts Chem. Res.*, 2007, **40**, 1217.
143. H. Machida, Y. Sato and R. L. Smith, *Fluid Phase Equilibr.*, 2008, **264**, 147.
144. C. A. Nieto de Castro, E. Langa, A. L. Morais, M. L. M. Lopes, M. J. Lourenço, F. J. Santos, M. S. Santos, J. N. C. Lopes, H. I. Veiga and M. Macatrão, *Fluid Phase Equilibr.*, 2010, **294**, 157.
145. D. Xiao, J. R. Rajian, S. Li, R. A. Bartsch and E. L. Quitevis, *J. Phys. Chem. B*, 2006, **110**, 16174.
146. P. J. Griffin, A. L. Agapov and A. P. Sokolov, *Phys. Rev. E*, 2012, **86**, 021508.
147. A. Brodin, R. Bergman, J. Mattsson and E. Rössler, *Eur. Phys. J. B*, 2003, **36**, 349.
148. A. Brodin and E. A. Rössler, *Eur. Phys. J. B*, 2005, **44**, 3.
149. M. Nakanishi, P. Griffin, E. Mamontov and A. P. Sokolov, *J. Chem. Phys.*, 2012, **136**, 124512.
150. P. J. Griffin, J. R. Sangoro, Y. Wang, A. P. Holt, V. N. Novikov, A. P. Sokolov, Z. Wojnarowska, M. Paluch and F. Kremer, *Soft Matter*, 2013, **9**, 10373.

151. S. Capaccioli, M. Paluch, D. Prevosto, L.-M. Wang and K. Ngai, *J. Phys. Chem. Lett.*, 2012, **3**, 735.

152. R. Richert and K. Samwer, *New J. Phys.*, 2007, **9**, 36.

153. B. Aoun, A. Goldbach, M. A. González, S. Kohara, D. L. Price and M.-L. Saboungi, *J. Chem. Phys.*, 2011, **134**, 104509.

154. K. Fumino, A. Wulf and R. Ludwig, *Angew. Chem. Int. Ed.*, 2008, **47**, 3830.

155. H. Shirota, T. Mandai, H. Fukazawa and T. Kato, *J. Chem. Eng. Data*, 2011, **56**, 2453.

156. O. Yamamuro, Y. Minamimoto, Y. Inamura, S. Hayashi and H.-O. Hamaguchi, *Chem. Phys. Lett.*, 2006, **423**, 371.

157. J. Leys, R. N. Rajesh, P. C. Menon, C. Glorieux, S. Longuemart, P. Nockemann, M. Pellens and K. Binnemans, *J. Chem. Phys.*, 2010, **133**, 034503.

158. J. Sangoro, C. Iacob, S. Naumov, R. Valiullin, H. Rexhausen, J. Hunger, R. Buchner, V. Strehmel, J. Kärger and F. Kremer, *Soft Matter*, 2011, **7**, 1678.

159. A. Triolo, O. Russina, B. Fazio, R. Triolo and E. Di Cola, *Chem. Phys. Lett.*, 2008, **457**, 362.

160. A. A. Freitas, K. Shimizu and J. N. Canongia Lopes, *J. Chem. Eng. Data*, 2014. DOI: 10.1021/je500197x

161. J. Dudowicz, K. F. Freed and J. F. Douglas, *J. Chem. Phys.*, 2006, **124**, 064901.

162. K. Kunal, C. G. Robertson, S. Pawlus, S. F. Hahn and A. P. Sokolov, *Macromolecules*, 2008, **41**, 7232.

163. J. Dudowicz, K. F. Freed and J. F. Douglas, *J. Phys. Chem. B*, 2005, **109**, 21350.

164. S. F. Swallen, P. A. Bonvallet, R. J. McMahon and M. Ediger, *Phys. Rev. Lett.*, 2003, **90**, 015901.

165. A. P. Sokolov and K. S. Schweizer, *Phys. Rev. Lett.*, 2009, **102**, 248301.

166. X. Xia and P. G. Wolynes, *Phys. Rev. Lett.*, 2001, **86**, 5526.

167. R. Richert, *J. Chem. Phys.*, 2005, **123**, 154502.

168. R. Richert, K. Duvvuri and L.-T. Duong, *J. Chem. Phys.*, 2003, **118**, 1828.

169. D. L. Sidebottom and C. M. Sorensen, *J. Chem. Phys.*, 1989, **91**, 7153.

170. N. Petzold and E. A. Rössler, *J. Chem. Phys.*, 2010, **133**, 124512.

171. G. Li, W. Du, X. Chen, H. Cummins and N. Tao, *Phys. Rev. A*, 1992, **45**, 3867.

172. R. Casalini, K. Ngai and C. Roland, *Phys. Rev. B*, 2003, **68**, 014201.

173. J. Thar, M. Brehm, A. P. Seitsonen and B. Kirchner, *J. Phys. Chem. B*, 2009, **113**, 15129.

174. D. A. Turton, T. Sonnleitner, A. Ortner, M. Walther, G. Hefter, K. R. Seddon, S. Stana, N. V. Plechkova, R. Buchner and K. Wynne, *Faraday Discuss.*, 2012, **154**, 145.

175. M. H. Ghatee, M. Bahrami and N. Khanjari, *J. Chem. Thermodyn.*, 2013, **65**, 42.

176. P. J. Griffin, A. P. Holt, Y. Wang, V. N. Novikov, J. R. Sangoro, F. Kremer and A. P. Sokolov, *J. Phys. Chem. B*, 2014, **118**, 783.

177. G. P. Johari and M. Goldstein, *J. Chem. Phys.*, 1970, **53**, 2372.

178. Y. Wang, P. J. Griffin, A. Holt, F. Fan and A. P. Sokolov, *J. Chem. Phys.*, 2014, **140**, 104510.

179. C. Hansen, F. Stickel, T. Berger, R. Richert and E. W. Fischer, *J. Chem. Phys.*, 1997, **107**, 1086.

180. C. Gainaru, R. Meier, S. Schildmann, C. Lederle, W. Hiller, E. Rössler and R. Böhmer, *Phys. Rev. Lett.*, 2010, **105**, 258303.

181. L.-M. Wang, Y. Tian, R. Liu and R. Richert, *J. Chem. Phys.*, 2008, **128**, 084503.

182. M. Beiner and H. Huth, *Nat. Mater.*, 2003, **2**, 595.

183. M. Beiner, O. Kabisch, S. Reichl and H. Huth, *J. Non-Cryst. Solids*, 2002, **307**, 658.

184. E. Hempel, H. Huth and M. Beiner, *Thermochim. Acta*, 2003, **403**, 105.

185. A Triolo, O. Russina, R. Caminiti, H. Shirota, H. Y. Lee, C. S. Santos, N. Sanjeeva Murthy and E. W. Castner Jr, *Chem. Comm.*, 2012, **48**, 4959.

186. A. Huwe, F. Kremer, P. Behrens and W. Schwieger, *Phys. Rev. Lett.*, 1999, **82**, 2338.

187. V. Adamec and J. Calderwood, *J. Phys. D Appl. Phys.*, 1981, **14**, 1487.

188. K.-D. Kreuer, *Chem. Mater.*, 1996, **8**, 610.

189. N. Agmon, *Chem. Phys. Lett.*, 1995, **244**, 456.

190. L. Vilčiauskas, M. E. Tuckerman, G. Bester, S. J. Paddison and K.-D. Kreuer, *Nature Chemistry*, 2012, **4**, 461.

191. L. J. Bellamy, *The Infra-red Spectra of Complex Molecules*, Wiley, New York, 1975.

192. M. Wierzejewska-Hnat, Z. Mielke and H. Ratajczak, *J. Chem. Soc. Farad. T. 2*, 1980, **76**, 834.

193. K. Bica, J. Shamshina, W. L. Hough, D. R. MacFarlane and R. D. Rogers, *Chem. Comm.*, 2011, **47**, 2267.

194. A. Swiety-Pospiech, Z. Wojnarowska, S. Hensel-Bielowka, J. Pionteck and M. Paluch, *J. Chem. Phys.*, 2013, **138**, 204502.

195. M. Köhler, P. Lunkenheimer and A. Loidl, *Eur. Phys. J. E*, 2008, **27**, 115.

196. C. Roland and K. Ngai, *J. Rheol.*, 1992, **36**, 1691.

197. G. Katana, E. Fischer, T. Hack, V. Abetz and F. Kremer, *Macromolecules*, 1995, **28**, 2714.

198. G. A. Jeffrey, *An Introduction to Hydrogen Bonding*, Oxford, New York, 1997.

199. L. Pauling, *General Chemistry*, Dover, New York, 2012.

200. A. Li, Z. Cao, Y. Li, T. Yan and P. Shen, *J. Phys. Chem. B*, 2012, **116**, 12793.

201. Z. Wojnarowska, C. Roland, A. Swiety-Pospiech, K. Grzybowska and M. Paluch, *Phys. Rev. Lett.*, 2012, **108**, 015701.

202. T. Dippel and K. Kreuer, *Solid State Ionics*, 1991, **46**, 3.

Vita

Philip J. Griffin was born in Lake Forest, Illinois on July 26th, 1986. Following graduation from Lake Zurich High School in Lake Zurich, Illinois, Philip attended the University of Illinois at Urbana-Champaign, where he received a B.S. in engineering physics with a minor in mathematics in May 2008. Yearning to experience the Appalachian culture—and live somewhere where the land is not completely flat and covered in corn—he moved to Knoxville, TN in August 2008. He is currently finishing his doctoral studies in physics at the University of Tennessee, Knoxville, where he was recently awarded the Paul H. Stelson Fellowship for Professional Promise. He is the author or co-author of nine peer-reviewed publications.